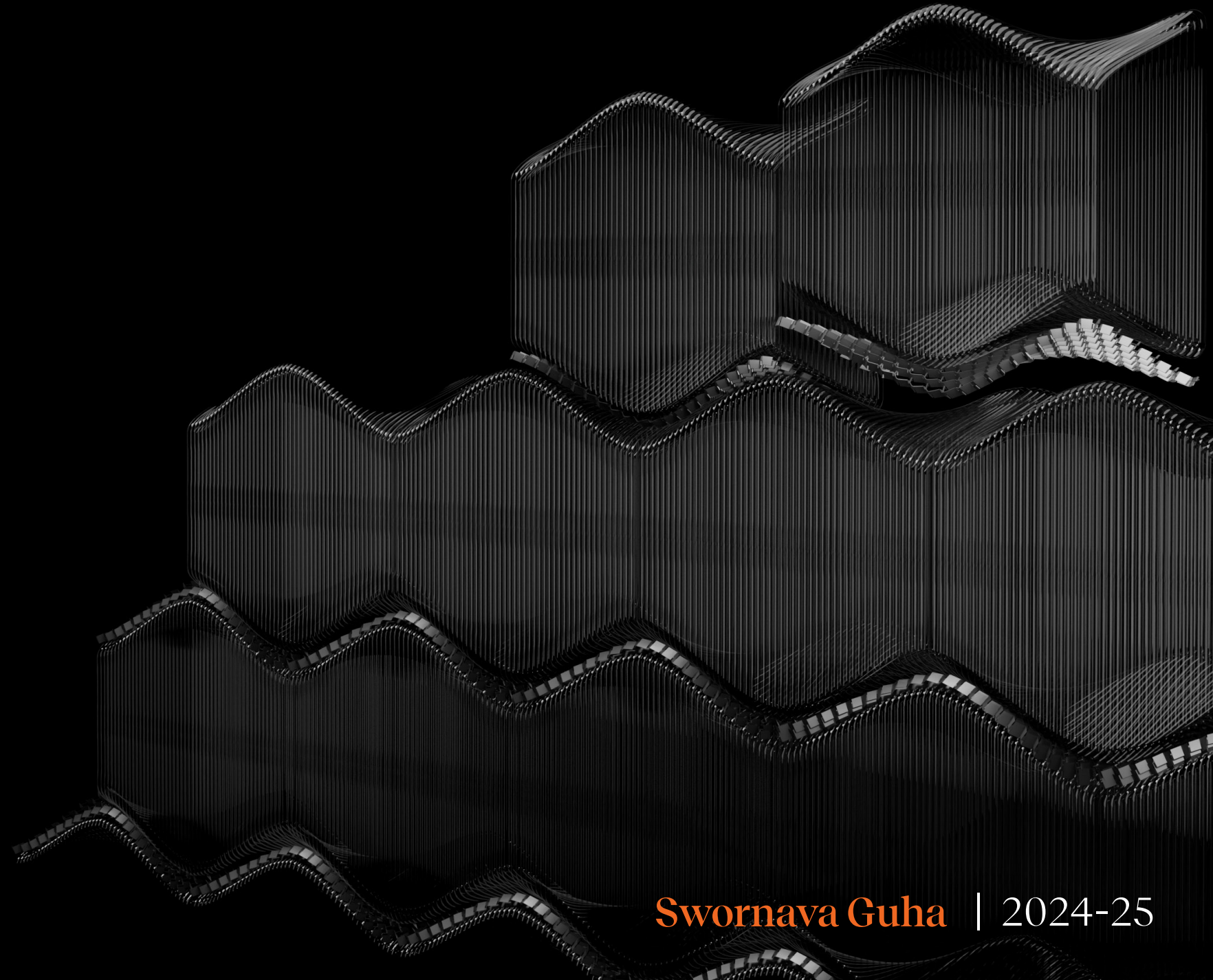


3DP Glass Assemblies

A novel Workflow for **Circular Assembly**
using **3D-Printed Glass Masonry** Units
with a **Kirigami inspired interlayer**



Swornava Guha | 2024-25



Depaartment	MSc. Architecture, Urbanism and Building Sciences (AUBS)
Track	Building Technology Graduation Studio 2025
Mentors	Dr. Faidra Oikonomopoulou Dr. Charalampos Andriotis
Student	Swornava Guha - 5961815



Abstract

This thesis presents assembly methods for reversible structures using 3D printed glass units with a innovative interlayer solution inspired by the traditional Japanese art of Kirigami. It investigates the design and optimisation of a dry-assembled compression-only glass vault with variable interlayers to reduce geometric imperfections and enable structural performance. Three parametric models- a freestanding wall, a catenary vault, and a doubly curved shell- were developed to verify the relationship between geometry, interlayer stiffness, and global behavior under load. A multi-objective optimization workflow was constructed via Grasshopper, ANSYS, and OptiSLang, using surrogate modeling strategies including Kriging and polynomial regression to determine target stiffness values for the interlayer. Based on these targets, a kirigami-inspired interlayer was reverse-engineered and optimized to satisfy the required elastic stiffness via another surrogate-assisted optimization procedure. Final structures were validated using finite element simulations, but further experimental testing must be done to assess long-term behavior, particularly creep and interface performance with glass. Tension activated Kirigami (TAK) samples were fabricated and tested under compression, revealing that the surrogate models require refinement to accurately capture their mechanical response- an area identified for future research. The assembly system described here has promise for reversible, scalable construction, but requires further detailing for disassembly, formwork integration, and physical prototyping. Overall, the research demonstrates a framework for material-driven, performance-based design in dry-assembled glass structures.

Keywords: 3D printed glass, dry-assembly system, masonry structures, kirigami metamaterials

Acknowledgements

This thesis gave me the opportunity to delve into both structural and computational design, making it interdisciplinary. I feel privileged to collaborate with leading experts in glass innovation, and to have connected with many individuals whose guidance, support, and encouragement helped shape this work. I would like to sincerely thank each and every one of them.

Firstly, I thank my mentors Faidra Oikonomopoulou and Charalampos Andriotis for their advice and understanding throughout the course. Their expertise helped me navigate through this complex and challenging topic. I would like to thank Daniel Massimino from Fabrication Indegrated Design Lab, MIT for patiently answering my questions and taking the time to engage with my long emails. Special thanks to Thomas Bigler from MIT as well, for his valuable insights on the kirigami activation and related technical aspects. Unofficially, in this journey I have had several other mentors who I want to thank. I'd like to thank Telesilla Bristogianni, Wilfred Damen, Clara Garcia Sanchez, Lisa-Marie Mueller, and Kaitlyn Becker for giving valuable inputs everytime we met and over emails. I'd particularly like to thank Wilfred Damen who spent hours providing technical and moral support when tools would not work as expected. I'm also grateful to Maiko van Leeuwen, Fred Veer for their help with the testing process within a very short timeline, and to everyone who assisted in preparing the samples for testing. Thanks to my family back in India for believing in me. I would like to thank my friends who helped me stay calm throughout the journey. Sharath MG, thank you for being a constant source of encouragement during the seemingly endless loop of simulations and setup. And to Harshita Sethi- thank you for being the home away from home that I'm grateful for.

"What if glass could be printed like plastic, assembled like LEGO, and disassembled—over and again?"

Contents

Part A- Background

1.0 Research Framework.....	14
1.1 Introduction	
1.2 Research objective	
1.3 Research question	
1.4 Methodology	
1.5 Time planning and Schedule	
2.0 Case Study 1 - Robotic Glass Vault.....	20
2.1 Introduction	
2.2 Design goals	
2.3 Form study	
2.4 Tessellation	
2.5 Interlayer	
3.0 A Review of 3D printing glass	26
3.1 Overview and benefits	
3.2 Limitations, Restraints	
3.3 Latest Advancements	

Part B- Literature

4.0 Design goals.....	32
4.1 Vision	
4.2 Research Sub-questions	
5.0 Design Approach.....	34
5.1 Designing a pure compression structure	
5.1.1 Tension Compression analogy- the Catenary principle	
5.1.2 The compression only model- Heymann's model	
5.1.3 Force Density Method	
5.1.4 Thrust Network Analysis	
5.1.5 Membrane Equilibrium Analysis	
5.1.6 Applying Airy stress function to NURBS patches	
5.2 Case Study 2 - The Armadillo Vault	
5.2.1 Introduction	
5.2.2 Design goals	
5.2.3 Form Study	

5.2.4 Tessellation	
5.3 Overview of tools to design a concave pure-compressive shell	
5.3.1 Comparison of currently available tools	
5.3.2 Designing the compression only shell	
5.4 Tessellations and brick geometry	
5.4.1 Tessellations	
5.4.2 Cast glass- dry assemblies	
5.4.3 Osteomorphic brick shape	
5.5 Optimization approaches	
5.5.1 Form optimization	
5.5.2 Standardization	
5.5.3 Material Optimization	
5.6 Chapter Conclusions	

6.0 The Interlayer.....	50
6.1 Cast glass assemblies- Review of adhesive based Interlayer systems	
6.2 Interlayer for Cast glass- Dry Assemblies	
6.3 Interlayer properties for selection	
6.4 Meta-materials- Why Kirigami?	
7.0 A Kirigami inspired interlayer	54
7.1 Kirigami - An introduction to types	
7.1.1 Ribbon Kirigami	
7.1.2 Zig-zag Kirigami	
7.2 Design of a Kirigami structure	
7.2.1 Ribbon Kirigami Design	
7.2.2 Zig-zag Kirigami Design	
7.3 Kirigami as an interlayer material	
7.3.1 Design Intent	
7.3.2 Geometry	
7.4 Chapter conclusions	

Part C- Design

8.0 Designing the Assembly	62
8.1 Parametric Design Approach	
8.2 Tessellations	
8.3 Defining geometric parameters	

Contents

8.3.1 Catenary vault	
8.3.2 Free standing wall	
8.3.3 Compression only shell	
8.4 Chapter conclusions	
9.0 Parameter Optimization.....	70
9.1 FEA Tools and Workflow	
9.1.1 Parametric Finite Element Analysis(FEA)	
9.1.2 Workflow	
9.1.3 Methods (Sampling, surrogate and optimization)	
9.2 Constraints and Objectives	
9.2.1 Material	
9.2.2 Variables, Responses and Objectives	
9.3 Parameter Sensitivity (2D arches analysis)	
9.4 Optimizing the Catenary Vault	
9.4.1 Variables and Sampling	
9.4.2 Loads and Boundary Conditions	
9.4.3 Surrogate model for optimization	
9.4.4 Optimization and Best designs	
9.4.5 Clustering of Best designs	
9.5 Validation	
9.6 Brick Amplitude	
9.7 Chapter Conclusions	
10.0 Engineering the Kirigami Interlayer	92
10.1 Defining the target stiffness range	
10.2 Target stresses for the kirigami	
10.3 Material and Method	
10.4 FEA on kirigami geometry	
10.4.1 Parametric model of kirigami	
10.4.2 FEA Analysis setup and workflow	
10.5 Kirigami Surrogate model	
10.6 Reverse calculating the Kirigami geometry	
10.7 Validation	
10.8 Kirigami Interlayer Performance	
10.9 Chapter Conclusions	

11.0 Validation	104
11.1 Kirigami stiffness for Osteomorphic surface	
11.2 Vault Design with 3DP units	
11.3 Final Vault Design	
Key take-aways for design	
12.0 Assembly and detailing	112
12.1 Assembly process and form-work	
12.2 Scaled Model demonstration	
13.0 Conclusions.....	120
13.1 Conclusion	
13.2 Future Work and Discussions	
14.0 Reflection	124
15.0 References	130
Appendix 1 - Form finding, Tessellations	132
Appendix 2 - Structural Analysis.....	138
Appendix 3 - Kirigami prototypes.....	148



Part A | Background

*Design / Photo Credit:
Foster + Partners / Aaron Hargreaves
mapleglassprinting.com*

1.0 | Research Framework

1.1 Introduction

"Glass is inherently multi-functional. The material is structurally sound, optically transparent, and chemically inert...What if these properties become fully tunable spatially and temporary such that glass becomes a multifunctional transparent building block?"

-Chikara Inamura, 2017

With the first ever 3D printed glass object (Figure 1), the Mediated Matter Group at MIT sparked a new beginning of looking at glass structures for the built environment. In 2015, (Klein et al., 2015), the MIT media lab introduced a novel technique: G3DP, a large-scale 3D printed glass technology, followed by G3DP2 in 2018, they showcased three-meter-tall glass columns (Figure 2) optimized for structural and optical efficiency (Inamura et al., 2018). The technology has been rapidly evolving ever since. Other studies, including Baudet et al., (2019) and Zhang et al. (2021) showcase the versatility of 3D-printed glass, overcoming challenges and maintaining original glass properties.

Additive manufacturing (AM) or 3D printing (3DP) is a computer-aided design and manufacturing technique that builds objects layer by layer. This rapidly evolving method offers key advantages, including reduced material waste, mass-efficient, structurally optimized products, lower development time and cost, and the **ability to create complex geometries unattainable with traditional methods**. Its potential in architectural applications has been explored using materials like ceramics, metal, and concrete (Qaidi et al., 2022; Tessman et al., 2022).

Fused Deposition Modeling (FDM), also known as Fused Filament Modelling (FFM) or Fused Filament



Figure 1: One of the first 3DP object (Source: Inamura, 2017)



Figure 2: 3D-printed glass columns displayed during Milan Design Week 2017 (Source: Inamura et al., 2018)



Figure 3: G3DP2 platform (Source: Inamura et al., 2018)

Fabrication (FFF) of glass, or more commonly AM or 3DP of glass involves a computer-controlled heating nozzle moving along the x-plane, selectively applying molten glass onto a work table, followed by rapid cooling (Huang et al., 2020; Sood et al., 2010; Popescu et al., 2018). MIT researchers developed G3DP2 (Figure 3) to produce industrial scale glass products for structural and architectural applications (Inamura et al., 2018). **Owing to its infant stages of developments, we have seen very limited application of 3DP glass at an architectural scale.**

Current 3DP glass constraints ($32.5 \times 32.5 \times 38$ cm) necessitate segmentation into masonry units for larger assemblies. Massimino et al. (2024) introduced 3DP glass interlocking units, inspired by cast glass systems (Oikonomopoulou et al., 2018). **Adhesive applications in projects like the Crystal House and Atocha Memorial hinder deconstruction and recyclability** (Oikonomopoulou & Bristogianni, 2022). Interlocking units avoid adhesives, relying on glass features for lateral load resistance, but **require interlayers to prevent contact, level tolerances, and transfer loads** (Massimino et al., 2024). Unlike cast glass, 3DP glass

Figure 4: The Robotic glass vault (credit: Maciej Grzeskowiak)

enables customizable masonry unit geometries thereby creating the possibility to standardize the interlayer using architected materials or (meta)materials for programmable stiffness and flexibility.

Kirigami, the ancient art of transforming flat sheets into 3D structures, imparts tunable properties, making it a (meta)material. Its flexibility, stretchability and the ease of manufacturing with sheets of material, it has many applications in lightweight, energy-absorbing panels, structures, and equipment (Corrigan et al., 2023; Sun et al., 2021).

This thesis employs a research-through-design approach to develop a **kirigami-inspired interlayer system for assembling 3D-printed glass masonry units**. It focuses on optimizing masonry structures to design the interlayer geometry. Drawing on cast glass interlocking systems (Oikonomopoulou et al., 2018), it explores kirigami-based interlayers for 3DP glass bricks in dry assembly of a wall, a catenary vault and a purely compressive shell structure, comparable to the adhesively bonded Robotic Vault (Parascho et al., 2020).

1.2 Research objective

"In comparison to traditional glass casting, glass additive manufacturing (AM) presents an opportunity to increase design flexibility and reduce tooling costs for the production of highly variable geometries." - Massimino et al., 2024

This thesis leverages the advantages of 3D printing non-standard glass units to standardize the interlayer design for specific assemblies. **The primary goal is to develop a methodology for designing assemblies using 3D printed glass units, along with a strategy to engineer the interlayer for targeted performance.**

Kirigami is a technique that imparts mechanical properties to sheet materials through strategically placed cuts and the application of an activation force. This method offers a simple, scalable approach to manufacturing from flat sheets. For these reasons, kirigami is employed to engineer the interlayer, enabling precise control over its properties while ensuring ease of production and scalability. The thesis develops a parametric method to optimize a dry-assembled masonry structure using 3D-printed glass bricks and reverse-engineers a kirigami-based interlayer. It addresses the structural design and optimization of the assembly while considering the current limitations of 3DP glass technology.

The novel interlayer solution could also be adapted for the dry assembly of cast glass units or similar applications. Future work may involve further optimizing the interlayer for other masonry structures and expanding its applicability.

1.3 Research Question

Given the Research objectives, the research question is framed as follows:

Can a Kirigami-inspired interlayer be the solution for a reversible dry-assembly system with 3D-printed glass bricks in the built environment? What are the key considerations?

Secondary goals supporting the exploration of the method's potential have been categorized into two owing to the two-faced research strategy. They are as follows:

Global Design and performance:

1. What are the suitable tessellation strategies for various dry-assembly structural typologies, and how do they influence geometric and mechanical compatibility?

2. How do local design parameters—such as load, support conditions, and unit arrangement—affect the overall structural performance of dry-assembled systems globally?

3. What is the optimal stiffness range for the interlayer material to ensure mechanical stability and compatibility within a given dry-assembly configuration?

Interlayer design:

4. How can the target stiffness values be translated into a feasible kirigami-based interlayer design, considering

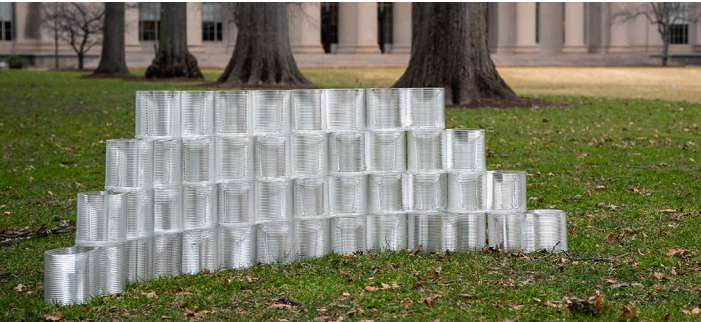


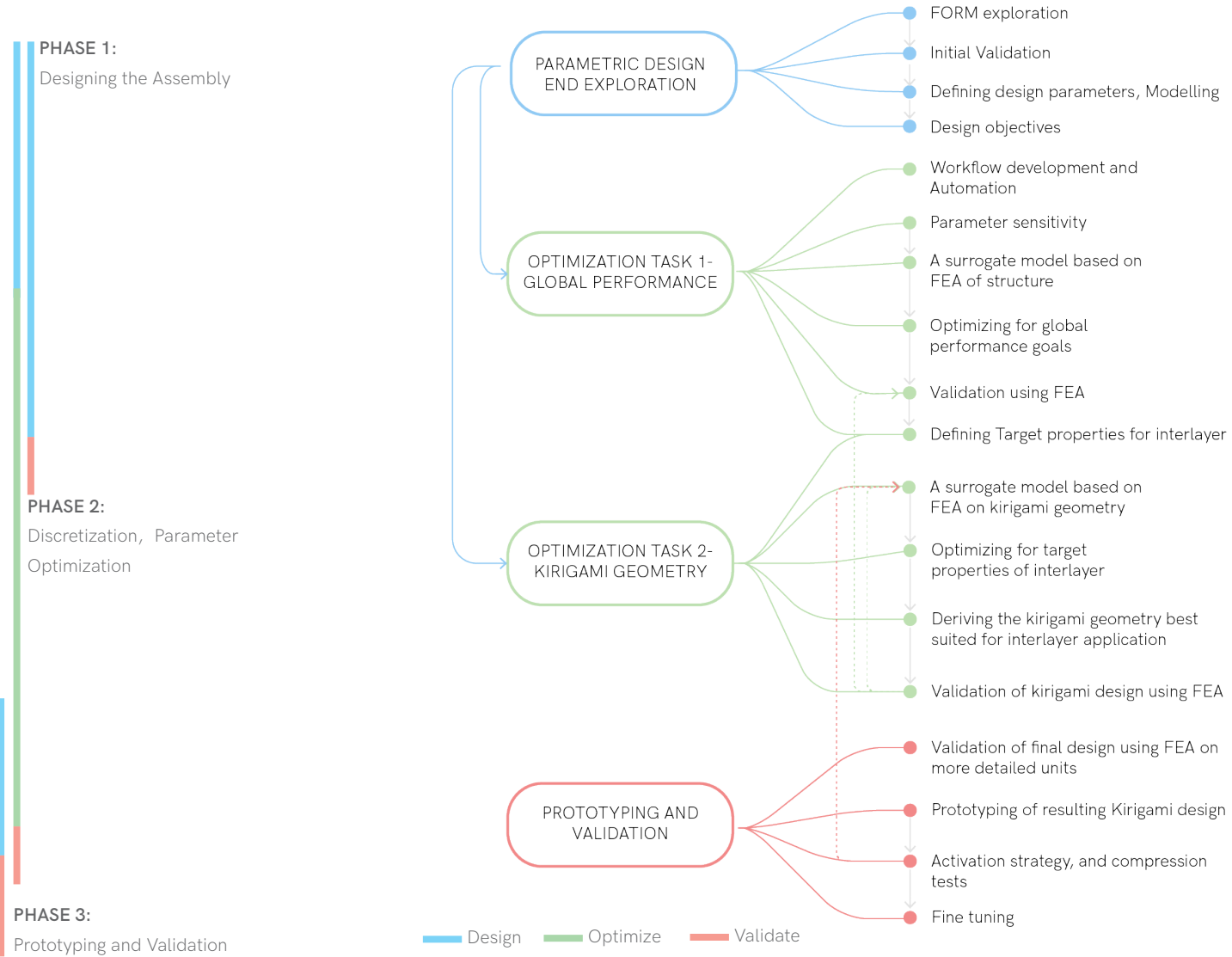
Figure 5: 3DP glass Interlocking units (Source: Massimino et al., 2024)

1.4 Methodology

material properties and manufacturing constraints?

5. How can a surrogate model be created and fine-tuned, to help predict the performance of interlayer-assembly systems, and how can these tools accelerate the design-space exploration through simulation?

Owing to the idea of Research through design, the Methodology followed in this thesis is simplified as shown in the figure below. The process is categorized into mainly three overlapping phases.



1.5 Time Planning and Schedule

The Building Technology Graduation studio officially started on November 7th, with my P1 presentation on November 15th. The research is currently directed towards reviewing relevant literature to establish the research objectives and sub goals. My aim is to complete this graduation project within the originally designated time frame, which allows for approximately 29 weeks. This research is also in collaboration with the Fabrication Integrated Design lab, MIT who are also working on engineering kirigami to target performances. Therefore, this calls for a strict time frame, for a fruitful collaboration- and feedback from the externals. This section provides the time frame that has been followed till date.

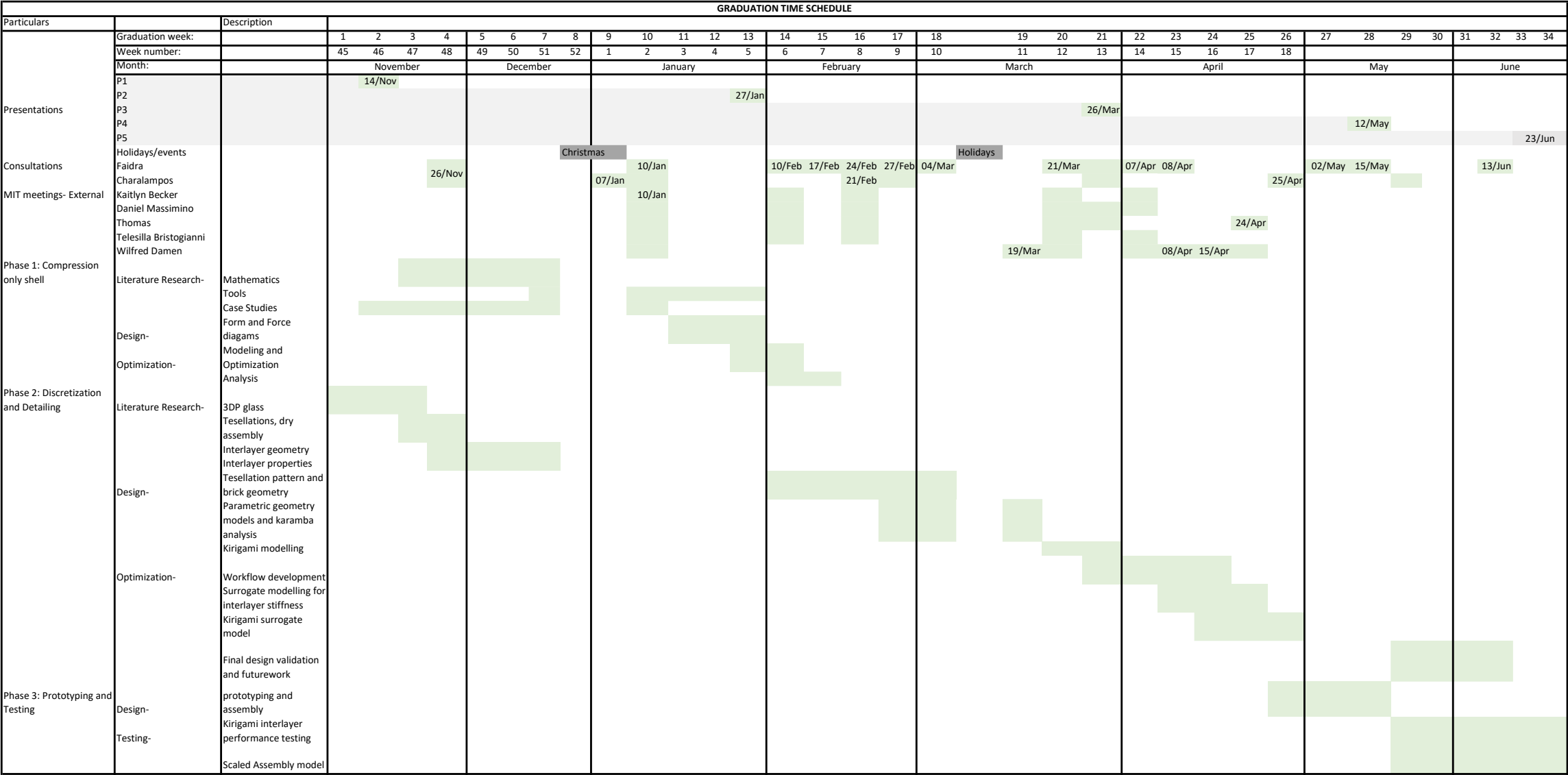


Figure 6: Schedule (Source: Own)

2.0 | Case Study 1 - Robotic Glass Vault

2.1 Introduction

Choosing the case study:

Glass is not commonly used as a structural material, but its exceptional compressive strength makes it well-suited for application in compression-only shell structures (Beghini et al., 2020). The closest comparable masonry application for the problem at hand is cast glass masonry structure. In contemporary architecture, glass masonry units primarily consist of cast or hollow pressed glass blocks. Traditional fabrication techniques for these blocks involve disposable molds for intricate designs or costly reusable molds for simpler forms (Oikonomopoulou et al., 2020). Cast glass masonry units offer valuable structural strategies that can be adapted for using glass additive manufacturing as a production method for construction components (Massimino et al., 2024). However, we have only seen glued applications for load bearing cast glass masonry at an architectural scale- The robotic glass vault, Crystal houses, and the Qammat Pavillion. Out of these, the Robotic glass vault has a more complex doubly curved geometry and varying interlayer dimensions - that aligns with our idea of developing standard interlayer and varying 3DP units. Therefore, we have chosen this as our primary case study and a project to compare our outcomes with.

The initial concept aimed to design a unique compression-only shell considering constraints such as ease of assembly, dry construction, and scaffold-free erection. However, a review of literature on discrete construction and interlocking geometries led to the selection of a geometry similar to the Robotic Glass Vault, but more symmetrical. This choice was made for its compatibility, minimal scaffolding requirements,

and the avoidance of solving for irregular block shapes. Further details are discussed in Section 5.4 of this report.

Robotic Light Vault- An Introduction:

The LightVault project- also known as Robotic glass vault, a collaboration between SOM, Princeton University's c.r.e.A.te lab and Form Finding Lab,



Figure 7: Prototype of assembled brick vault at Princeton University (Source: Parascho et al., 2021)

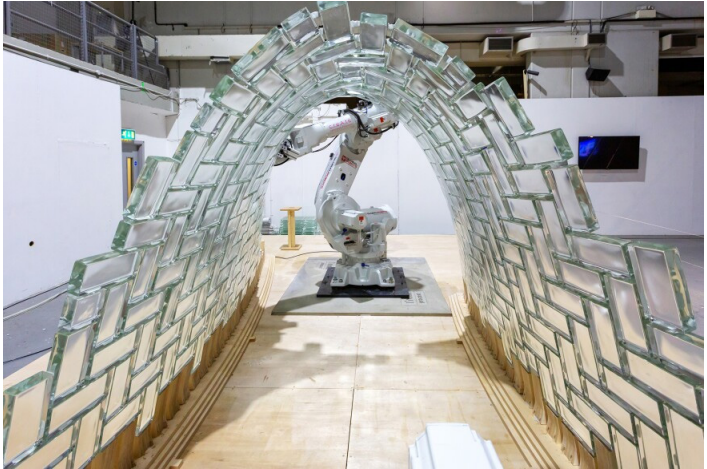


Figure 8: Final constructed vault (Source: Beghini et al., 2020)

and the TU Delft Glass Group, aims to showcase the potential of automated robotic construction. This project focuses on the robotically assembled, scaffold-free construction of a large-scale, double-curved glass brick vault measuring approximately 2 meters in height and 2.6 meters in width (Parascho et al., 2021). The first full scale model prototype was built using concrete and cast glass units at Princeton University (Beghini et al., 2020)(Figure 7). Finally assembled live on-site by two robots during SOM's Anatomy of Structure 2020 exhibition in London (Figure 8), the vault features a herringbone pattern and was designed as a purely compression-only structure. However, an adhesive medium was applied to stabilize the structure during assembly due to the absence of scaffolding.

In this section, the Robotic glass vault has been reviewed in terms of its compression only geometry design, tessellations, and its interlayer properties. The further details about the robotic assembly of the structure is disregarded.

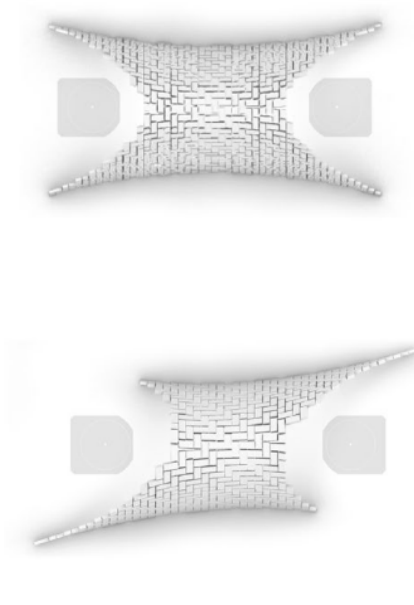


Figure 9: Original and Final vault shape based on robotic arm placement (Source: Beghini et al., 2020; Parascho et al., 2021)

2.2 Robotic glass vault- Design goals

- i. Automated construction- Robotic
- ii. No falsework- eliminate the guides
- iii. Use of standard size bricks
- iv. Compression only structure- form finding method based on Airy Stress function

2.3 Form Study

The vault consists of leaning arches that grow larger outward from the central, robot-built arch. The leaning arches are stable without requiring falsework, following the ancient technique discussed as shown below (Figure 9). Additionally, the vault's geometry is made asymmetric to prevent conflicts between the robot's movement and the structure, as shown in Figure 10.

Height of Vault: 2.0m
Width of Vault: 2.6m
Length ~6m

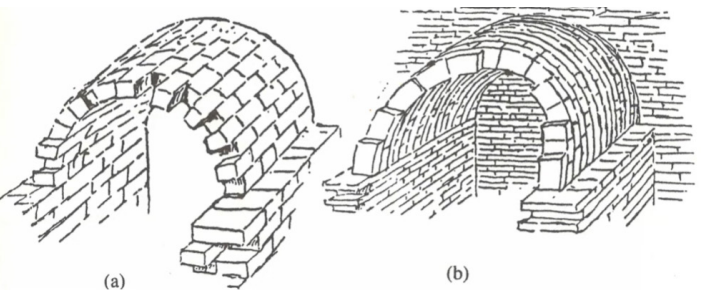
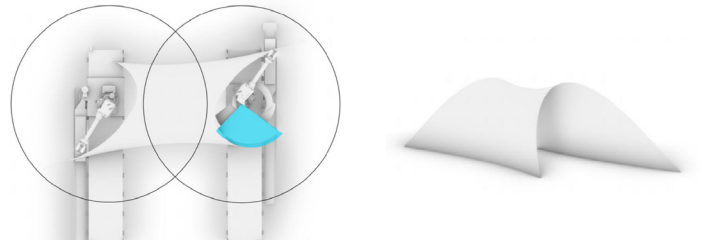


Figure 10: Barrel vault Techniques (Source: Heyman, 1995)



Prototype section (Figure 2.1) : $3.3 \times 2.6 \times 2.0$ m
 No. of bricks: 233 full bricks (250x110x50mm)
 32 half bricks (125x110x50mm)

The original symmetric shape of the vault as shown below (Figure 11) is selected for our design problem. The compression-only form of the Robotic vault has been developed using their in-house custom tools using an outdated grasshopper plugin called Mothra which is later explained in this report in Section 5.3. We initially planned to recreate the shape using the same strategies used here as shown in Figure 9. (Parascho et al., 2021)

2.4 Tessellation

Tessellation pattern in this case was chosen to employ a constant brick shape and size as use of standard cast glass bricks were a fabrication constraint due to costs. The herringbone pattern was chosen for its stability during construction- which allows the blocks to naturally lock into place and ensure higher structural stability, although several different tessellations were considered for scaled prototyping (Figure 14). Gaps between bricks were optimized to range from 6mm (to avoid clashes during robotic placement) to 50mm (to minimize epoxy use and maintain aesthetics). The final tessellation is shown in Figure 9.

An iterative process was used to ensure equilibrium at each stage of construction using finite state analysis and discrete element method. (Source: Beghini et al., 2020). A central arch supports the vault construction serving as a backbone (Figure 13). However, this technique failed and a more stepped construction was followed.

3DP eliminates the requirement of moulds, and therefore does not require standardization. Therefore, the tessellation pattern would depend on the dry assembly performance.

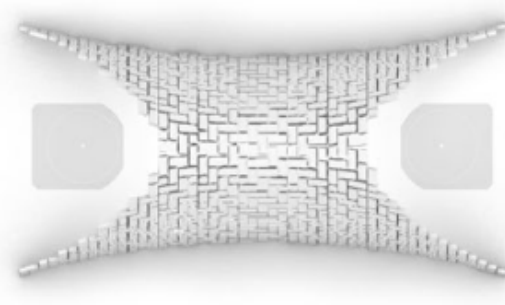


Figure 11: Original vault shape of the Robotic Glass Vault (Source: Beghini et al., 2020)

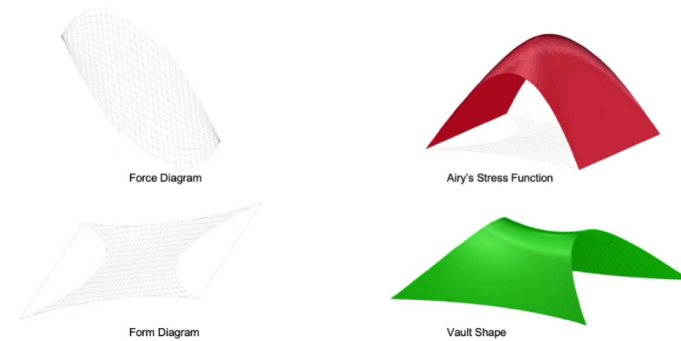


Figure 12: Force and Form Diagram and vault shape derived from Airy Stress function (Source: Beghini et al., 2020)

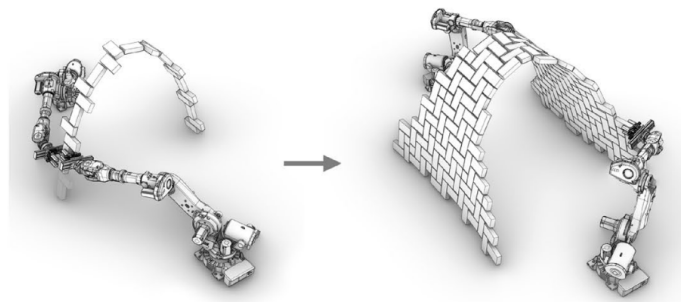


Figure 13: First phase: the middle arch is built by alternating the robots used to place and then support the structure. Second phase: the construction is continued on either side of the middle arch (Source: Beghini et al., 2020; Parascho et al., 2021)



Figure 14: Tessellation (Source: Beghini et al., 2020)

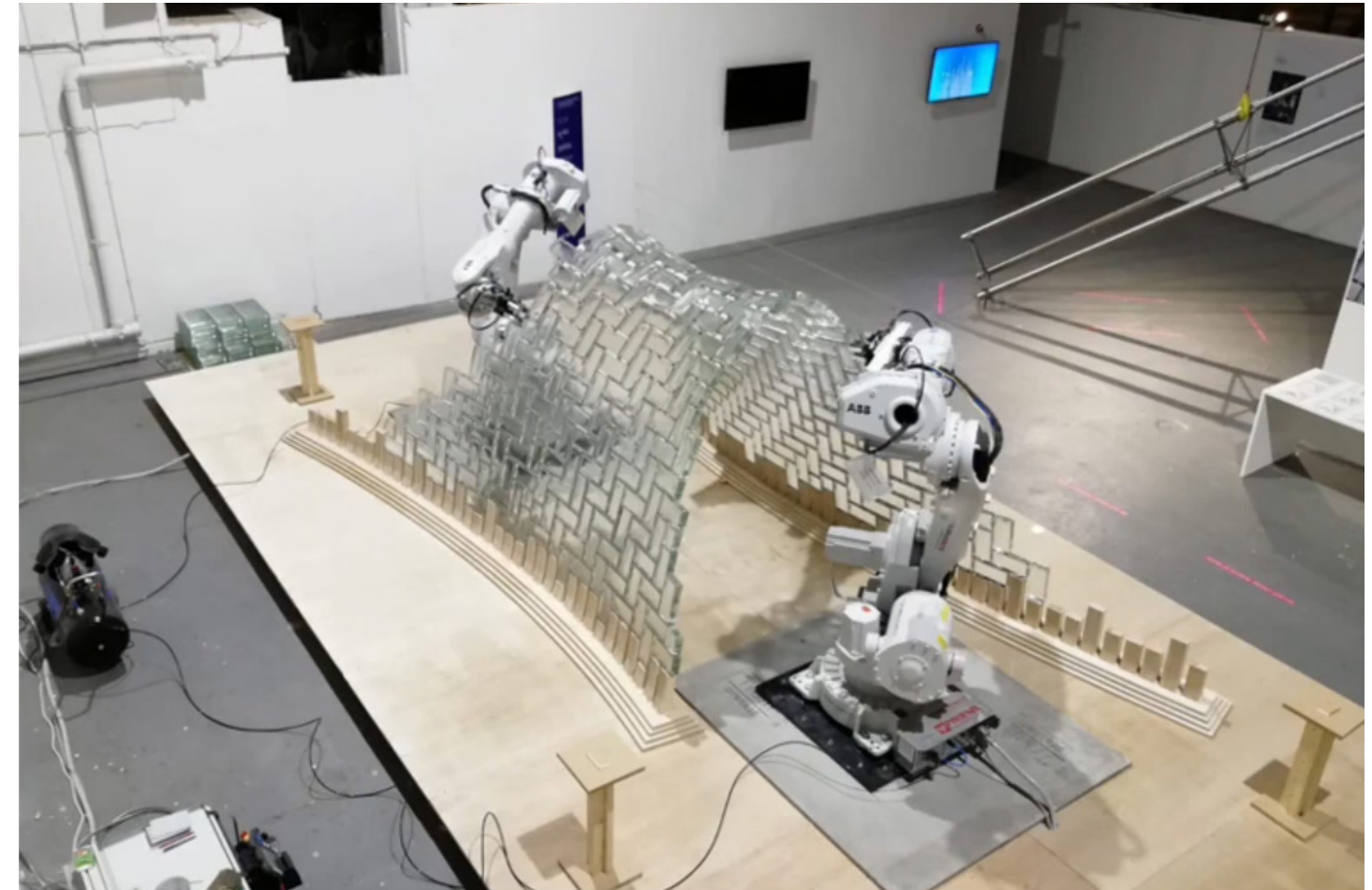


Figure 15: Final Vault construction (Source: Beghini et al., 2020)



2.5 Interlayer

The Interlayer for the Glass vault, as summarized from (Oikonomopoulou & Bristogianni, 2022):

Required properties (Prioritized in order):

High gap-filling capability

Fast assembly

Economic construction & Good creep resistance

Chosen interlayer: Fast setting Rigid epoxy putty in combination with acrylic pieces in case of the larger gaps

Gap filling capacity: 20mm

Color: Grey

Experimental Validation: Applicability tests on adhesive pre-selection small and large-scale prototyping of assembly

Selecting an interlayer with gap filling capability as well as resistance to creep was the major challenge. A putty form of epoxy was finally chosen which does not generally have structural applications and has different properties than regular stiff epoxy. Strength was not a major factor of concern as the geometry was a designed as compression only.

Key take-aways

-Inferring from parallel research on tessellations and dry-assembly systems presented in later sections of the report, the a symmetric version of the vault (Figure 11) is chosen to be recreated for our design assignment.

-Considering inclined barrel vault techniques (Figure 10) from Heymann's is promising and is considered for the final design as it will avoid stress concentration along the unsupported edges.

-We considered the grasshopper tool Mothra created for the form developed- which is however found to be outdated and is discussed later in this report.

-Defining a concave Airy's stress function is assumed to be a potential solution to form-find such a concave compression only shell.- but is not further explored in this thesis

-Herringbone tessellation is excluded, as it relies on standard brick modules and self-supported robotic construction. In contrast, 3D printing allows for non-standard units without the need for molds.

-The tessellation will instead be guided by dry interlocking performance and assembly detailing. While staggered patterns (like the 90° orientation shown) help support half-bricks during adhesive curing, such cantilevering is unsuitable for a dry assembly process and will be avoided.

-Our research idea has arrived mainly from the challenge faced in finding an interlayer solution in this case. The properties of interlayer required in our case remain the same as mentioned here.

3.0 | A Review of 3D printing glass

3.1 Overview and benefits

Contemporary architectural trends demand complex glass forms and large-scale production of custom-tailored, doubly curved panels. Additive manufacturing (AM), or 3D printing (3DP), offers a revolutionary approach to producing glass components layer by layer with key benefits such as reduced material waste, shorter development time, lower costs, and the ability to create intricate geometries unattainable by traditional methods (Qaidi et al., 2022).

Various methods to additively manufacture glass have been researched on, and they include Fused Deposition Modelling(FDM), Stereolithography (SLA) and Digital Light Processing (DLP), Selective laser sintering/melting (SLS), and Direct Ink Writing. An overview of the methods can be found in Table 1. Pioneering research by MIT's Mediated Matter Group, KIT Klein Lab, and NIMTE has advanced 3D glass printing technology for custom architectural components. The G3DP2 platform comprising of a 4-axis motion by MIT demonstrated the feasibility of industrial-scale 3D-printed glass, opening pathways for high customization and sub-millimeter precision in glass processing (Inamura et al., 2018; Zhang et al., 2021). *Thereby, FDM is regarded as the most promising for industrial scale, and we consider MIT's latest G3DP3 (Figure 17) platform for our study.*

Despite its promise, large-scale applications remain limited. 3DP glass is also one of the most sustainable fabrication techniques, enabling intricate and customized structures with minimal waste, offering significant opportunities for innovation in design, geometry, and structure (Oikonomopoulou, 2023; Inamura et al., 2018).

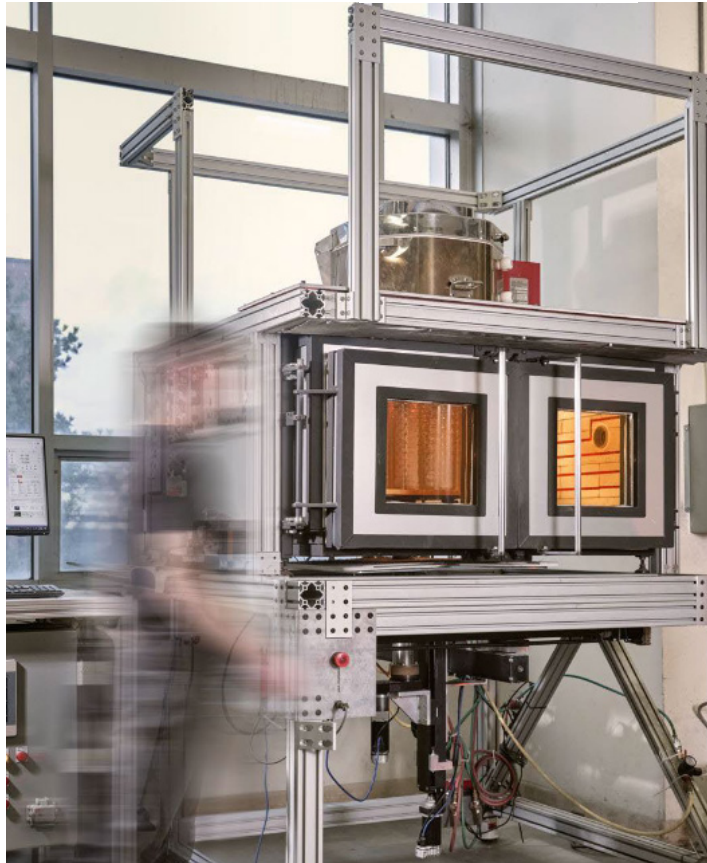
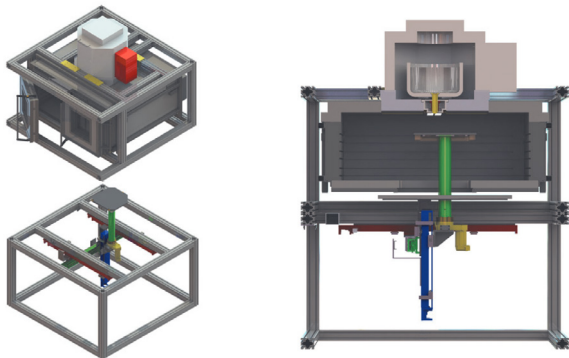


Figure 17: Photograph of Evenline's G3DP3 Molten Glass 3D Printer (Source: Stern et al., 2024) and exploded view of printer (above) (Source: Klein et al., 2015)

Criteria:	FDM (glass)	SLA and DLP	SLS	DIW
Operating principle:	Glass extrusion	Photopolymerization	Powder sintering	Semi-solid ink extrusion
Material:	Glass (specific formulation)	Limited glass options	Limited glass options	Glass-based inks
Print Speed	Moderate to fast	Slow to Moderate	Moderate	Slow
Suitability for Large Objects	Feasible	Limited	Limited due to setup	Limited
Applications	Prototyping, functional parts,	Prototyping, small parts	Complex glass structures	Complex structures, soft robotics

Table 1: Qualitative Analysis of 3DP glass techniques (Source: Own)

3.2 Limitations, Restraints

The FDM method limits the control of discharge shape and achieving results under operating temperatures. Printed samples lack precision (sometimes), show "step effects,"- have surface flaws; the structural strength also depends of geometry. Therefore, it has lower structural performance and visibility of layering, presenting developmental limitations (Zhang et al., 2021; Oikonomopoulou, 2023).

There are fabrication limitations due to the continuous filament deposition (Inamura, 2017). The Glass 3D Printer 3 (G3DP3) represents the third generation of molten glass printing technology. The printer characteristics of G3DP3 have been summarized in table 2.

Although recently the potential and feasibility of using recycled glass(soda lime container glass and recycled float produced window glass) for 3DP has been demonstrated by (Stern et al., 2024), the applications of the same at an architectural scale and recyclability of the 3DP product itself is still unknown.

	Unit	G3DP3
X-Axis	mm	325
Y-Axis	mm	325
Z-Axis	mm	380
Print volume	cm3	40, 100
Bead height	mm	3.0-6.0
Bead width	mm	9.0-16
Feed rate	mm/s	6-20
Path curvature radius	mm	6-15
Max overhang angle	Degrees	30-35
Minimum path length	mm	300-475
Max extrusion temp.	oC	1200
These limitations can be exceeded for certain shapes, but require additional testing.		

Table 2: Qualitative Analysis of 3DP glass techniques (Source: Stern et al., 2024)

3.3 Latest Advancements

'3D printing techniques have brought new life to the ancient material, glass' (Zhang et al., 2021)

There has been a rapid development in 3DP of glass, and thus a growing interest for applications in the built environment. Latest advancements include-

Interlocking 3DP glass units of different types using the G3DP3 platform- the latest and third generation of the printer currently owned and operated by Evenline Inc.

Hollow interlocking unit(Figure 18) produced using recycled soda-lime float glass using G3DP3; also establishing a conclusion that the printer can be re-calibrated for different glass formulations. Prints were also made on top of float glass as a base as shown in Figure 20. (Massimino et al., 2024; Stern et al., 2024)

Architectural scale applications include 3D-printed glass columns displayed during Milan Design Week 2017 (Figure 19)

Evenline studio and Maple glass have been exploring 3DP glass objects; Maple glass in collaboration with RMIT Architecture have developed Glass 3D Printed Architectural Facade Prototype (Stern, n.d.; Maple Glass Printing, n.d.).

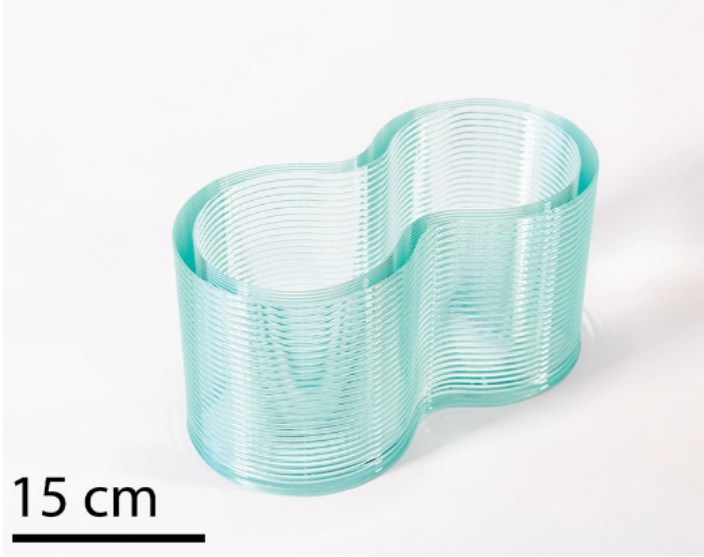


Figure 18: Hollow 3DP glass unit using recycled soda-lime float glass (Source: Massimino et al., 2024)



Figure 19: Interlocking units assembled in a Wall configuration (Source: Massimino et al., 2024)



Figure 20: Hexagon form printed on Optifloat float glass and high temperature coated float glass (Source: Stern et al., 2024)

Key take-aways

Following are key takeaways from literature and outcome of initial discussions with the MIT Team:

- FDM is regarded as the most promising for industrial scale, and we consider MIT's latest G3DP3 platform for our study.
- Maximum size limitation for a single printed unit: 32.5 x 32.5 x 38cm. Path curve radius of 6-15mm and other characteristics summarized in table 2.
- Printed unit has to be designed to accommodate a Continuous path during slicing (develop a custom slicing tool in gh).
- 2 faces (bottom and top) of the printed object has to be parallel and horizontal. - Brick units can be used with loading in the perpendicular direction as to printing.
- The assumed masonry unit for our design assignment is assumed to be hollow units- with a possibility to be printed over float glass- for a closed/shaded vault structure.
- There are signs of anisotropic behavior of printed glass objects due to FDM, but we will disregard the effect of the same for this research.
- Although crucial, we will not delve deeper into glass characterization/ viscosity and printing calibration.



Part B | Literature

4.0 | Design Goals

This section outlines our vision and goals, emphasizing the key aspects we aim to address in this thesis.

4.1 Vision

Using an example assembly of a masonry vault- we aim to develop a method to engineer an innovative interlayer solution capable of accommodating required properties of gap filling while providing creep resistance. This interlayer can be further optimized for assembling other interlocking masonry structures, making it a versatile and universal solution. To demonstrate and analyze we attempted to put forward methods to assemble a simple wall, a singly curved structure (a catenary vault) and a doubly-curved compression only vault with 3d printed glass blocks designed for the assembly system.

4.2 Research sub-questions

As briefly mentioned earlier in Section 1.2, in this section we state how the sub research questions would be answered as per the current methodology planned. We have categorized the sub questions into two categories as here under. *This also reflects in the chapters categories that come after, with each chapter that define a 'goal' in the beginning.*

Global Design and performance:

1. What are the suitable tessellation strategies for various dry-assembly structural typologies, and how do they influence geometric and mechanical compatibility?

Chapter 8 of the report demonstrates tessellation strategies for a wall, a catenary vault and the doubly curved compression only shell based on force flow in the structure, ease of assembly and construction limitations.

2. How do local design parameters- such as load, support conditions, and unit arrangement- affect the overall structural performance of dry-assembled systems globally?

Chapter 9 demonstrates parameter sensitivity and optimization and a developed workflow for automation of FEA to create a surrogate model for optimization.

3. What is the optimal stiffness range for the interlayer material to ensure mechanical stability and compatibility within a given dry-assembly configuration?

Chapter 9 also documents an optimization done with structural performance objectives on the developed surrogate in order to derive the required optimal stiffness in terms of its young's modulus of the interlayer assumed as a solid in this case. This process is demonstrated with the case of the dry assembled catenary vault as per design.

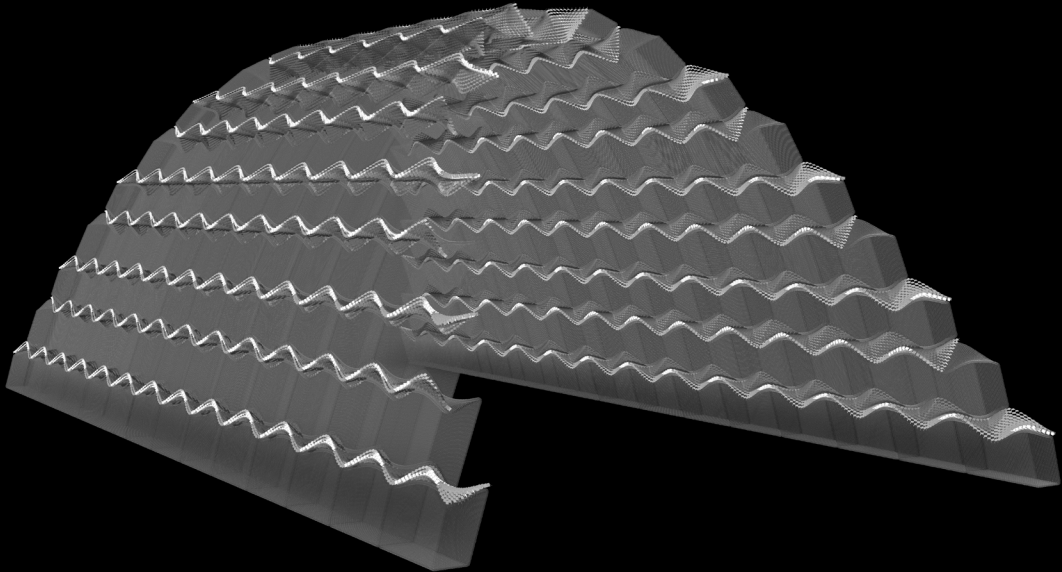
Interlayer design:

4. How can the target stiffness values be translated into a feasible kirigami-based interlayer design, considering material properties and manufacturing constraints?

Chapter 10 demonstrates a method to reverse engineer the kirigami geometry from the target stiffness range based on an optimization task performed on the surrogate. This is planned to be fine tuned based on physical tests in the following month

5. What role can machine learning and surrogate modeling play in predicting the performance of interlayer-assembly systems, and how can these tools accelerate the design-space exploration through simulation?

Chapters 9 and 10 demonstrates a workflow for creating surrogate models and validate the optimization outcome with FEA.



5.0 | Design Approach

5.1 Designing a pure compression structure

Veenendaal & Block (2012) classified the methods of form finding into three main families (Figure 21): Stiff Matrix Method- based on standard elastic and geometric stiffness matrices; Geometric stiffness methods- material independent, only with geometric stiffness; and Dynamic Equilibrium- steady state solution equivalent to static solution of static equilibrium.

In this section we discuss the background and methods of form finding of pure- compression shells with respect to computational tools to realize the same. The idea is to find with trying out different methods and find the appropriate method for our design goal to create a similar concave compression only form similar to the Robotic glass vault discussed earlier.

5.1.1 Tension Compression Analogy - the Catenary principle

"As hangs the flexible line, so but inverted will stand the rigid arch." -Robert Hooke, 1676

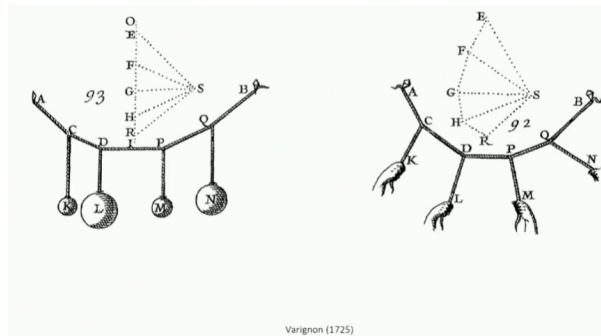


Figure 22: Use of Tension-compression analogy and graphic statics to solve equilibrium. Right: models from Gaudi, Heinz Isler *

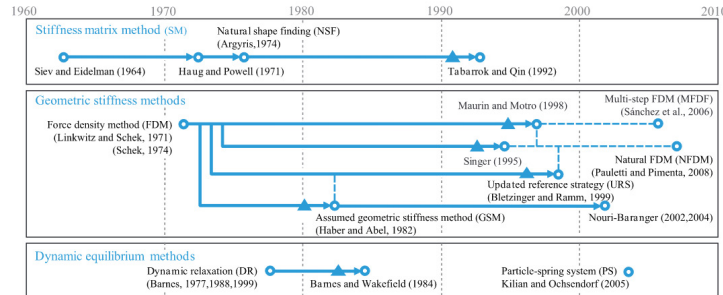
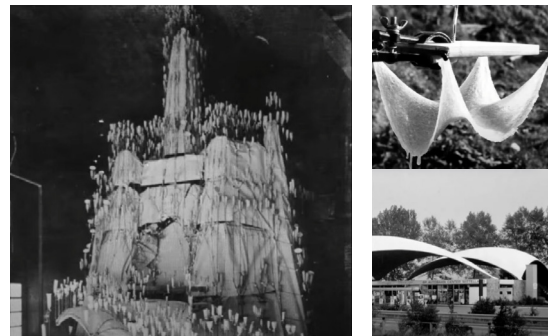


Figure 21: Development and categorization of form finding methods (Source: Veenendaal & Block, 2012)

If you have a system in pure tension without any flexure, the geometry if frozen, can be inverted to create compression-only structure. The idea to create such compression only shells goes back centuries and notable pioneers are Antonio Gaudi, Heinz Isler 1968, Frei Otto's soap bubble experiments and so on.

The methods of *graphic statics* as shown in the figure 21 were developed to create force diagrams and solve equilibrium problems that were otherwise very complex. This is what is the basic idea the more modern methods of Thrust Network analysis is built upon. (Marmo & Rosati, 2017)



5.1.2 The compression only model- Heymann's model

In 1966, Heymann defined the idea of Limit Analysis to assess the safety of masonry structures, based on following three assumptions

- Stone has no Tensile strength
- The compressive strength of stone is effectively infinite
- Sliding of one stone upon other cannot occur

Considering these assumptions, Limit analysis allows us to apply Safe Theorem and Kinematic Theorem to ensure stability of the designed structure.

Safe theorem: The structure will not collapse if a pure compression stress field exists that balances the external loads.

Kinematic theorem: The structure will collapse if a deformation mechanism exists where the external loads' work exceeds the internal energy dissipation. This is the base idea that Membrane equilibrium Analysis is derived from which also uses graphic statics.

5.1.3 Force Density Method (FDM)

Schel, 1974 presented the Force Density Method that analyzes (rope) networks using force-length ratios (force densities) for each branch. These parameters effectively describe the equilibrium state of any network. Node coordinates are determined by solving a single linear equation system, derived through a Gaussian transformation of the branch-node matrix.

These concepts are seen in the grasshopper plugin Kangaroo- a grasshopper (Rh) plugin that solves for an equilibrium condition with given loads using

dynamic relaxation- a numerical method where forces and displacements are iteratively updated to simulate physical behavior. Form finding principles of RhinoVAULT 2 also overlap with FDM

5.1.4 Thrust Network Analysis(TNA)- Rigid block Equilibrium

It is very difficult to draw conclusions from stress analysis of unreinforced masonry even for a simple 2D problem (Block, 2009). The equilibrium of vaulted structures is analyzed through a network of thrusts, representing compressive forces balanced with the applied loads. A thrust network is representative of the thrust forces that equilibrate the external loadings. (Marmo & Rosati, 2017) reformulated the original version of TNA originally developed by Block, added horizontal forces and boundary conditions thereby significantly enhancing the computational performances. The thrust network as shown in figure 22 can be described by nodes- N_n and branches N_b , where $N_n = N_i + N_e + N_r$. N_i , N_e , N_r are the internal, edge, and external (restrained) nodes. The generic branch is identified by two end nodes and corresponding thrust force: $t^{(b)} = (t_x^{(b)}, t_y^{(b)}, t_z^{(b)})$.

Nodes are loaded with an external force $f^{(n)} = (f_x^{(n)}, f_y^{(n)}, f_z^{(n)})$.

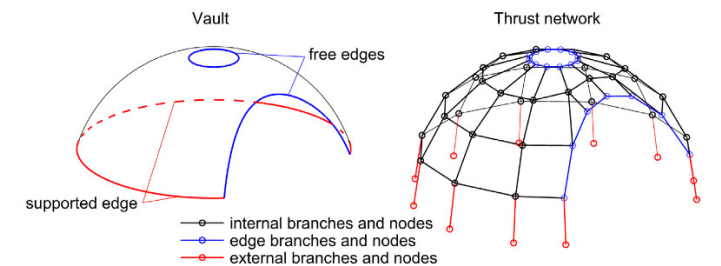


Figure 23: Representation of the thrust network. (Source: Marmo & Rosati, 2017)

$f_y^{(n)}, f_z^{(n)}$ and equilibrium conditions are employed to evaluate position of all nodes and branch thrusts.

Force components $f_x^{(n)}, f_y^{(n)}$ and thrust forces relative to branch b , $t_x^{(b)}, t_y^{(b)}$ enter the horizontal equilibrium conditions, and their z-components constitute vertical equilibrium. To do so, the network is projected onto a 2D surface using graphic statics as shown in figure 5.4. The evaluation of the nodes and branches have not been presented here, and can be reviewed at (Block, 2009) and (Marmo & Rosati, 2017).

RhinoVAULT, a plugin for Rhino developed in 2015 by Matthias Rippmann uses TNA approach to explore compression-only structures by using reciprocal diagrams to solve horizontal and vertical equilibrium conditions of a network of nodes and branches. It has been used in designing structures such as the Armadillo vault. There were further versions -2 and 3 of the RhinoVAULT plugin but is currently unavailable.

5.1.5 Membrane Equilibrium Analysis (MEA)

Membrane Equilibrium Analysis(MEA) is developed by Carlo Oliveri, 2021 that uses a thrust-membrane derived from thrust-line solution from Heymanns Model as shown in figure 25, and uses a continuum approach to solve the equilibrium using *Airy Stress Function*- definition of a function and solving a single biharmonic equation instead of multiple equilibrium equations.

Carlo Oliveri, 2021 developed FORMERLY-Math a constrained Form- Finding through MEA in Mathematica openly available at https://github.com/colivieri89/FORMERLY-Math/blob/main/FORMERLY-Math_Documentation.pdf

The tool using FEM, it takes into account the thickness of shell and non uniform loading and therefore is more suitable for optimization volume of the shell as

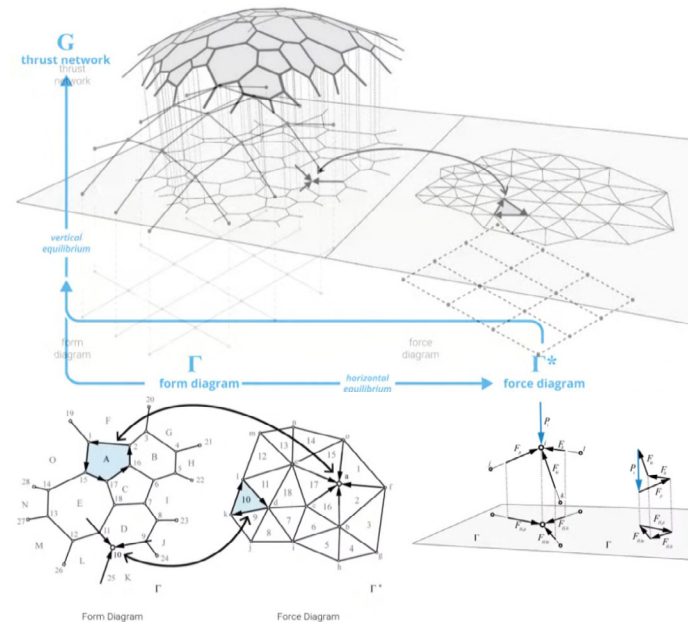


Figure 24: Representation of the thrust network. (Source: *)

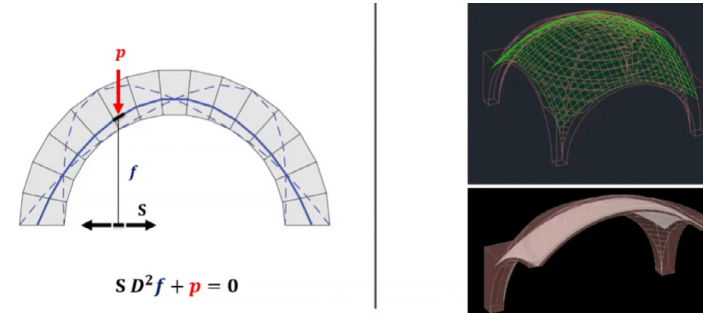


Figure 25: 2D Thrust line to 3D Membrane (Source: **)

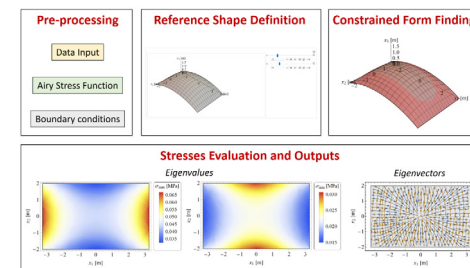


Figure 26: FORMERLY-Math (Source: **)

(Source: *Philippe Block-Reimagining Shell Structures <https://www.youtube.com/watch?v=vAavRx7uoeA&t=2174s>)

**Carlo Olivieri - Airy Stress-based Approach for Assessment and Design of Compressed Shells <https://www.youtube.com/watch?v=tU7uLn36mRg&t=1474s>

opposed to TNA that is only a representative of thrust forces that equilibrate external loadings.

5.1.6 Applying Airy stress function to NURBS patches

Computing Airy Stress Function is proven to be an effective solution to solve equilibrium- and thus help design parametric- self-supporting surfaces (Miki et al., 2015a). Miki et al. (2015b) presented a new computational tool 'Mothra' for computing compression-only shell applying Airy Stress Functions to NURBS patches in Rhino+grasshopper (Figure 27).

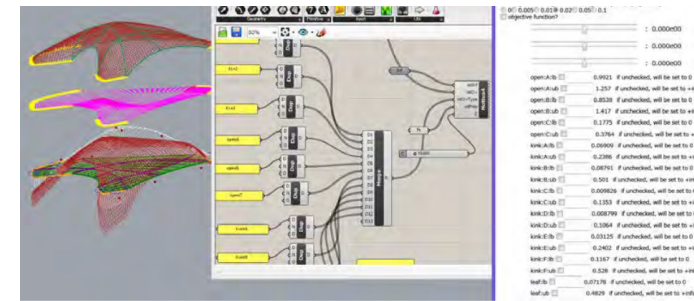


Figure 27: Mothra plugin (Source: Miki et al., 2015b)

Mothra uses NURBS surface patches in grasshopper as an input, computes an airys stress function and then computes the equilibrated structure based on certain user inputs of boundary conditions as shown in figure 27. This tool was used to generate the custom tool to create the Robotic glass vault's compression only shell.

Mothra (although a decade old) is open source and is available at <https://github.com/mikity-mikity/Mothra5>, however, due to dependencies on a discontinued Microsoft environment, cannot be further used.

Key take-aways

Following are key takeaways from compression-only shell theories and tools-

-Graphic statics- developed centuries ago has been adapted into different conditions to design shell structures. It helps make computational tools more effective with graphical representations.

-Dynamic relaxation can help achieve equilibrium and therefore kangaroo solvers can be used for form explorations. However, they would (might) not generate compression only structures.

-Both MEA and TNA draw from the Heyman's model for discretization

-Thrust Network analysis using RhinoVAULT is one of the promising tool to be used initially, also used to design discrete dry assembled shells like the Armadillo vault. However, it does not consider material and volume.

-FORMERLY-Math is also considered as it the latest research that overcomes the material and thickness applicability. However, upon using it is inferred that there are input shape constraints and might need modification.

-Mothra plug-in for grasshopper is considered to be most promising as it follows a grasshopper interface which would fit well for the parametric process. However, upon trying, mothra has dependencies on Sho .NET Microsoft environment which has been discontinued.

-Karamba3D and Kiwi3D are other optimization tools also considered for analysis and validation of form-founded shells.

5.2 Case study 2- The Armadillo vault

Owing to its discrete- dry assembly, and a prime example of Form finding using TNA (Block et al., 2015) in RhinoVAULT, the Armadillo Vault (2016) by the Block Research group, ETH Zurich has been chosen as a case study. This is to mainly understand the form finding and tessellation process.

5.2.1 Introduction

The Armadillo Vault is an unreinforced, freeform vault made using 399 discrete interlocking limestone blocks with thickness ranging from 5-12cm.

Total area : 75m²
Span : >15m
Weight: 23.7 tons

The triangular stone vault, located in the exhibition space, spans the central walkway and wraps around existing columns, which penetrate its surface through large openings. Supported by 20 mm steel plates, the structure's weight is evenly distributed, while steel ties absorb horizontal thrust, as no floor connections were permitted. The vault's voussoir geometry results from tessellation patterns defining stone rows. Figure 28 outlines the design, fabrication, and assembly process. The process follows the following outlined steps:

- Design of a Thrust surface through a form-finding process (RhinoVAULT).
- This surface is taken as the middle surface of the cross-section of the vault and offsetted for a thickness.
- Tessellation pattern developed using an elaborate method described here.
- Discretized into voussoirs following a tessellation pattern taking into account the fabrication and assembly requirements
- Stability verified with discrete element modelling (Rippmann, Matthias et al., 2016)

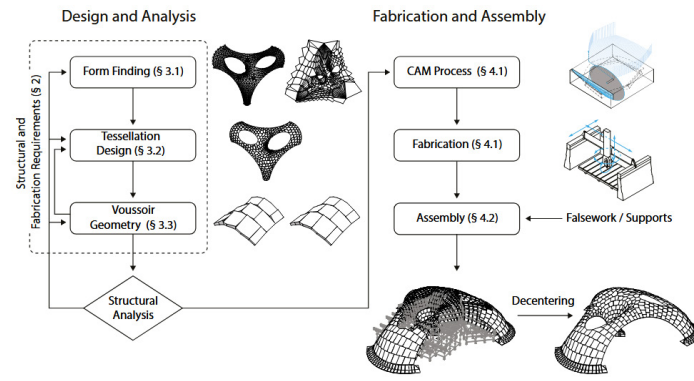


Figure 28: Flowchart for constructing Armadillo vault (Source: Rippmann, Matthias et al., 2016)

5.2.2 Design Goals

- Mortar-less construction- interlocking design with a high degree of precision.
- Compression only funicular design
- Fabrication limitations for the limestone

5.2.3 Form Study

The form finding is through TNA described earlier. (Rippmann, Matthias et al., 2016)

- Design alternatives created using RhinoVAULT plugin
- Obtained mesh was refined for functional and aesthetic considerations.
- Obtained mesh used as 'target' for a 'best-fit' procedure. Its an iterative procedure defined at Van Mele et al. 2014.

An initial pair of reciprocal diagrams generated and rescaled to align the thrust network with the target. Through iterative optimization, thrust forces are redistributed, and force densities are refined while maintaining parallelism between form and force diagrams until achieving an optimal solution

- Corresponding thickness computed based on experience, aesthetic considerations and common

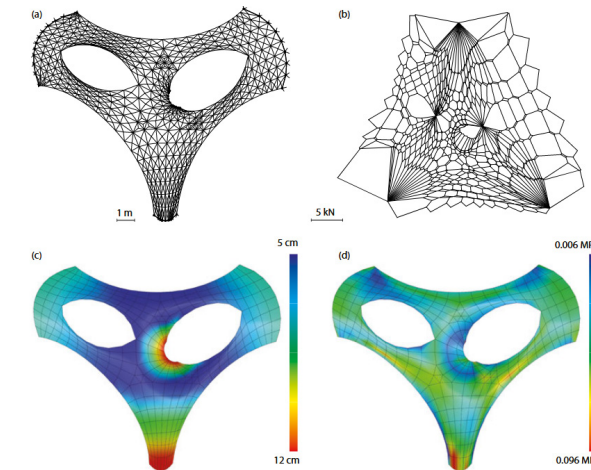


Figure 29: a. form diagram b. force diagram c. thickness distribution d. resulting stress due to force and thickness (Source: Rippmann, Matthias et al., 2016)

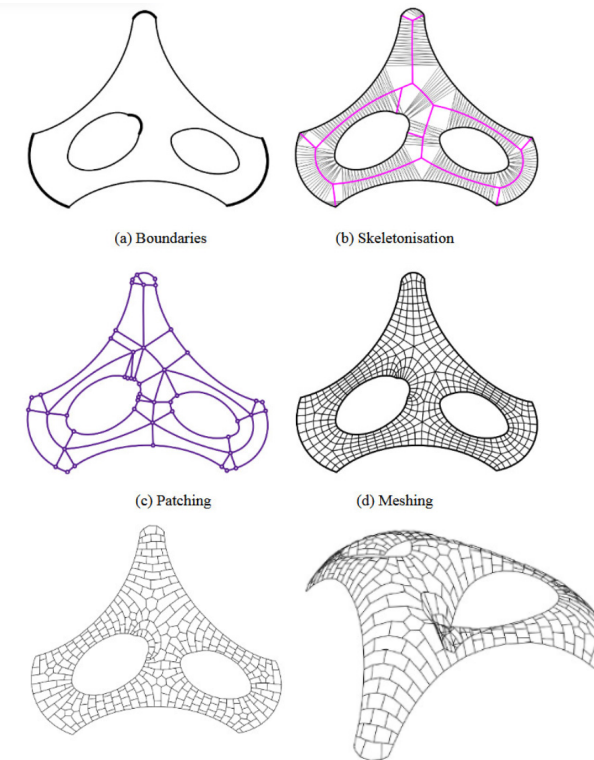


Figure 30: Tessellation design overview (Source: Oval et al., 2017)

sense- varies from 12cm-5cm on top.

5.2.4 Tessellation and unit geometry

As summarized by Oval et al.(2017) and Rippmann & Block (2018), the tessellation of the vault can be strategized into five steps as shown in figure 30. The tessellation pattern is created from meshing using certain strategies that align with production limitations. It is a manual process as described by Rippmann & Block(2018) and is further discussed in section 5.4 of the Report.

Key take-aways

Following are key takeaways from Armadillo Vault-

- The structure has been designed for disassembly, but it does require a network of scaffolding for construction.
- RhinoVAULT is used only for initial form finding of thrust surface. The form and force diagrams are then modified using an iterative process stated in Van Mele et al. 2014.

-Thickness is not optimized computationally as TNA does not take into account the volume of the structure as discussed earlier. Rather thicknesses are applied as per experience, aesthetics and common sense.

-Tessellation is formed by a segmenting procedure to create controlled patterns- this will be later discussed in section 5.4.

5.3 Overview of tools to design a concave pure-compressive shell

This Section gives an overview of workflow of the different tools being explored to form-find our desired shape in mind for a doubly curved vault shape. The applicability of these tools are mentioned earlier in the report.

5.3.1 Comparison of currently available tools

i. Rhino gh + Kangaroo3D

Kangaroo uses Dynamic relaxation with principles of FDM to arrive at a relaxed solution which can be assumed to be in equilibrium under the application of the specified forces only.

STEP1: Input topology.

STEP2: Define supports-anchors and edges

STEP3: Define elasticity factor and forces

STEP4: Relax mesh in 3D

Analyze mesh using karamba.

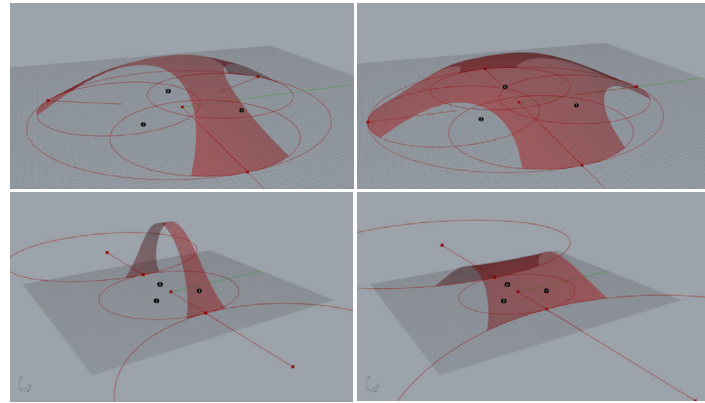


Figure 31: Parametric form exploration using Karamba (Source: Own)

We use Kangaroo only for initial form exploration. If this method is chosen as primary- then it will have to be coupled with evolutionary solvers maybe coupled with Karamba to allow only compression only stresses in the geometry.

ii. Rhino + RhinoVAULT v1

RhinoVAULT uses defined form and force diagrams projected on a flat surface.

STEP1: Input Topology- can be 2D patch or a Rhinomesh.

STEP2: Create relaxed projected pattern

STEP3: Create force diagram from the form diagram

STEP4: Horizontal equilibrium with angle deviations < 5

STEP5: Vertical equilibrium with height constraint.

These are further elaborated in the next sections since this tool has been considered for the design.

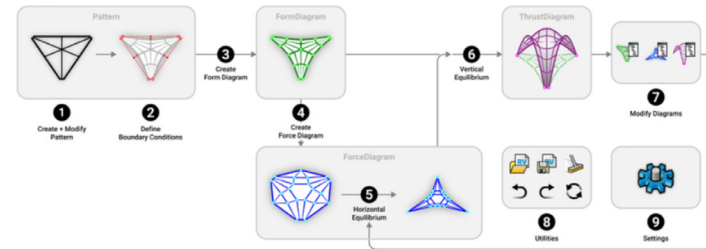


Figure 32: RhinoVault Workflow (Source: Food4Rhino.com)

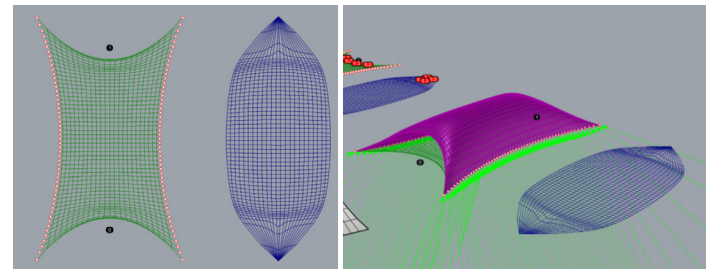


Figure 33: RhinoVault exploration (Source: Own)

As shown in figure 33, the equilibrated form tends to always be convex- it is a prime consideration for Thrust network analysis.

In case this method is chosen, further modifications in the force diagram need to be done and iterative methods mentioned in Van Mele et al., 2014 will have to be utilized.

iii. FORMERLY-Math - A mathematica tool

Formerly-Math by Carlo Oliveri as stated earlier has been explored. It generates promising solution based on given shell material properties- and also calculates a force distribution as shown in figure 34.

```
in[52]:= R = ImplicitRegion[-1/2 <= x1 <= 1/2 && -b/2 <= x2 <= b/2, {{x1, -1/2, 1/2}, {x2, -b/2, b/2}}];
Ω = DiscretizeRegion[R, "MeshOrder" -> 2, MaxCellMeasure -> size];
CentroidMeshPoints = AnnotationValue[{Ω, 2}, MeshCellCentroid];
Show[Ω]
```

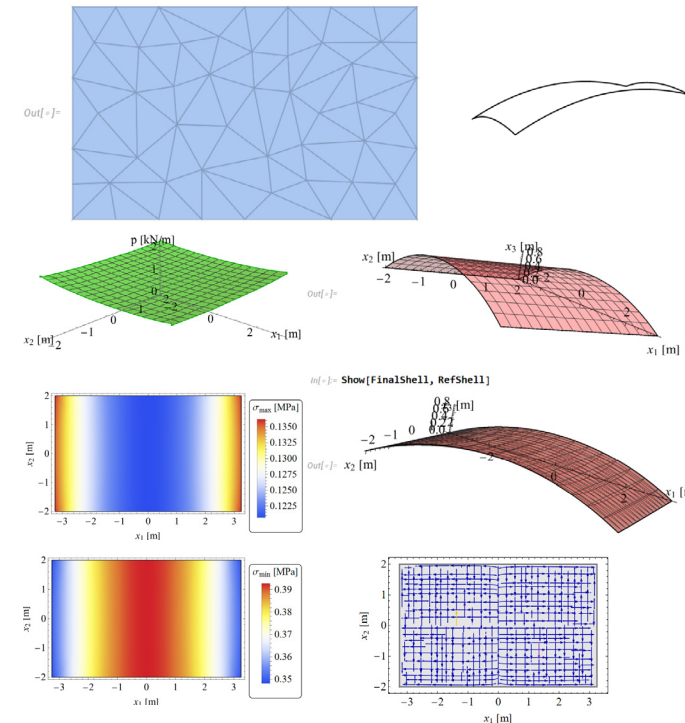


Figure 34: Formerly-Mathematica. An Attempt to create a concave rectangular shell using a quartic Airy Stress function (Source: Own)

This method can be promising as inferred to earlier. If this method is chosen then the tool has to be modified to accept other boundary conditions than a rectangle.

iv. Rhino gh + Mothra

Mothra- the grasshopper plugin also used for designing the Robotic glass vault as mentioned earlier is also attempted, with provided example files- however, the plugin has dependencies on SHO a .NET Microsoft environment which has been discontinued.

If this plugin is still chosen, it has to be recreated by changing dependencies using their Github repository.

v. Rhino gh + Kiwi!3D

Kiwi!3D is yet another grasshopper plugin based on Isogeometric Analysis (IGA) to directly integrate structural analysis into CAD. It uses B-Splines- NURBS instead of discrete meshes unlike Karamba, therefore can be more accurate. This method has not been explored in this thesis.

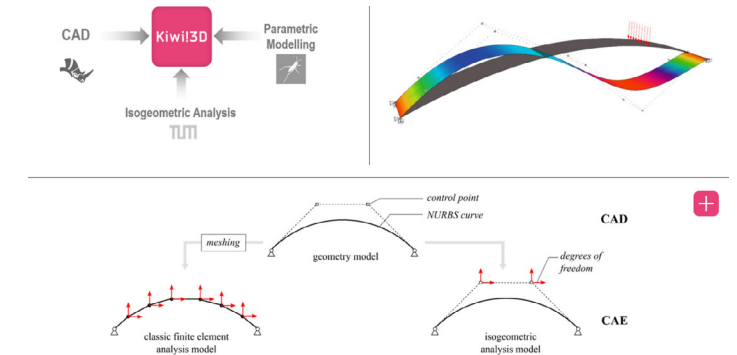


Figure 35: (Source: <https://www.kiwi3d.com/>)

5.3.2 Designing the compression-only shell

Initial explorations were done using kangaroo plug in grasshopper with the idea of tension compression analogy. However, it resulted in mixed-tension compression shells as demonstrated in Appendix 1 of the report. It was also observed that the free edges play a crucial role in determining the vaults compression-only state.

The intention was to design a symmetric version of the glass vault (Beghini et al., 2020) as shown in figure 36. The researchers have not demonstrated the creation of the shape or its verification as a compression only shell. Based on the analysis done using karamba and form exploration, it is assumed that the glass vault designed as a mixed compression-tension shell and it takes tension within the limits as glass units are bonded to each other with spacers.

The tools mentioned in the previous sections were explored, and Rhino Vault 1 was found to be the only applicable(working) tool to create a compression only shape by mere inputs of a 2D form diagram.

RhinoVAULT 1

RhinoVAULT is a plugin for Rhinoceros 3D based on Thrust Network Analysis (TNA). It helps design funicular (compression-only) structures like masonry vaults or fabric forms by aligning the geometry with the flow of forces.

Draw the form diagram - Create a 2D network outlining the desired boundary and connectivity of the structure.

Generate the force diagram - RhinoVAULT builds a reciprocal diagram representing internal force directions and magnitudes.

Adjust force densities - Modify edge lengths in the force

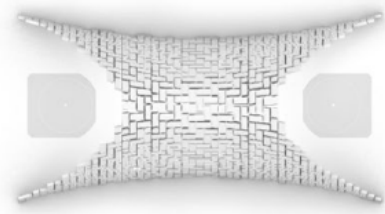


Figure 36: Intended design of glass vault (Source: Beghini et al., 2020)

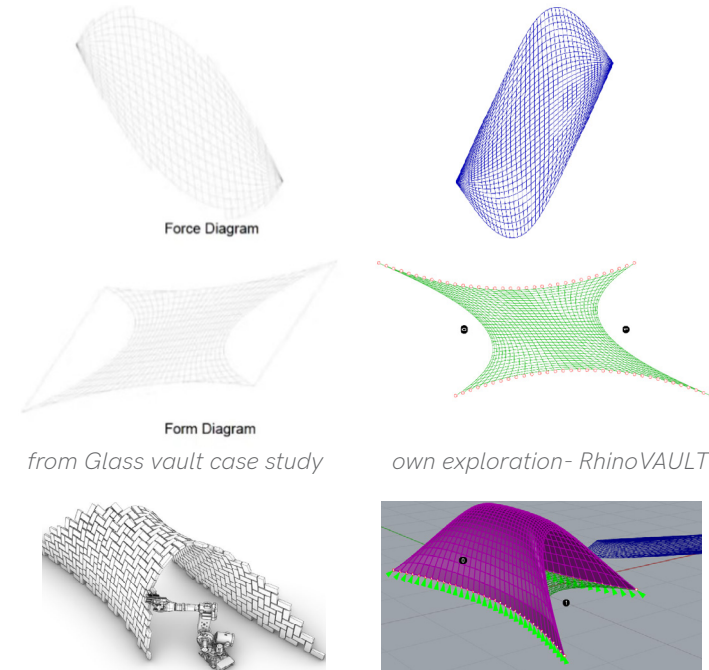


Figure 37: Glass vault using RhinoVAULT (Source: Beghini et al., 2020 ; Own)

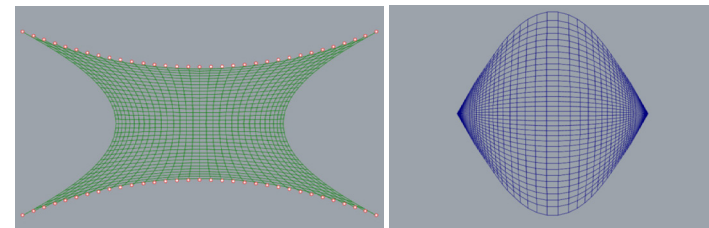


Figure 38: Final compression-only shell force and form diagram (Source: Own)

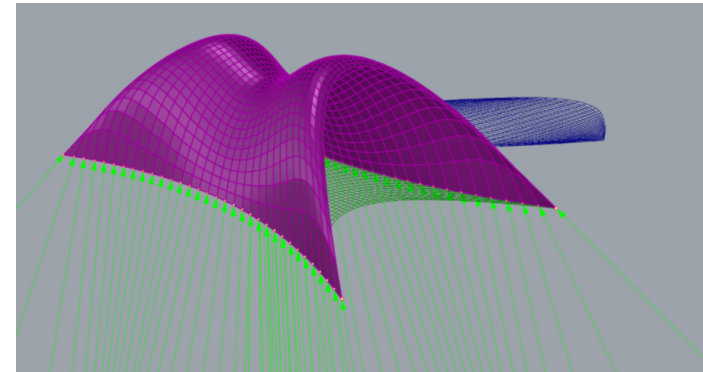


Figure 39: Final compression-only shell (Source: Own)

diagram to control how forces flow through the structure.

Lift to 3D form - The software uses TNA to raise the form diagram into a 3D shape in vertical equilibrium.

Refine the geometry - Tweak positions, weights, and constraints to optimize the structure's shape and force distribution.

Export the final funicular form - The result is a compression-only surface ready for analysis, visualization, or fabrication.

Figure 37 shows the form founded shape using RhinoVAULT when a form diagram of the glass vault design was used. The equilibrated shell did have similar force diagram, but the vertical equilibrium resulted in a shape as seen in the figure.

Figure 38, and 39 shows the symmetric compression only form considered for showcasing a dry assembly.

The idea was to avoid curvature in all directions as we have constraints for 3DP glass that adds more restrictions to the tessellation process making it not feasible. The compression only form is thereby chosen so as to keep the dry assembled block at an equilibrium without necessitating additional supports.

Final Vault Design: (Figure 39)

Span= 2.6m(max) ; Height= 1.8m(min)

Thickness of the vault is decided as per tessellations in the part C of the report so as to keep the equilibrated thrust network within the shell thickness.

The resulting design does not seem to be promising for application, and further exploration is not done in this direction since it is out of scope for the thesis.

Key take-aways

-Multiple tools were explored for form-finding compression-only shells, each with different methods and applicability based on constraints.

-Kangaroo3D (with Grasshopper) uses dynamic relaxation for free-form shape exploration but results in mixed tension-compression shells unless coupled with advanced optimization.

-RhinoVAULT1, based on Thrust Network Analysis (TNA), was found to be the most applicable tool for designing compression-only forms with simple 2D input diagrams.

-Formerly-Math showed promising results by calculating forms based on material properties but lacks flexibility in boundary conditions.

-Mothra and Kiwi!3D have potential but face limitations: Mothra requires redevelopment due to outdated dependencies, while Kiwi!3D was not explored further in the thesis.

-The final vault design- thrust network for a symmetric dry-assembled compression-only glass vault- was achieved using RhinoVAULT, but was not pursued for application due to design constraints and scope limits.

5.4 Tessellation and Brick geometry

This Section presents a review of literature studied for tessellation of masonry shell structures and relevant interlocking brick geometries inferred from existing Cast glass dry assemblies.

5.4.1 Tessellation Patterns

Oval et al. (2017) summarized a method to create discrete compression only masonry structure. The best way to do is by using a 'feature preserving' and structured quad mesh. (Figure 40, 41, 42). Rippmann et al. (2018) further established rules for tessellating geometries considering their structural integrity (Figure 5.16). Some of the key considerations for tessellations are-

- The intersections should be as perpendicular as possible to the direction of force flow
- Joints should not align between courses-a staggered pattern can be developed by removing every second edge (Figure 40)
- Singularities- where multiple (more than 3) blocks meet should be avoided (Figure 40)

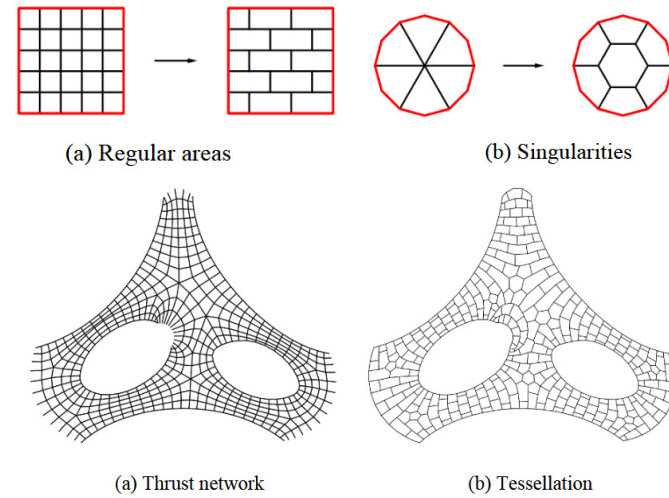


Figure 40: Transformation rules of regular areas and solving singularities of mesh into tessellation described with an example of Armadillo vault (Source: Oval et al., 2017)

It is also to keep in mind that with tessellating free form geometries, Wang et al. inferred that topological interlocking assemblies generally end up with many unique blocks. (Figure 44)

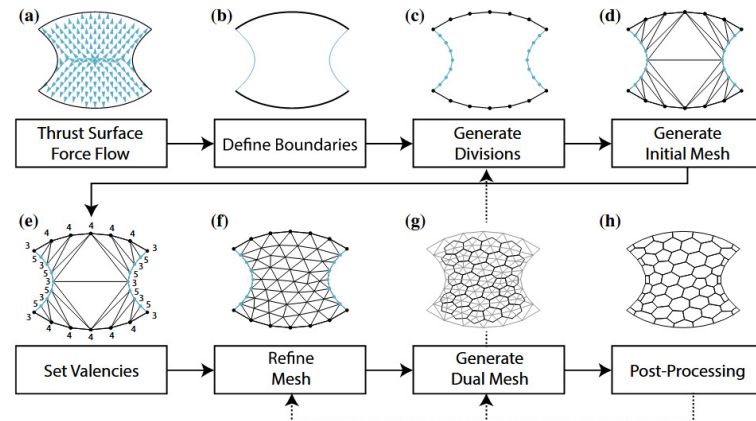


Figure 41: Flow Diagram showing sequential steps of the developed tessellation algorithm by Rippmann et al. (Source: Rippmann et al., 2018)

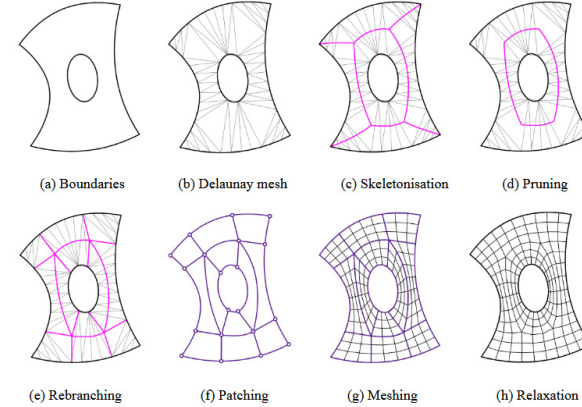


Figure 42: Generating a smooth quad mesh by (Oval et al., 2017)

5.4.2 Cast glass Dry Assemblies

With references from (Aurik 2017; Aurik et al. 2018; Snijder et al. 2016) a dry-assembled arched glass masonry bridge and an interlocking cast glass column (Akerboom 2016), Oikonomopoulou et al. (2018) developed promising interlock geometries for application of cast glass assemblies (Figure 43). Design criteria followed interlocking requirements and criteria imposed by glass as a building material by casting.

- Limited volume. 10kg mass limitation
- Rounded shape and equal mass distribution - equal cross sectional area
- Limited number of units- lesser moulds

The authors consider osteomorphic blocks (types A and B as shown in figure 43) the most promising for further development due to their multifunctionality, ease of assembly, and ability to reduce peak stress during casting and loading. The smooth concave-convex interlocking mechanism of the elements ensures its high shear capacity, however an interlayer is necessary to avoid glass-to-glass contact.

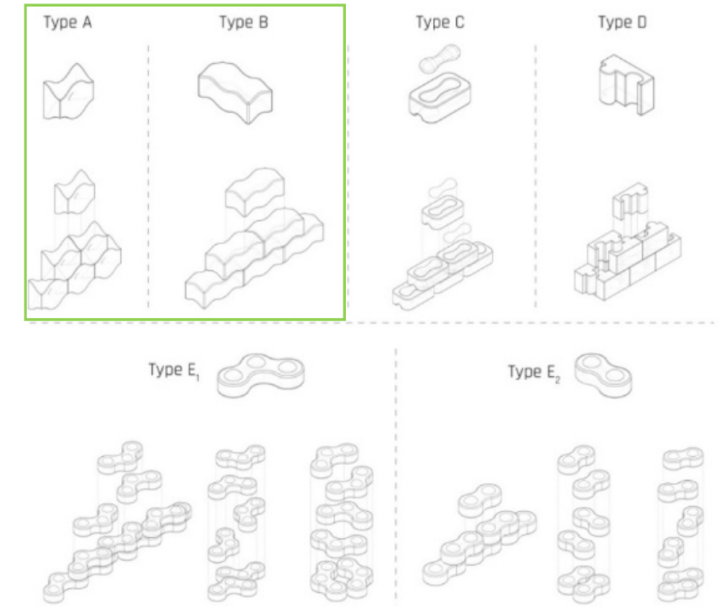
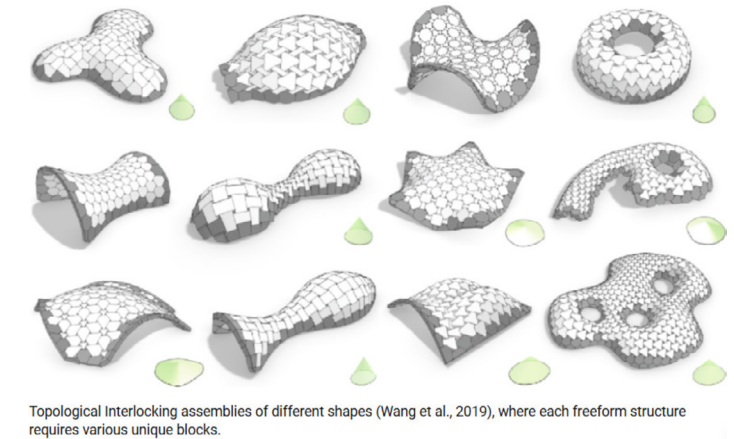


Figure 43: Developed interlocking designs. Type A, B - Osteomorphic Bricks defined by Dyskin et al. 2003 (Source: Oikonomopoulou et al., 2018)



Topological interlocking assemblies of different shapes (Wang et al., 2019), where each freeform structure requires various unique blocks.

Figure 44: Topologies Interlocking assemblies (Source: Wang et al., 2019)

5.4.3 Osteomorphic Brick geometry

The osteomorphic geometry as proposed in Dyskin et. al, 2003 derives its shape from a Cosine/Sine trigonometric identity. General Sine/cosine function:

$y(x) = A \sin\left(\frac{2\pi}{\lambda} x\right)$

Where A=Amplitude, λ=Wavelength. The amplitude of the brick A is ideally 0.5h as to create a symmetric curvature of the block. However, the amplitude of the full sine/cosine curve does not need to match the amplitude of the half curve on the 'h' side of the block as shown in the figure 46.

The proportions of the block can be varied within manufacturing constraints of 3DP glass. The main consideration is the maximum amplitude(A) of the brick 3D printable. The maximum A will vary based on the wavelength λ, therefor the length of the brick is set to be constant = 300mm in order to find the maximum amplitude printable.

Maximum overhang angle: θ=60° from base

Slope of sine curve:

$\frac{dy}{dx} = A \cdot \frac{2\pi}{\lambda} \cdot \cos\left(\frac{2\pi}{\lambda} x\right)$

$\left|\frac{dy}{dx}\right|_{\max} = A \cdot \frac{2\pi}{\lambda} \qquad \cos(\cdot) = 1$

For maximum slope 60°,

$\left|\frac{dy}{dx}\right|_{\max} = \tan(60^\circ) = \sqrt{3}$

$A \cdot \frac{2\pi}{\lambda} = \sqrt{3} \Rightarrow A = \frac{\sqrt{3} \cdot \lambda}{2\pi}$

Therefore for length λ=300mm,

$A = \frac{\sqrt{3} \cdot 300}{2\pi} \approx \frac{1.732 \cdot 300}{6.283} \approx \frac{519.6}{6.283} \approx 82.7 \text{ mm}$

Therefore the maximum amplitude for a 3DP glass unit with length 300mm is 82mm. For simplification of further analysis and to utilize maximum sizing limits of 3DP glass units, table 3 shows constraints and variables that are set for an osteomorphic masonry unit.

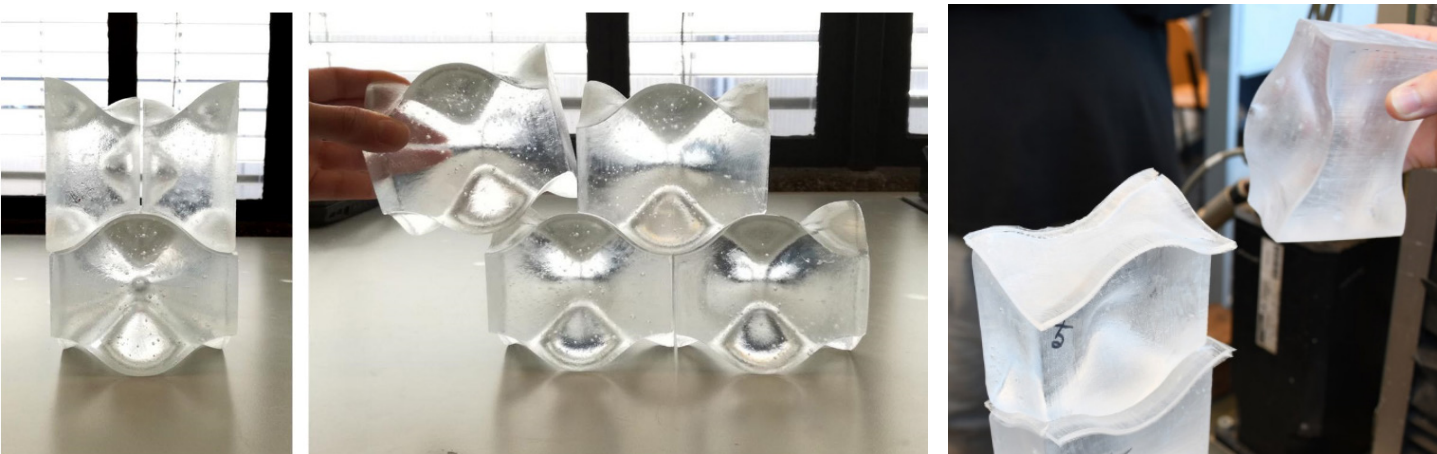


Figure 45: Osteomorphic Interlocking units with Cast glass (Source: Oikonomopoulou et al., 2018)

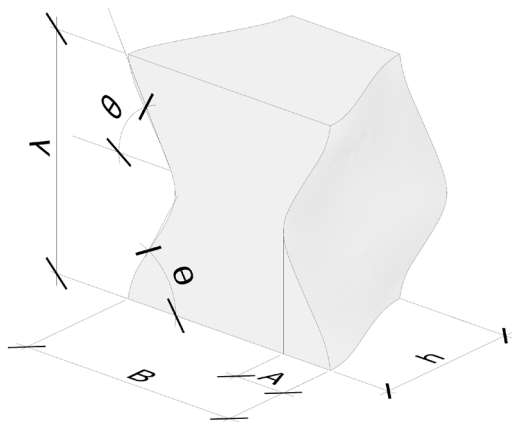


Figure 47a: Osteomorphic Interlocking unit parameters (Source: Own)

Constants			Variable
3DP Osteomorphic glass unit	Length (L)	300mm	Amplitude 0-82mm
		constant per design	To be optimized based on design
	Width (B)	~200mm	Thickness (h)

Table 3: Osteomorphic Interlocking unit parameters considered (Source: Own)

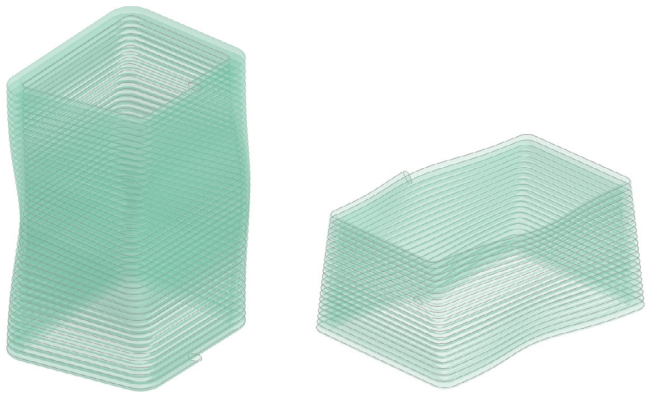


Figure 47b: Possible Orientations for 3DP an osteomorphic geometry with glass (Source: Own)

Key take-aways

The rules for tessellations provided by Oval et al. (2017) have been considered to create effective tessellations. The main criteria is that the seams should not be parallel to the direction of force flow. Ideally, they should be perpendicular.

It has also been inferred from (Wang et al.,2019) tessellation of free-form structures creates various unique blocks. (Figure 5.20) Therefore a standardizing procedure has to follow.

From cast glass assemblies, we infer that osteomorphic geometries are the best performing for masonry applications- brick amplitude and height are crucial geometry aspects. For ease of further optimization, the length of the brick is set to be constant, and the maximum amplitude calculated based on glass 3DP overhang constraint is 82mm. The thickness (h) is a parameter to be optimized as per design.

5.5 Optimization Approaches

Here we overview various methods for an efficient form and tessellation of the geometry that have been implemented in this thesis

5.5.1 Form optimization

We initially aimed to optimize the form using Airy Stress Function, and/or minimizing stresses using parametric modelling and Karamba analysis. The main parameters to be looked at were the vault sizes and the thickness of the vault.

The overall vault sizes are decided to be constant in case of catenary vault, and a the form founded compression only shell was set as the constant size for the assembly process and are discussed later in chapter 8 of the report. The only parameter affecting the overall sizing that is kept to be parametric is the thickness of the vault- *it is assumed that the thickness will largely affect the structural performance as well as the stiffness of the interlayer required for the dry assembly system. The design parameters are further explained in Part C of the report.*

5.5.2 Standardization

One of the main advantages of using 3D printing is the ability to produce customizable geometry without extra material waste, but it is not practical to create entirely unique masonry units for construction. Having all unique units would significantly complicate the assembly process, making it highly time-consuming and inefficient.

To address this challenge, we aimed to minimize the number of unit typologies while preserving the structural and architectural intent of the design. In section 8.1, we present a standardization method for the units used to assemble a catenary or a single curved

vault where 50% of the units can be used to assemble any other straight wall or a vault of another size. It was inferred that standardization for a doubly curved geometry designed was not possible as explored with tessellations and given the manufacturing limits, they are further discussed in chapter 8. We proposed a tessellation method derived from the Armadillo vault by Block Research group as overviewed in chapter 5.4, resulting in unique units for the doubly curved compression only shell designed. *There is further research and experimentation required to find a way to standardize units for a doubly curved geometry.*

5.5.3 Material Optimization

Even though its crucial for structure's self weight, and cost, the optimization of geometry for material efficiency with 3DP is considered out of scope for this thesis. This study focuses on optimization of overall geometry parameters which affect the structural performance. It focuses on material optimization of the interlayer in terms of its Young's modulus, in order to engineer the interlayer to meet the required properties.

5.6 Chapter Conclusions

Based on the study of compression only shell structure design, RhinoVAULT emerges as a promising tool for initial form-finding, as seen in projects like the Armadillo Vault, though it lacks considerations for material and volume. Newer advancements, such as FORMERLY-Math, address material applicability but face input shape constraints. Among parametric tools, Mothra shows potential but is hindered by outdated dependencies. Karamba3D and Kiwi3D remain valuable for optimization and validation.

For the Armadillo Vault, scaffolding requirements and the non-computational optimization of thickness reveal areas for further improvement. Tessellation strategies, as discussed by Oval et al. (2017) and Wang et al. (2019), underscore the need for standardized procedures to balance unique geometries and assembly efficiency. This is eventually where we decided to use a more symmetric and one-way spanning vault rather than a complex multi supported shell like the Armadillo. Therefore we plan to replicate the symetric initial form of Robotic glass vault as dicussed in section 2.

Finally, the potential of osteomorphic geometries in cast glass assemblies demonstrates their superiority in masonry applications, emphasizing the importance of controlling brick amplitude and height for optimal performance. Moving forward, the challenge remains to define initial geometries effectively and create efficient tessellations for concave, compression-only shells. Adding to that, the 3DP blocks would be hollow sections and therefor need a bracing design as mentioned earlier in section 3.

6.0 | The Interlayer

6.1 Interlayer properties for Selection

Based on (Oikonomopoulou, 2019), the selection of bonding media for cast glass assemblies revolves around the following key characteristics:

- i. Visual Performance- transparency
- ii. Structural performance- Bond (shear) strength, Resistance to creep, Elongation to failure, Service temperature suitability
- iii. Ease of Assembly (Constructability): Gap-filling capability to ensure proper alignment and bonding during assembly
- iv. Budget Constraints: Post-processing requirements for glass components, influencing production costs and time.
- v. Additional Considerations like UV resistance, aging, and weathering durability, Toxicity and emission safety, Processing properties (e.g., viscosity, curing conditions, surface preparation) and Low shrinkage during curing

To achieve our design goal, the interlayer criteria is inferred from the review of Robotic vault's interlayer by (Oikonomopoulou & Bristogianni, 2022) and are mentioned in section 2.5. An illustration of the R&D Method for selection of interlayer system for the Robotic glass vault is depicted in figure 48. We can see how the brick geometry and the adhesive selection both depend on the Key performance criteria. *Therefore we need to define the performance criteria along with the final design of the vault.*

6.2 Cast glass assemblies- Review of adhesive based Interlayer systems

Adhesive interlayers for cast glass assemblies are

categorized into three:

- (i) flexible, soft-elastic adhesives, which include silicones, polyurethanes and MS polymers
- (ii) stiff adhesives, which include epoxies and acrylates
- (iii) cement-based mortars and tile adhesives, typically employed in hollow glass brick structures

Table 4 provides a curated comparison of adhesive properties as curated from (Oikonomopoulou & Bristogianni, 2022). *In all the applications discussed in the paper, a significant concern was the high degree of precision required and the necessity for post-processing glass bricks, both of which are less desirable. Additionally, the creep resistance of the interlayer emerged as a critical property for the interlayer system.*

6.3 Interlayers for Cast glass- Dry Assemblies

Dry-stacked glass under axial load is unlikely to fail due to its high compressive strength. However, because glass cannot undergo plastic deformation, any **surface irregularities or imperfections at the contact points can lead to localized tensile stress concentrations.**, thereby necessitating an interlayer (Oikonomopoulou et al., 2018). Some key considerations noted from the research are:

- i. The stiffness of the interlayer need to be within a certain stiffness as to not decrease the stability of the overall structure- ideally only a little lower than glass.
- ii. It should have good short and long term compressive behavior and resistance against creep.
- iii. Accommodate dimensional discrepancies and yet be consistent in thickness-at least 2-3mm
- iv. Time-dependency response and resistance to creep
- v. A maximum service temperature of 50 °C

vi. Flexible for forming into osteomorphic surface.

The paper presents several designs and interlocking mechanisms, as reviewed in section 5.4.2. Using vertically stacked osteomorphic cast glass bricks, the research evaluated two different interlayer materials(initially concluded from an FEA) : PU70 3mm and Neoprene 5mm and concluded that PU70 rubber is the best fit for the application in terms of its structural

performance and shaping potential.

The key factors contributing were its consistent thickness and flexible as to match the curves of the brick surfaces. The research also proposes a solution to be a composite with a softer external interlayer to accommodate surface deviations and displacements under axial load and a stiff, resistant inner core.

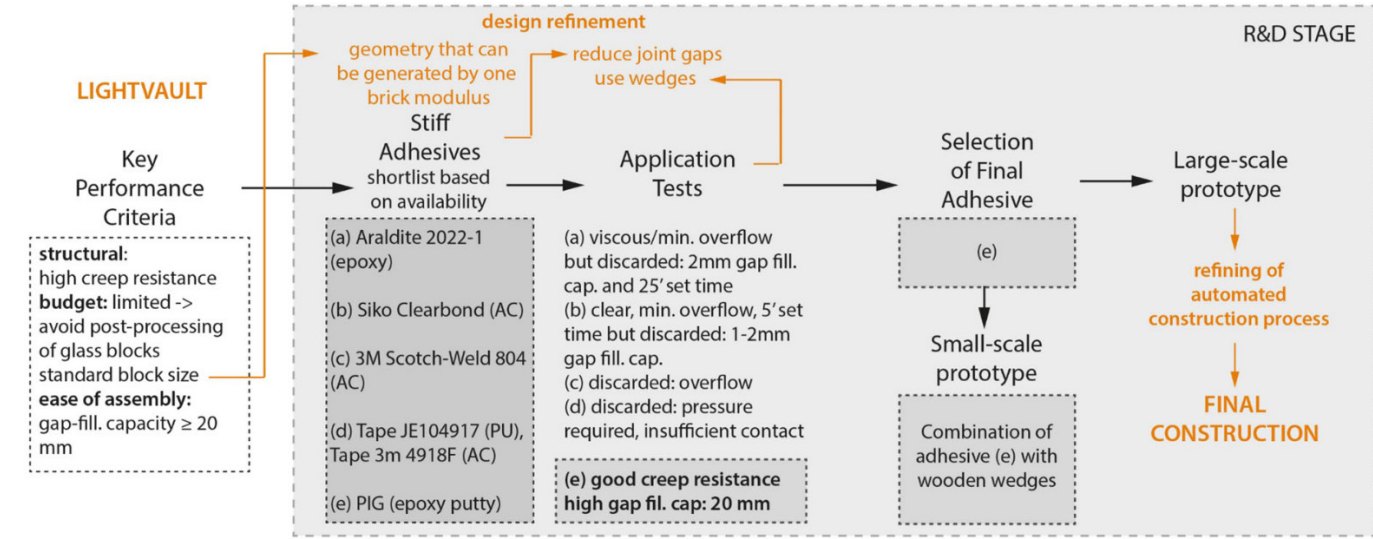


Figure 48: Illustration of the R&D Methodology for interlayer selection for the Robotic glass vault. (Source: Oikonomopoulou & Bristogianni, 2022)

Strength					Ease of Assembly		Visual
Adhesive family	Bond strength	Creep resistance	Service temperature range	Failure mode	Gap-fill capability	Post-processing of cast glass components	Transparency
Stiff (epoxies, acrylates)	High	High	High; yet stress concentrations may occur due to differences in thermal expansion	Rigid joint: brittle, sudden	Low (< 1 mm)	Yes (CNC-polishing)	High
Flexible (PU, MS polymers, silicones)	Low	Low	High	Visible deformation prior to failure	High (1–10 mm)	Not required	Medium/ high
Cement-based mortars & tile adhesives	Low (TS < 1 MPa g)	Satisfactory	Tile adhesives typically used only for interior applications	Visible warning prior to failure	High (3–7 mmg)	Yes (sand-blasting or 3D geometry of connection surfaceh)	Opaque

Table 4: Adhesive interlayer properties (Curated from: Oikonomopoulou & Bristogianni, 2022)

6.4 (Meta)materials- Why Kirigami?

Based on the requirements of unique properties of interlayer as discussed in the previous section, the research is driven towards (meta)materials. There are various similar terms like architected materials, and programmable materials which have an overlapping idea as (meta)materials.

"A metamaterial is a 3D structure with a response or function due to the collective effect of meta-atom elements that is not possible to achieve conventionally with any individual constituent material.

A metasurface is a 2D version of a metamaterial where the structural elements are confined to a 2D plane."
Source: UK Metamaterials Network

In other words, metamaterials are engineered materials designed to exhibit properties that do not naturally occur in their original form. Since these properties are externally induced, in many cases could be programmable.

Kirigami

Kirigami is a traditional Japanese art form of cutting paper that dates at least 15 centuries back. The new cut shape acquires new structural configuration by stretching/compressing. Kirigami also often involves cutting and folding (the art of Origami) that can further enhance the structural configuration. Kirigami is thus a technique that can create metamaterials and meta structures with extraordinary properties like negative Poisson's ratio. (Sun et al., 2021)

Kirigami patterns are generally crated on a 2D surface, thereby enabling one to program the material at any scale. (Sun et al., 2021) This increases the productability as well as transportation. The stiffness and flexibility of kirigami has been widely explored for

different applications such as lightweight structures, and sandwich panels and well as shock absorbing materials (Sun et al., 2021; Parra Rubio et al., 2023; Qi et al., 2024)

Owing to the evidence of its unique configurable properties, its simple manufacturing process and its scalability, Kirigami is chosen as a concept for further research of the novel interlayer solution.

Key take-aways

Following are key takeaways from the initial interlayer study

- *Suitable interlayer should be stiff- ideally little lower than glass so as to withheld the structural integrity*
- *The interlayer good short and long term compressive behavior depending on the structure*
- *A minimum thickness of 2-3mm (for cast glass surfaces). For 3DP glass as inferred from section 3, a bead height min. 3mm would require ~6mm minimum interlayer only to take care of surface variations of 3mm(min) on either side.*
- *Should be flexible as to curve into osteomorphic surfaces*
- *PU rubber could be a promising material for the external layers of a sandwich interlayer so as to take surface geometry tolerances of a 3DP masonry unit.*
- *Transparency might not be a crucial factor for selection of interlayer material in this case.*

We are interested in finding the possibilities of an interlayer solution- even though it is labor intensive.

7.0 | Kirigami inspired Interlayer

7.1 Kirigami- an introduction to types

Kirigami is an ancient Japanese art form that creates metamaterials by simply making cuts on a sheet material. It is often combined with Origami- the art of folding to create 3D geometries. (Sun et al.,2021)

Researchers Sun et al. (2021) classified kirigami into mainly two types- (a)cut-only and (b)cut-and-fold with sub categories as shown in Figure 49. On reviewing these types it was inferred that the for our application Ribbon kirigami and Zig-zag kirigami could be considered for further exploration as they showcase transformability of 2D to 3D structure. The other types are thus not presented further in this report. The cut-and-fold kirigami involves an extra step pf folding and is thereby less preferred even though it can exhibit better stiffness values.

7.1.1 Ribbon Kirigami

The ribbon kirigami pattern, originally used to improve graphene's ductility, undergoes four deformation stages under tension: initial hinge rotation, elastic deformation with stress concentration, yielding due to hinge stress, and eventual tearing.

Studies highlight the influence of geometric parameters, such as slit size and hinge design, on stretchability and buckling resistance. Adjustments like adding grooves or modifying patterns can control deformation modes and enhance programmability. Also known as Tension-Activated Kirigami(TAK), Ribbon kirigami improves elasticity with simple manufacturing, making it versatile for applications in graphene, metallic glasses, shape

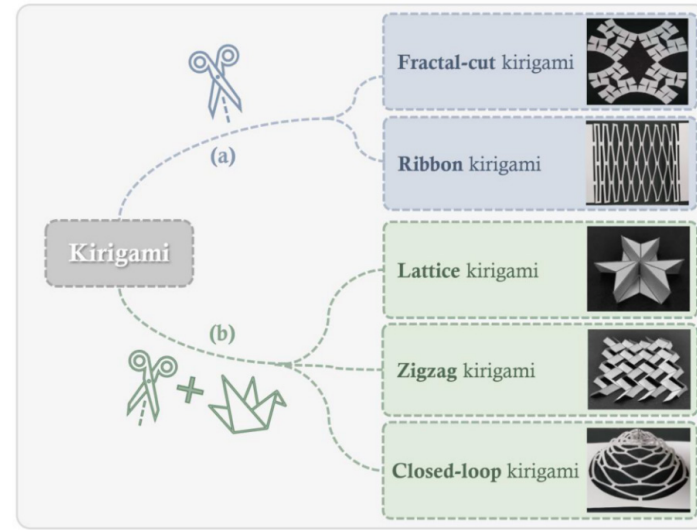


Figure 49: Kirigami types (Source: Sun et al., 2021)

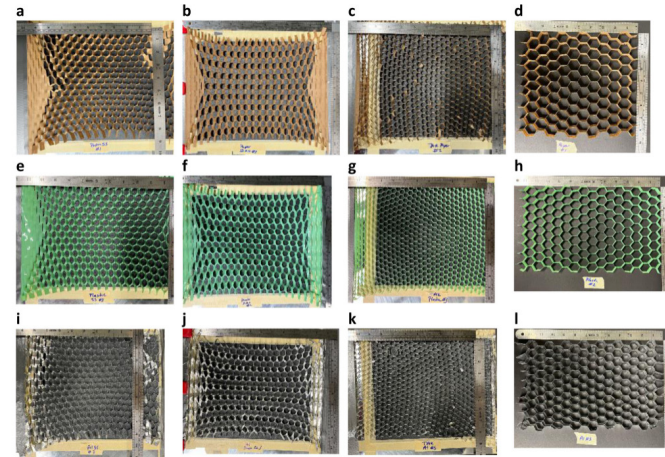


Fig. 4 Samples prepared for compression testing. **a** Single-slit TAK—parallel (paper). **b** Single-slit TAK—alternating (paper). **c** Folding-wall TAK (paper). **d** Constructed honeycomb (paper). **e** Single-slit TAK—parallel (plastic). **f** Single-slit TAK—alternating (plastic). **g** Folding-wall TAK (plastic). **h** Constructed honeycomb (plastic). **i** Single-slit TAK—parallel (aluminum). **j** Single-slit TAK—alternating (aluminum). **k** Folding-wall TAK (aluminum). **l** Constructed honeycomb (aluminum).

Figure 50: Compression testing of Kirigami forms in paper, plastic and aluminum(Source: Corrigan et al., 2023)

memory alloys, and energy/biomedical devices, while offering significant strain capacity and energy efficiency. (Sun et al.,2021; Corrigan et al., 2023)

Corrigan et al.(2023)'s research assesses the stiffness of ribbon kirigami types and creates a TAK novel hexagon pattern that was found to be 84% of the specific strength of a full honeycomb construction which is more production-intensive. (Figure 50) Another finding of the research was the lockability of the deformed state- it was found that multi layered TAK interlocked themselves thereby maintaining their deformed state.

7.1.2 Zig-zag Kirigami

The zigzag kirigami pattern, inspired by the Miura-ori (a notable Origami pattern), features the unique property of negative Poisson's ratio and rigid folding. Miura origami, due to its stiffness has already been explored in creating lightweight and stiff sandwich panels as seen in Wang et al. (2023). Further configurability of the zig zag kirigami in discussed in the next section.

7.2 Design of a Kirigami structure

In this section we discuss the configurability of the ribbon and zig-zag Kirigami as inferred from (Sun et al.,2021; Corrigan et al., 2023).

7.2.1 Ribbon Kirigami Design

Ribbon Kirigami mainly consists of single slits - parallel or alternating TAK as shown in Figure 51. Corrigan et al., (2023) demonstrated that materials arranged in an alternating configuration exhibit lower initial stiffness but demonstrate notably higher stiffness and strength after undergoing significant strain, compared to those

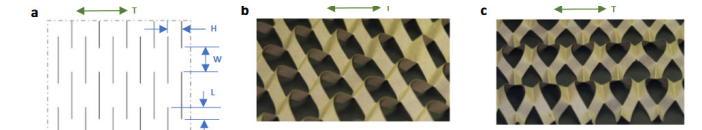


Fig. 1 Single-slit tension activated kirigami. **a** Schematic of the single-slit TAK pattern. **b** Deployed single-slit TAK in parallel configuration. **c** Deployed single-slit TAK in alternating configuration.

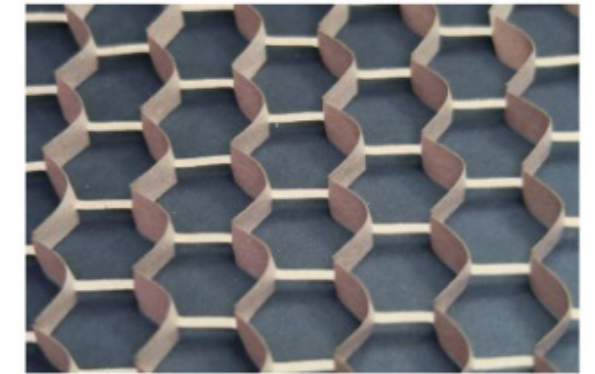


Figure 51: TAK- regular single slit and designed double slit (Source: Corrigan et al., 2023)

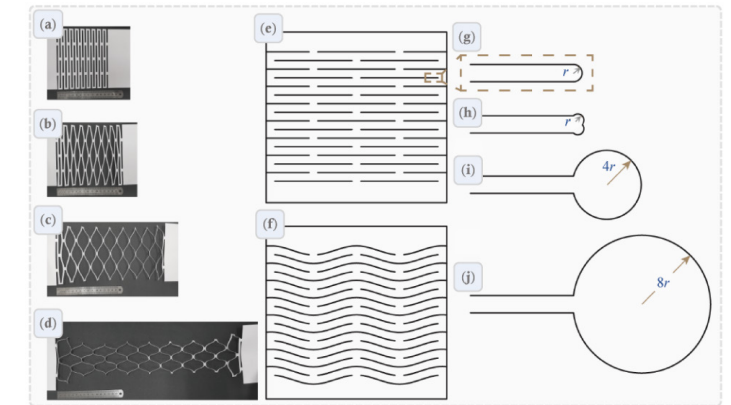


Figure 52: TConfiguring hinges into Ribbon Kirigami (Source: Sun et al., 2022)

in a parallel configuration. *The geometry variation after deformation -its relation to the parameters depends upon material and has to be figured out.*

The ribbon Kirigami also shows varying deformation pattern based in the end configurations as shown in figure 52.

7.2.2 Zig-zag Kirigami Design

The Zig-zag kirigami pattern has been represented by Eidini & Paulino, (2015) as a base unit cell BCH_n (Base unit cell with Hole) that is parametrized. The parameter representation is shown in figure 53. The expressions defining the geometry are as below:

$$w = 2b \sin \phi, \quad \ell = 2a \frac{\cos \alpha}{\cos \phi}, \quad h = a \sin \alpha \sin \theta, \quad b_1 = b/n,$$

ℓ = projected length of zigzag strips along x axis in xy plane; relationship between angle ϕ and fold angle θ is given by:

$$\tan \phi = \cos \theta \tan \alpha.$$

For the zigzag kirigami with $n = 2$, the in-plane Poisson's ratio of the approximately infinite BCH_2 (figure 53 right) is expressed as

$$\nu_{\infty} = -\tan^2 \phi \frac{4\lambda \cos \alpha - \cos^2 \phi}{4\lambda \cos \alpha + \cos^2 \phi}$$

The sign of Poisson's ratio depends on the sign of the numerator in the equation. Eidini & Paulino (2015) further proposed a misplaced pattern (figure 53 left) that affect the folding of the overall pattern as shown in figure 55. The Kirigami retains the characteristics of Miura-ori including negative Poisson's ratio as well as stackability and rigid folding, but however has lower density- is lighter and higher programmability.

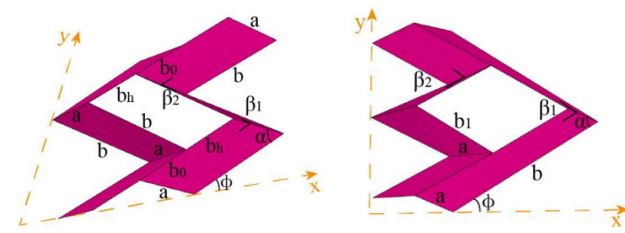


Figure 53: Base unit cells representation (Source: Sun et al., 2022)

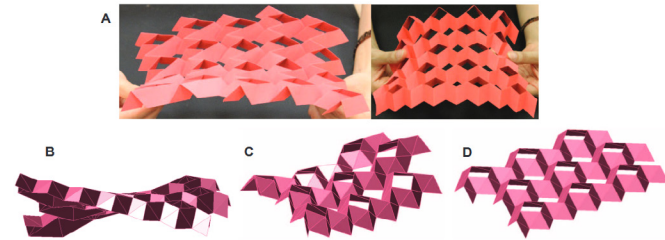


Figure 54: Behavior of BCH_2 sheet (Source: Eidini & Paulino, 2015)

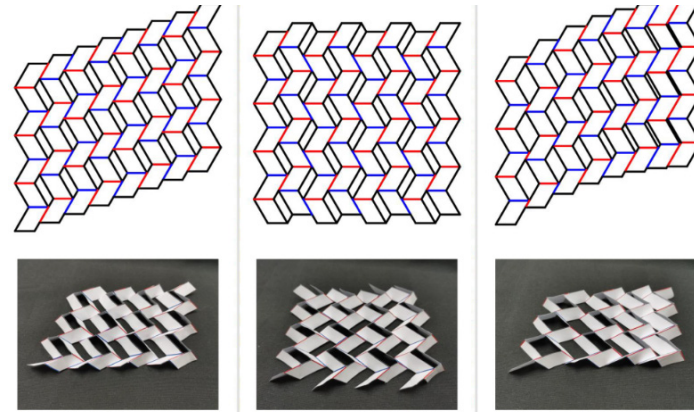


Figure 55: displaced pattern creating varying folds globally. (Source: Eidini & Paulino, 2015)

7.3 Kirigami as an interlayer material

Based on the literature summary of the kirigami types, the ribbon kirigami also represented in researches as tension activated kirigami or Buckling induced Kirigami only involves cutting of the sheet material and then activation. And on the other hand the other type(s) of kirigami also involves folding in order to activate.

As per the required properties for the interlayer discussed in chapter 6, resistance to creep is a property that can be achieved with a certain stiffness in the interlayer. It was seen in the previous chapter, that the interlayer property requirements also keep changing based on applications.

Kirigami - being simple to manufacture has seen several applications that present a stiffness range that are tuned with geometry parameters. Therefore Kirigami is chosen for creating an interlayer with tunable properties required for a particular assembly system.

7.3.1 Design Intent

Kirigami has a wide range of geometries and types as seen earlier. For the application as an interlayer material, following considerations are made:

- A constant-controlled thickness: It is crucial to have a precise and uniform thickness after activation because the 3DP glass units are manufactured to precision and should not be post processed due to the interlayer.
- Able to take tolerances: The kirigami interlayer should also be able to take tolerances of the 3DP unit surface and also tolerances during construction.
- A cut-only kirigami is most preferred in this case as to ease the manufacturing process by keeping it easily scalable.
- The geometry properties as well as material

properties would play a role in composite action with glass when applied in a dry assembly system, thereby material compatibility with glass is also to be considered while selecting the interlayer material. Especially for dry assemblies it can cause stresses in glass if the tolerances have not been incorporated.

- A more flexible material like PU70 as suggested for cast glass dry assemblies (Oikonomopoulou et al., 2018) can be considered on either side of the kirigami in case it is needed for tolerances- thereby developing a sandwich interlayer.

7.3.2 Geometry

In this thesis Kirigami is looked at as a method that can be applied to selected materials in order to tune

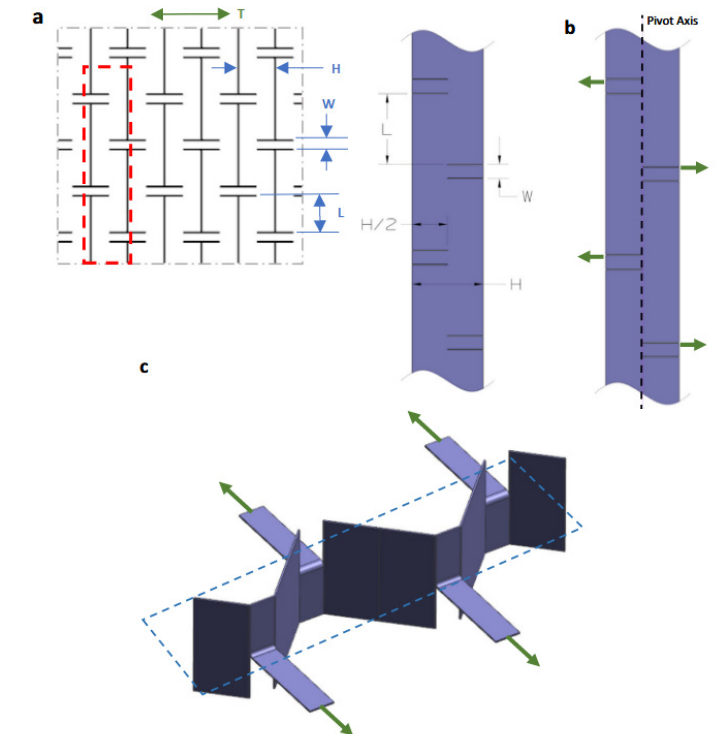


Figure 56: Tension Activated Kirigami (TAK) (Source: Corrigan et al., 2023)

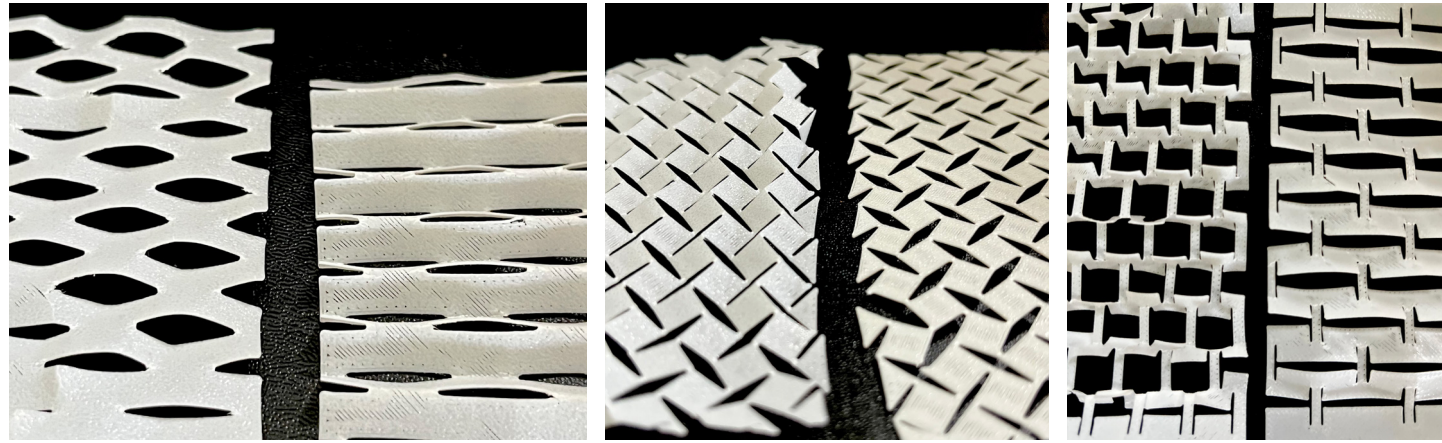


Figure 57: Initial Kirigami Explorations (Source: Own)

them to obtain desired target properties. Therefore, a promising geometry is selected from the literature for further exploration and application.

Tension Activated Kirigami (TAK)

Tension Activated Kirigami(TAK) is a novel pattern proposed by Corrigan et al.,2023 enabling a low-cost method to create wrapping material out of different material (figure 56). TAK pattern creates rows of material into vertical walls which demonstrate stiffness and strength comparable to honeycomb grated material. The concept and its activation is shown in figure 56. The researchers have made several iterations with paper, plastic and aluminum foil of 0.077mm thick demonstrating their promising application in the packaging industry.

As seen in figure 56, TAK has the parameters H, L, and W which drive the activated pattern. These patterns were considered as L = 5.8 mm, H = 5.8 mm, W = 1.2 mm; extended +50% for the samples in the research. In this thesis, we aim to utilize these to create an interlayer material of target thickness and stiffness. Further considerations regarding the geometry and model are discussed in chapter 10.

Key take-aways

Following are key takeaways from the initial kirigami study so far

-We have looked at various kirigami patterns there is a vast space and configurations to select from.

-We have also seen the configurability with custom cut patterns/ modified patterns for varying properties both in the case of ribbon and zig zag Kirigami.

-Zig-zag Kirigami as defined by Eidini & Paulino, 2015 was a novel research that drew its programmability ideas from Miura-ori. Although has extraordinary properties, it is less preferred due to an extra step of folding.

-Ribbon Kirigami- alternate or parallel configurations are a starting point for prototyping. The relationship of the strength with different thicknesses of material and architecture is to be determined.

-The research by Corrigan et al. (2023) already shed some light on the Tension activated Kirigami Ribbon patterns using aluminum thereby demonstrating its applicability and configurability. TAK is thus chosen for exploration in this thesis.

-Research on the ability of Kirigami patterns to stably

maintain their folded state or transition seamlessly between folded and unfolded configurations remains limited. Activation factors of kirigami needs to be taken into account which will affect its stiffness.

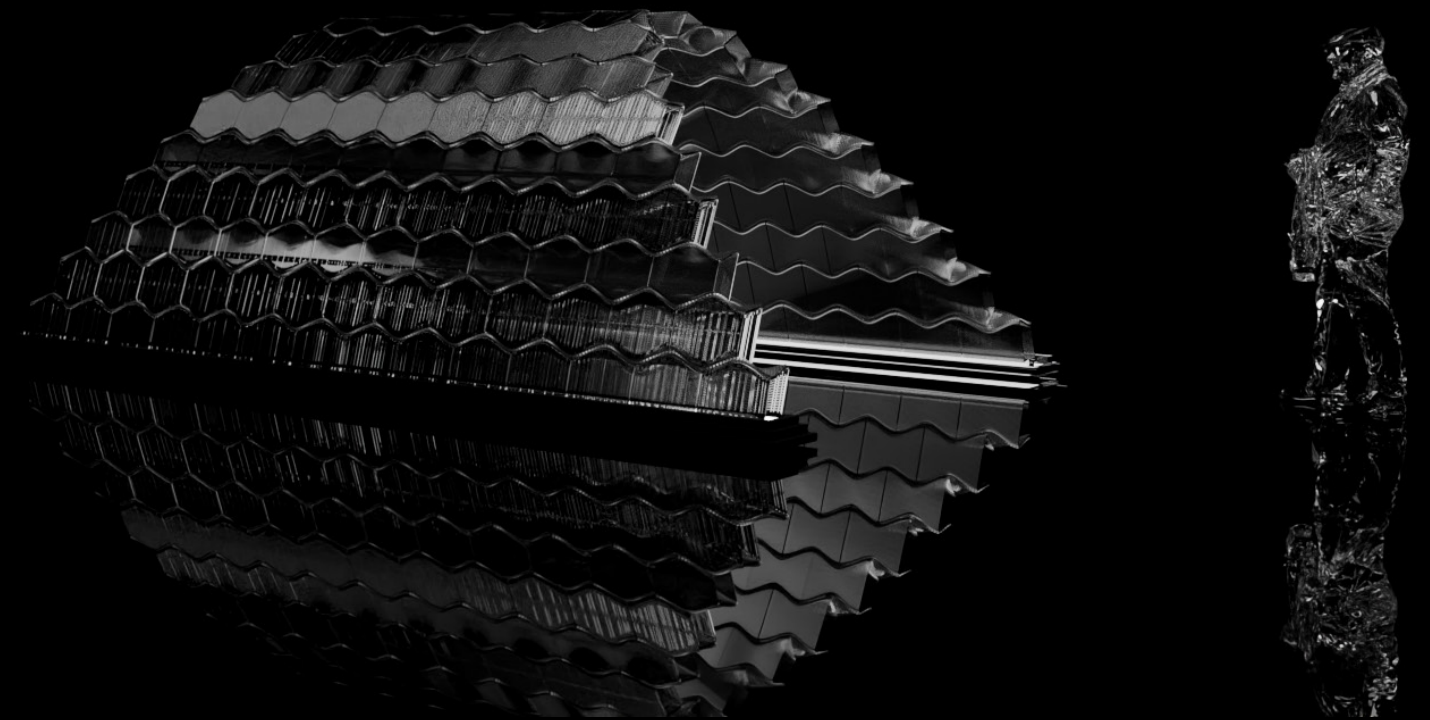
7.4 Chapter Conclusions

This chapter explained the kirigami principles as cut-only and cut-and-fold types based on Sun et al. (2021) and their subtypes within the context of transformable structures. Ribbon kirigami and zig-zag kirigami were among those most suitable for future research by virtue of the fact that they can transform flat sheets into three-dimensional structures, a property which is crucial for interlayer utilization. Whereas cut-and-fold styles can yield increased stiffness, the added folding complexity makes cut-only shapes like ribbon kirigami better suited for scalable, manufacturable applications.

The critical analysis focused on the tensile behavior of ribbon kirigami and its flexibility by way of geometric adaptation, supported by Corrigan et al.'s (2023) creation of a new TAK (Tension Activated Kirigami) motif. Zig-zag kirigami, derived from the Miura-ori motif, exhibited complex mechanical properties such as a negative Poisson's ratio and stiff folding, though less favored here due to its dependence on folding.

In conclusion, this chapter lays the groundwork for the choice of kirigami patterns with programmable mechanical properties, and the **outcome is the choice of TAK as a promising candidate for the development of an interlayer material with tunable stiffness and controlled deformation.**

Part C | The Design



8.0 | Designing the Assembly

Goal: To define the geometry for the assemblies as per design goals mentioned in chapter 4.

Since our goal is to establish an assembly technique and an interlayer solution, the design was not looked at as the primary objective in terms of designing-for-users or a specific case. Several Parametric models have been created for the process that are discussed in chapter 9 for parameter optimization. In this chapter, we discuss the parametric form, and tessellation for a simple straight wall, singly-curved, and doubly-curved dry-assembly system.

8.1 Parametric Design Approach

The idea was to define geometric and material property parameters that result in a structurally stable geometry while performing optimizing certain parameters.

- Since the thesis revolves around creating a circular design for disassembly, in order to maximize the re-use of the 3D printed blocks, the design of a catenary vault was proposed using 2 types of modules for a vault design as shown in figure 58-
- i. a standard module- that can be assembled into a straight wall or can be reused for assembling another arch with different dimensions.
 - ii. angular modules- that are specific for the curvature of the vault.

This approach reduces the number of unique modules for a curved geometry, allowing some amount of standardization. The idea is simplified for our application, deriving from (Sheth & Fida, 2020) who have explored osteomorphic form on funicular structures; however, results used gap filling techniques and tension cables for assembly. Therefore, for a doubly

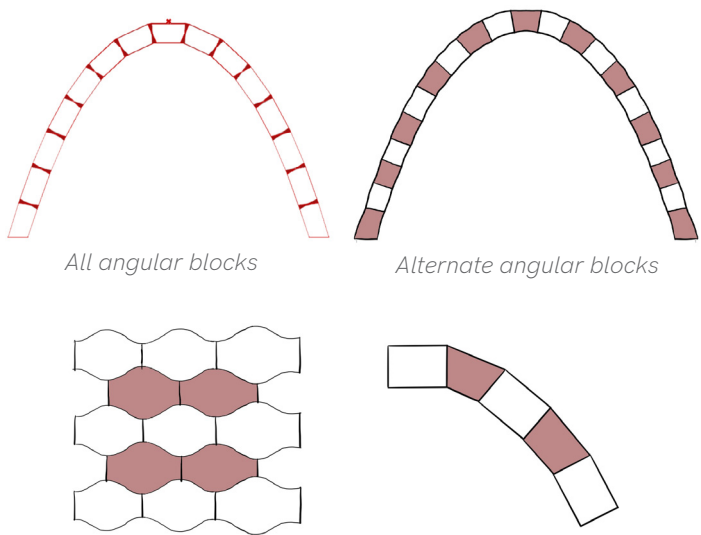


Figure 58: Unit Design Approach

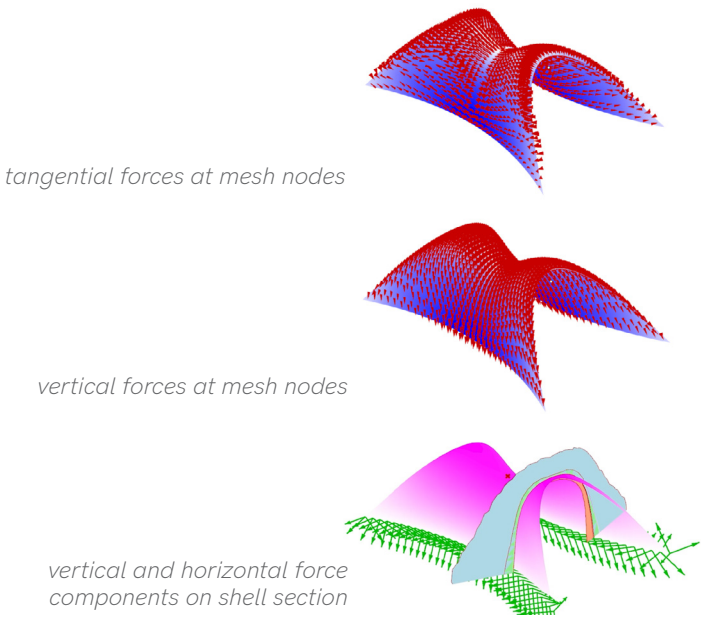


Figure 59: Force flow in designed compression only shell. (karamba analysis)

curved geometry, the osteomorphic form is not believed to be a suitable option for mortar-less construction, since there is force flow in both directions as shown in figure 59. In addition, there will be interlayers required in both directions in this case to avoid load transfer via glass-to-glass contact.

Looking at Block Research group's Armadillo vault as a prime example of a dry assembled doubly curved system as discussed in section 5.2, we propose trapezoidal glass units for a doubly curved assembly with interlayer application on both directions.

The overview of assembly properties is given here under in table 5.

	Wall	Single-curved structure Catenary Vault	Doubly-curved structure Compression-only shell
Dimensions	Length- 1.2m Height- 2.5m (one floor) Thickness-110m	Span- 2.2m Height- 1.9m Length ~4m	Span ~2.6m Height- 1.8m Length ~5m
Dry assembly	yes	yes	yes
Unit shape			
Unit customization	standard	standard+custom	custom
Unit 3DP configuration			
Scaffolding	not necessary	yes	yes

Table 5: Assembly design

The block geometry has been proposed based on trying various tessellation forms using osteomorphic shape as the initial 'ideal' shape. They have been further discussed in the next section. The main objective was to derive at a shape with manufacturing constraints mentioned in section 3.2, and is easy to assemble.

8.2 Tessellations

Based on the study on the tessellation patterns for dry assembly and chosen osteomorphic brick geometry, the goal was to use the osteomorphic faces of the brick in the direction perpendicular to the force flow, as you would do to assemble a wall. However, due to the complex sine-cosine curvature discussed earlier in section 5.4.3 and the manufacturing constraint of having at least 2 parallel geometry faces for 3DP, it was not possible to apply this unit geometry to a doubly curved compression-only form.

In this section, we have outlined several tessellation ideas along the same line, to arrive at feasible tessellation and block geometry for manufacturing and assembly.

1. Tessellation from Mesh geometry:

As seen in examples like Armadillo vault, the mesh is used as a base to create the tessellations. Since we are dealing with a vault shape (with two parallel supports), a quad mesh would be feasible to consider as per the size of manufacturable bricks. This idea was discarded as our obtained shape had mesh faces that varied immensely in area (as seen in figure 60).

2. Tessellation using projected patterns:

Lunchbox tools within grasshopper provide various tessellation patterns including staggered pattern. This was tried on an unrolled surface and projected back to the source surface. This resulted in a pattern that was difficult to control further. In addition, the pattern would not follow the shape as seen in figure 60.

4. Structured quad mesh:

In order to get a structured quad mesh that can be manipulated as per user inputs and controlled based on manufacturability of units, its essential to refine the initial mesh and post process as suggested in (Rippmann & Block, 2018). Deriving from the process,

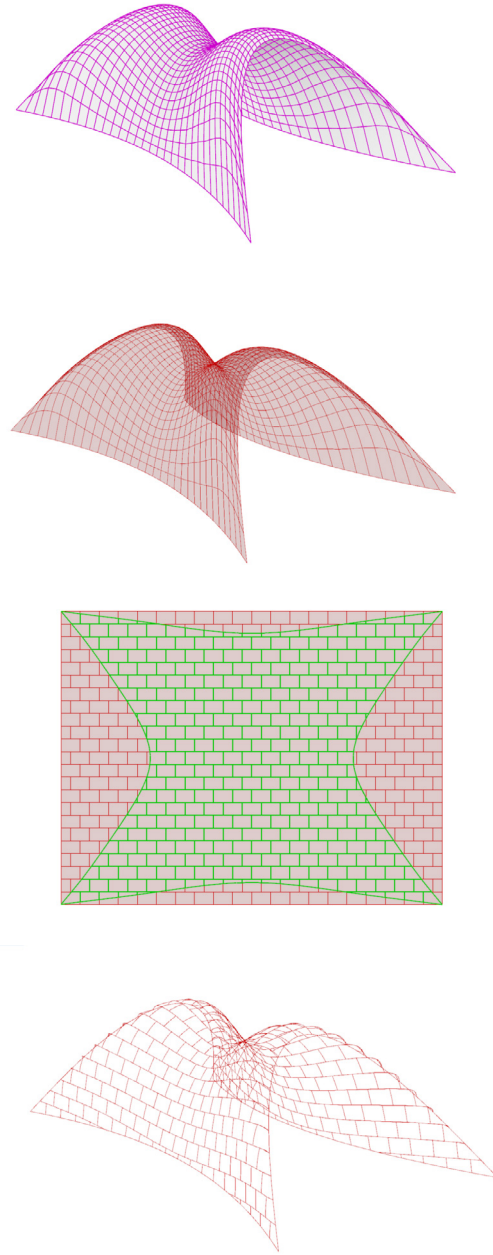


Figure 60: Tessellating a doubly curved surface

the idea of creating two different (mirrored) pattern on the intrados and extrados of the shell was found to be a feasible solution to create the osteomorphic form on a shell of certain thickness. This idea was first applied to the simpler catenary vault which has a single curvature as shown in figure 61. *It was also inferred that the sine-cosine surface gets distorted while applied to a doubly curved shell, and is unnecessary as the form is stable with lateral loads.*

Since its a curved shell, the osteomorphic surface does not help resist lateral loads as it does in case of a wall. The shape however, would immensely help during assembly so as to rightly place blocks into place in the staggered pattern.

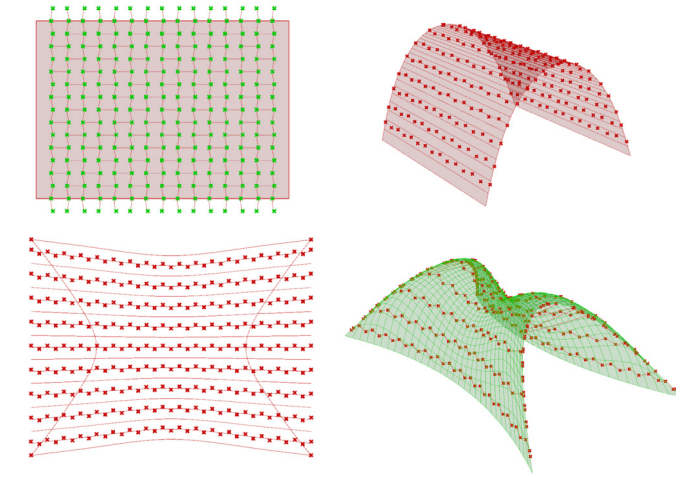


Figure 61: Osteomorphic Tessellation on curved surfaces

Several iterations of staggered pattern were done, and it was inferred that in case of a curved assemble, the shape would highly affect the ease of assembly allowing blocks to rightly place themselves in their respective locations. This was also seen in case of the Armadillo vault where stones edges were chamfered at angles. Figure 62 denotes the some tessellation options. These are done keeping the manufacturing constraints for block geometry in mind as discussed in chapter 5.4.3. Figure 63 shows the final tessellated geometries that are considered for the assembly optimization.

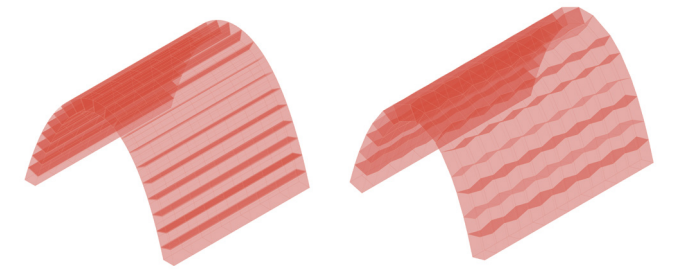


Figure 62: Possible Staggered Tessellation options for Catenary vault

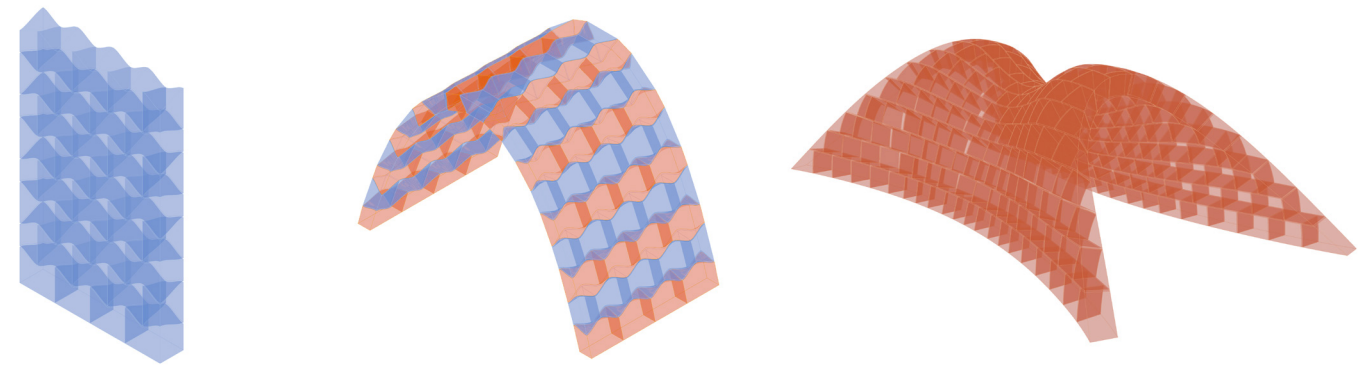


Figure 63: Final Tessellated geometries with 10mm thick interlayer

8.3 Defining Geometric Parameters

As discussed earlier, the overall parameters of the design were intended to be kept constant. However, certain geometric factors might affect the overall performance of the structure and would need optimization. Apart from the overall geometric shape parameters as in table 5, figure 64 depicts the parameters and geometries that have been considered to explore in this thesis.

not affect the structural performance. Figure 65 shows the Parametric model from grasshopper with constant parameters used and the parameters to be optimized as number sliders. The block size parameters entered here are only tentative upper limits, and they change with the thickness of the interlayer and the overall arch dimensions. The standard blocks in the alternate layers are consistent. The interlayer thickness is set to a constant value of 10mm as per initial parameter sensitivity analysis and ease of assembly discussed in

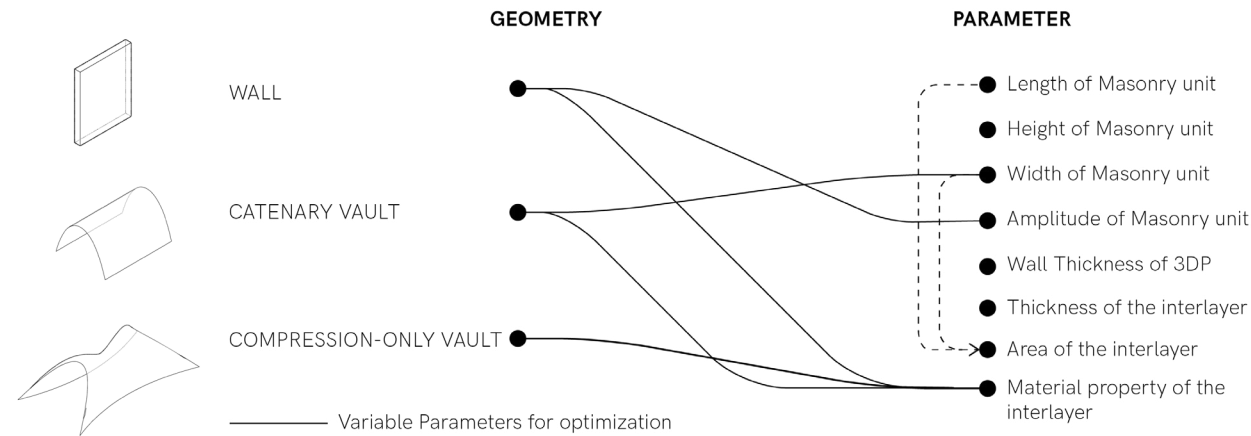


Figure 64: Geometry and parameter relationship.

In this section, an overview of the geometric parameters are presented for each of the geometries. Certain parameters for the Catenary Vault and a free standing wall are inter-related as we define the wall length, width and height based on the standard blocks defined from the catenary vault, and the loading conditions for the wall. Similarly, the amplitude of the brick is decided based on the performance of the wall under applied lateral loading and manufacturing constraints.

8.3.1 Catenary Vault

As discussed earlier regarding the brick geometry, we assume that the amplitude of the brick only affects the ease of assembly and varying the osteomorphic form will



Figure 65: Parametric model of the Catenary Vault

the subsequent chapters.

8.3.2 Free standing wall

We consider a 1m high free standing wall for our analysis, to be constructed using the 'standard' osteomorphic bricks defined for an optimized catenary vault. A straight wall is mainly considered to understand *what is the amplitude of the block* to be used if we consider a wall of length 1 meter and height (based on the thickness of the optimized catenary vault structure).

From the subsequent chapters, the best performing catenary arch based on considered interlayer stiffness is found to be around 110mm. A height of a free standing 110mm thick wall considering a lateral wind load of 0.5kN/m² was found to be 0.4m as documented in Appendix 1, and is not considered as in case of a dry assembly the upper block also has to be restrained. A height of 2.5m wall which could span a floor level is considered here, with a length of 1.2m.

A lateral load on the wall would help understand the effect of amplitude of the brick to be considered for such assemblies.

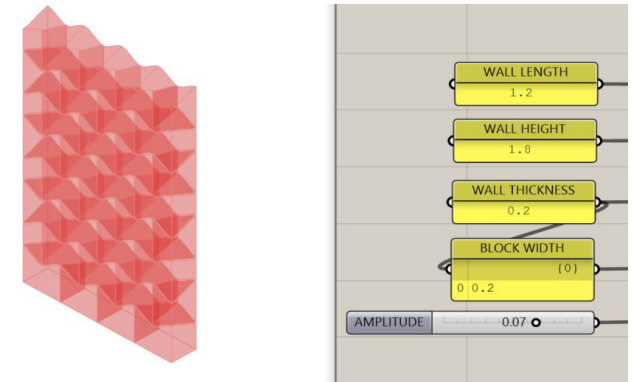


Figure 66: Parametric model of 1m free standing wall.

8.3.3 Compression only shell

The doubly curved shell does not relate to the geometric definitions of the other geometries. The units in this case are not standard and vary as per the shape of the geometry. Figure 67 shows model in this case. Since the vault is form founded in RhinoVault, it is not made parametric. The thickness of the vault is also made constant as to incorporate the form founded thrust network lie within the shell. It is further demonstrated in Appendix 1.2.

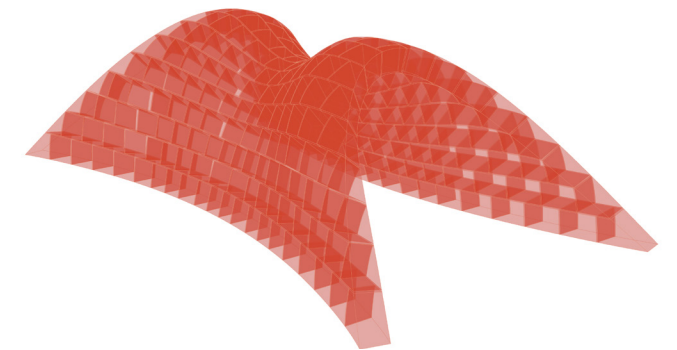


Figure 67: Model of compression only shell

8.4 Chapter Conclusions

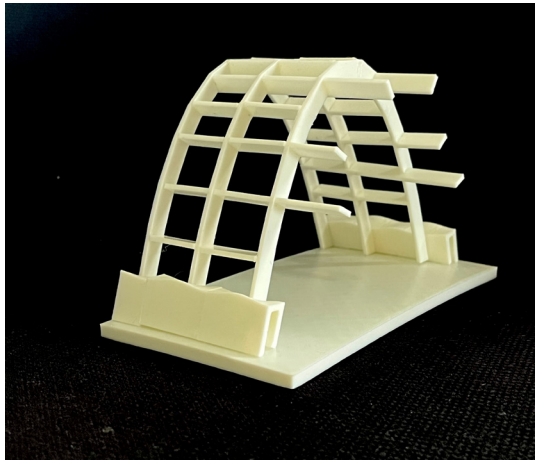
Three Parametric models were made to analyze the assembly process further. Some geometric parameters were set as constants as per the design intent and some parameters were considered to be varying based on the structure's performance. Following are the considerations summarized for each geometry-

i. A free standing wall of length 1.2m, thickness 0.11m and height 2.5m is considered with a lateral wind load of 0.5kN/sqm in order to determine the amplitude of the brick to be considered.

ii. A Catenary vault of span 2.2m and height 1.9m is considered. The amplitude is kept constant (defined by the altitude for the free standing wall) and it is assumed that it will not play a role in the overall performance of the structure. The thickness of the vault is the only geometric factor which is set to be optimized in the next steps.

iii. The form founded compression only geometry from section 5.3 is considered as the doubly curved shell geometry for the assembly process. It is tessellated using customized bricks of trapezoidal cross-section, therefore, the brick sizes vary with geometry however within manufacturable limits. In this case, no geometric parameter are to be varied for optimization, since the thickness of vault also depends on the thrust network of the vault. Considering more input factors lead to a complex relationship with output parameters under loading conditions as depicted in the following chapters.

The overview of the parametric models made has been depicted in Appendix 1 for reference to the tessellation process. 3DP unit sizes are defined to be kept within manufacturable limits but are controlled within the bounds by the geometry parameters.



9.0 | Parameter Optimization

This chapter is a documentation of the process to be followed for optimizing the structure based on certain boundary, load conditions.

Goal: To find a stiffness range of a solid interlayer with initial (arbitrary) properties. The process is demonstrated with our design case of the Catenary arch.

Since the study focuses on engineering the interlayer for application with respect to the dry assembly, it's essential to **identify the parameters** that would affect the properties of interlayer required for an acceptable structural performance. The following equation gives the stiffness of the interlayer assuming it as a simple linear spring(1D axial deformation with area A under uniform load and deformation):

$$k = \frac{EA}{t}$$

where, k = Stiffness of Interlayer (N/mm)
 E = Young's modulus of Interlayer (MPa)
 A = Area of the interlayer (mm²)(at one course)
 t = Thickness of the Interlayer (mm)

As seen in the above equation, the geometric parameters A, t and the material property E influence the stiffness of the interlayer. The first step was to study the parameter sensitivity with the performance of the overall structure.

This section presents an overview of the optimization process followed to derive the required stiffness of the interlayer based on objectives set for the structural performance globally. We understand the parameter sensitivity in a simplified 2D arch thereby defining the variables for the vault geometry.

9.1 FEA Tools and Workflow

9.1.1 Parametric Finite Element Analysis(FEA):

We chose Ansys for the Finite element analysis(FEA) of the discretely modelled masonry structures, and optimization process since it ingrates with python and several ML tools for optimization and sensitivity analysis. Ansys allows parametric analysis with MAPDL, however, all the parameters need to be defined within Ansys. In our case, the geometry was not considered to be recreated in Ansys CAD tools- Discovery/Design Modeller or Spaceclaim, since they are very limited compared to grasshopper.

9.1.2 Workflow:

The geometry was modelled parametrically in grasshopper, but, there is a lack of integration between Ansys and Rhinoceros+Grasshopper in order to consider geometric parameters from grasshopper. A new workflow had to be thus developed for automation of repeated analyses, incorporating geometric parameters that would affect the structural performance. The material properties were considered to be parametrized in Ansys, and the geometry is parametrized in grasshopper prior to performing the analysis in a loop for varying parameters. Ansys Workbench is used to perform multiple analyses by running Ansys programs in the background. Figure 9.1 shows an overview of the workflow developed integrating the tools for the process.

The workflow was made keeping in mind the time constrains for FEA, and system requirements. The idea was to utilize Delftblue supercomputers for the analysis process, but, further automation is required

to automate the creation of .dat input files by running Ansys Mechanical in batch mode, without manually having to export input solver files for each geometry. In addition, another automation is required for reading the solved files from Delftblue, without having to load each solved file in Ansys Mechanical. It was also found that Ansys Mechanical does not support 'Journaling' - a script that records all actions performed in Ansys for automating repetitive tasks. Hence, Delftblue was only used for Validation FEA runs only. Sample workflow and the python script components can be found in the github repository.

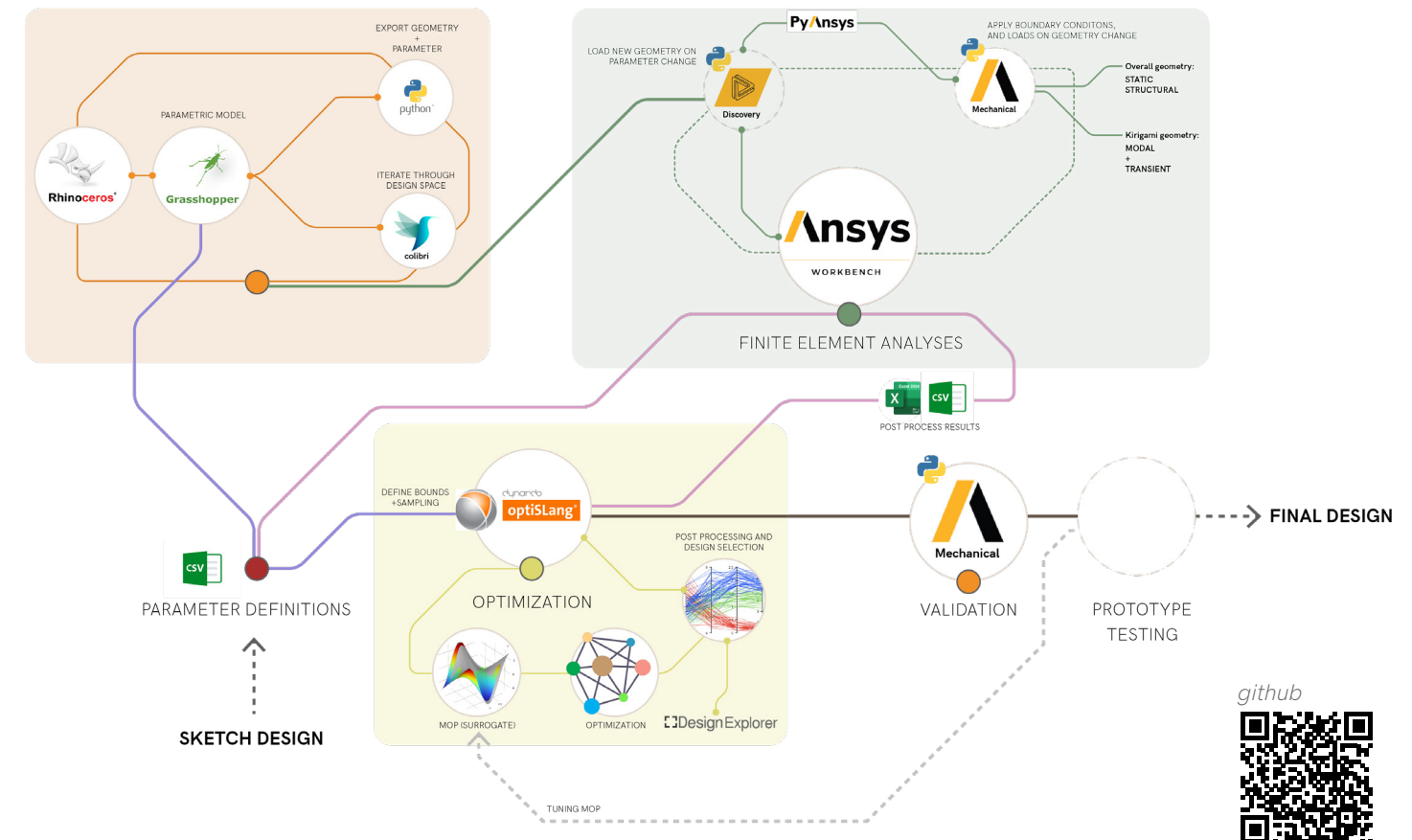


Figure 69: Developed Workflow for Surrogate based Optimization

9.1.3 Method:

As shown in the workflow diagram (figure 9.1), following steps outline the whole process from creating design samples to optimization:

(a) Parameter bounds are first decided based on constraints for 3DP glass and material properties- parameters vary for each design as discussed further in this chapter.

(b) A 100 samples are selected using Latin Hypercube Sampling(LHS) every time for each design. A 100 samples seemed to be a fair number for the time span of the thesis and available resources. The parameter values of these samples were imported in grasshopper and the geometry for each design was exported using python and a grasshopper plugin Colibri that automatically iterates over a given design space.

(c) The sample designs were imported to Ansys Workbench's Parameter set using Design of Experiments(DOE) to import the csv file with designs.

(d) Ansys Programming Design Language (APDL) is used to analyze all the design points by running Ansys tools in batch mode. Two python scripts (PyAnsys) are integrated within the tools- one to import the correct geometry on parameter value change, and another within Ansys mechanical to set the correct boundary conditions and load conditions. These scripts would change for different structures and loading/boundary conditions presented in the report.

(e) The evaluated results(inputs and outputs) for the 100 samples are then exported as a csv file for post processing in optiSLang and to create a Surrogate model to be used for the optimization task.

ANSYS tools Design explored, OptiSLang were initially explored for sampling and optimization process.

ANSYS OptiSLang was found to be more flexible and has more machine learning tools that can be leveraged.

i. Sampling:

With a sample size of 100 design points, Latin Hypercube Sampling (LHS) was used to effectively explore the parameter space. Because LHS can offer a more consistent and stratified coverage of the multidimensional parameter space, especially when working with a small number of samples, it was chosen over alternative sampling methods. By ensuring that every parameter range is sampled uniformly, LHS lowers the possibility of clustering and enhances the representation of the input space in contrast to simple random sampling. In high-dimensional models, where a full factorial design becomes computationally impractical, this is particularly crucial. The sampling was done in ANSYS OptiSLang by defining the variable parameters and their bounds and exported as an excel for further processes. Since OptiSLang samples were continuous, they were rounded off in excel.

ii. Surrogate Method:

The surrogate method used is Polynomial Regression, Moving least squares(MLS), Kriging (Gaussian Process Regression). OptiSLang was used to create Meta Model of Optimal Prognosis (MOP) using Polynomial +MLS + isotrop. Kriging. OptiSLang it chooses the best surrogate model per output parameter individually and is further mentioned in the chapters that follow.

iii. Optimization Algorithms:

ANSYS optiSLang provides a variety of local and global optimization algorithms, each with unique advantages based on the type of problem:. The following were looked into for a multi-objective optimization task:

- Adaptive Multi-Objective (AMO): Robust algorithm

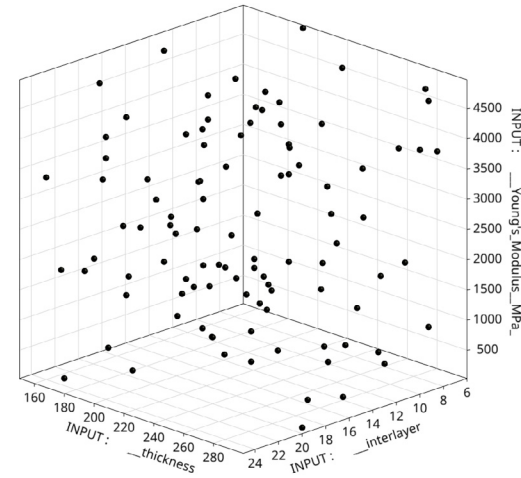


Figure 70: 3D scatter plot of designs for analysis of 2D arch

designed for multi-objective problems. It adaptively balances exploration and exploitation, suitable for highly nonlinear and constrained problems.

- Adaptive Metamodel of Optimal Prognosis (AMOP): An effective surrogate-based optimizer that lowers computational costs by creating predictive models (metamodels) of the design space.
- Evolutionary Algorithm (EA): A population-based global optimization method inspired by biological evolution. Capable of handling complex, non-convex, and multi-modal design spaces without requiring gradient information.
- Multi objective Particle Swarm Optimization (MOPSO): A heuristic optimization technique based on the collective behavior of particles. Well-suited for continuous and moderately nonlinear problems. This method was not further explored as they were found to be less robust than EA.

The Evolutionary Algorithm was chosen for its

robustness in handling multi-objective, non-linear, and non-convex optimization problems. While AMO is effective in multi objective tasks, it can require more iterations to converge in rugged landscapes. And, AMOP depends on surrogate model accuracy, which can be limiting for highly non linear problems like stress and deformations in glass. EA does not require gradient information. Its global search capability also reduces the risk of converging to local optima.

Figure 9.2 shows a 3D scatter plot of 100 samples in the design space with three variables used for initial study of 2D Arches discussed in chapter 9.3.

9.2 Constraints and Objectives

9.2.1 Materials:

The Material properties of standard soda-lime glass was used from Ansys Granta Material Data. They are as outlined hereunder:
Glass properties:
Density: 2465 kg/m³
1403 kg/m³ (calculated for eq. 3DP unit)
Young's Modulus: 69.93 GPa
Poisson's ratio: 0.2149
Tensile Yield strength: 32.56 MPa

Interlayer Properties:
Density: 1100 kg/m³
Poisson's ratio: 0
(A density of PU is considered and a poissons ratio assumed to be 0 as per the chosen kirigami geometry discussed in chapter 7.3.)

Note: Solid blocks with a density equivalent to a 3DP unit of the same size as mentioned in chapter 5.4.3 have been considered for the analyses in order to keep the model simple and make computation less expensive. Initially, glass units were considered to be discrete and max. stress in glass was to be monitored but not set as an objective. However, initial results on 2D arch implied on setting a multi-objective optimization. Even then, solid blocks were considered for the analyses, and were set to be later verified with a hollow block model of the optimized structure.

9.2.2 Variables, Responses and Objectives:

Initially all the geometric parameters that would affect the overall structural stability were listed. It was crucial to understand the parameter sensitivity with the performance for a specific application. Trying to optimize multiple geometric parameters was not feasible, as it would lead to higher computation time

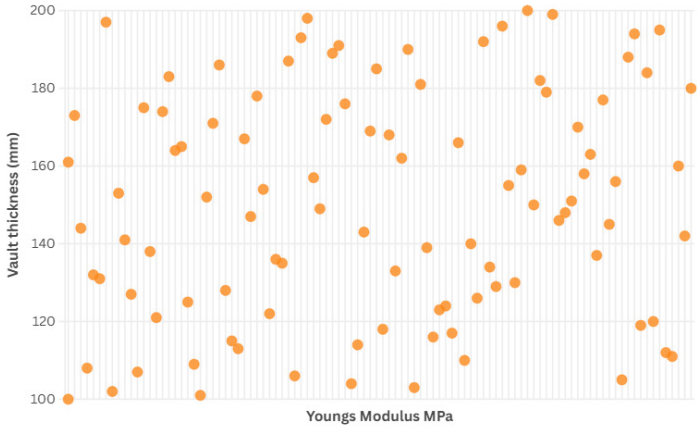


Figure 71: Sampling parameter bounds to create Design Space

and increase complexity.

Therefore, the parameter sensitivity was analyzed using an over-simplified 2D catenary arch section form the catenary vault designed, under self weight as discussed in the following chapter. Following this, the variables were decided for the Catenary vault optimization process. Certain parameters like the thickness of the interlayer were set to constant on the process, and geometric variables were kept at minimum. Geometric parameters were still considered in order to allow some flexibility in the engineering of the interlayer as well as optimize the overall mass of the design as per the performance objectives set.

Table 6 gives an overview of the bounds of the variable parameters and the constant parameters considered for each design. Figure 71 shows a scatter plot of a 100 designs sampled within the parameter bounds to create the design space.

GEOMETRY	INPUT			OUTPUT		OPTIMIZATION		
	Variables/ Constants	Bounds		Design samples	Response	Objective	Constraints	Limit State
2D Arch	Arch thickness (T) in mm	150	250	100	Max Tensile Stress in glass	minimize	none	-
	Interlayer thickness (I) in mm	6	25					
	Interlayer Young's Modulus (E) in Mpa	20	5000		Total deformation	minimize		
Catenary Vault				200	Max Tensile Stress in glass	minimize	none	Max Tensile Stress in glass<30MPa
					Total deformation	minimize		
	Arch thickness (T) in mm	100	200					
	Interlayer thickness (I) in mm		10		Max Tensile Stress in Interlayer			
	Interlayer Young's Modulus (E) in Mpa	20	1000		Max Compressive Stresses			
Wall	Amplitude of osteomorphic 3DP unit in mm	40	82	100	Total deformation	minimize	none	Max Tensile Stress in glass<30MPa
	Wall thickness (T) in mm		110		Max Tensile Stress in Interlayer			
	Interlayer thickness (I) in mm		10		Max Compressive Stresses			
	Interlayer Young's Modulus (E) in Mpa		250					
Compression only shell	Vault thickness (T) in mm		200		Total deformation	minimize	none	Max Tensile Stress in glass<30MPa
					Max Tensile Stress in Interlayer			
					Max Compressive Stresses			
	Interlayer Young's Modulus (E) in Mpa	50	1000		100			

Table 6: Parameter Bounds and Optimization Objectives used

9.3 Parameter Sensitivity

Analysis of 2D Catenary arches:

Two simplified Catenary arches from the catenary vault design as shown in figure 73 and 77 were made initially to set up the workflow, and were used to analyze the parameter sensitivity with the performance factors as outputs. This was mainly to minimize the geometric parameter variables and consider only the ones that could make an impact in terms of resources.

Material Properties: as mentioned in chapter 9.2.1

Boundary conditions: Fixed displacement supports.

Load: Self weight considering 0.3m thick shell

Number of designs: 100 (as sampled using LHS) Figure 72

Results:

ARCH 1- Solid Bricks:

Deformation in all designs were less than 1mm- inferring that the catenary shape is very stable with stiff geometry blocks like glass- and even for an interlayer with low young's modulus like 10Mpa, the units eventually settle down under their self weight.

It was also noticed that in this case the friction coefficient played a crucial role in the arch stability- and the solutions converged only when a higher friction coefficient was applied implying that the arch behaves as if the interlayer was bonded instead of being a dry assembly.

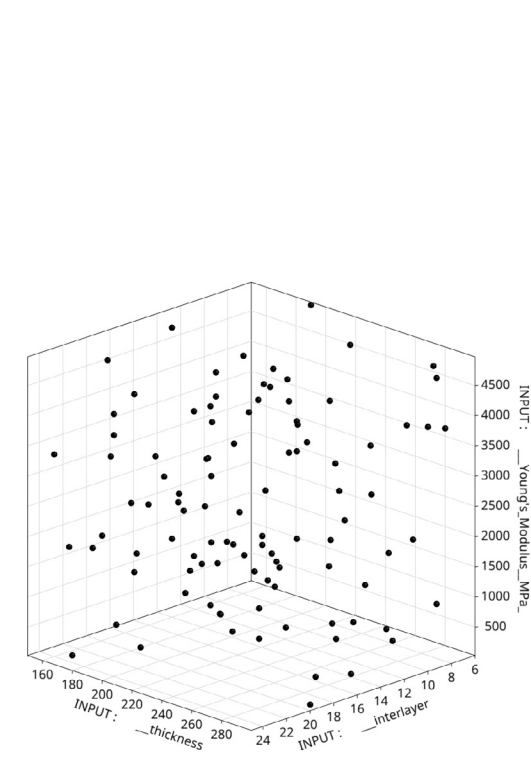


Figure 72: 3D scatter plot of designs for analysis of 2D arch

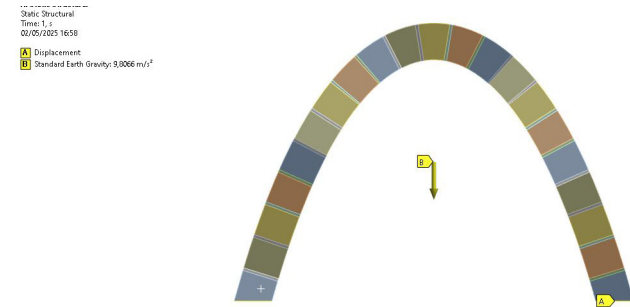


Figure 73: Boundary conditions and load

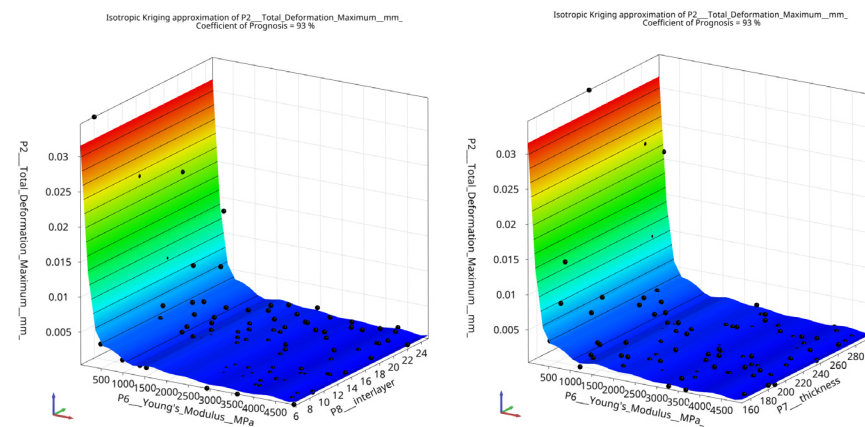


Figure 74: 3D scatter plot of designs for analysis of 2D arch

As seen in figure 75, the deformation inwards implies the stress patterns in the glass blocks- higher stresses where the blocks come together as the interlayer slides/compresses.

The 100 designs were used to build the Metamodel of Prognosis(MOP) or surrogate on OptiSLang, and the accuracy of the model reached 93% (for output total deformation) with inputs- Young's modulus of interlayer, Arch thickness, and interlayer thickness as seen in figure 74.

The relationships of the inputs with other responses were not significant and therefore have not been considered.

The parameter sensitivity for 2D arches as presented in

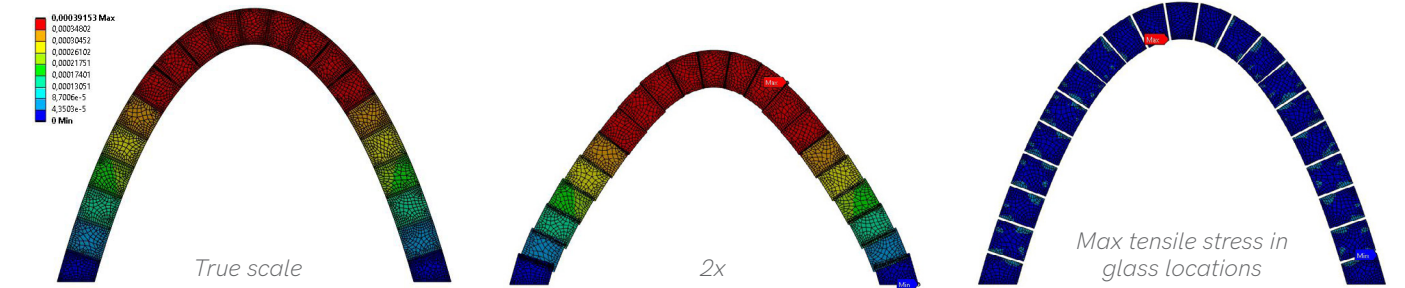


Figure 75: Solid block arch 2D Total deformation and Tensile stress locations in glass

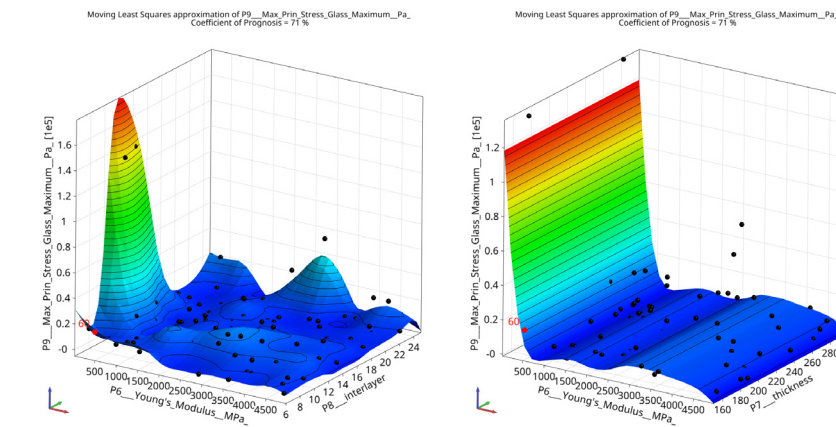


Figure 76: 3D scatter plot of designs for analysis of 2D arch

figure 76 shows that the interlayer thickness as well as the thickness of the arch does not have a clear relation to the total deformation of the arch or the maximum tensile stress in glass. Although the stiffness ($k = EA/t$)N/mm of the interlayer would depend on the area as well as the thickness of the interlayer, it would not directly affect the total deformation or the maximum stress in glass. It would depend on the young's modulus for the given thickness. For eg. a very soft interlayer which has low thickness is more likely to cause stress in glass as compared to the same interlayer but with more thickness.

It was decided to keep the interlayer thickness as constant- as it would mainly play a significant role during the assembly of the vault, and tolerances needed. The thickness of the vault was the only geometric factor to

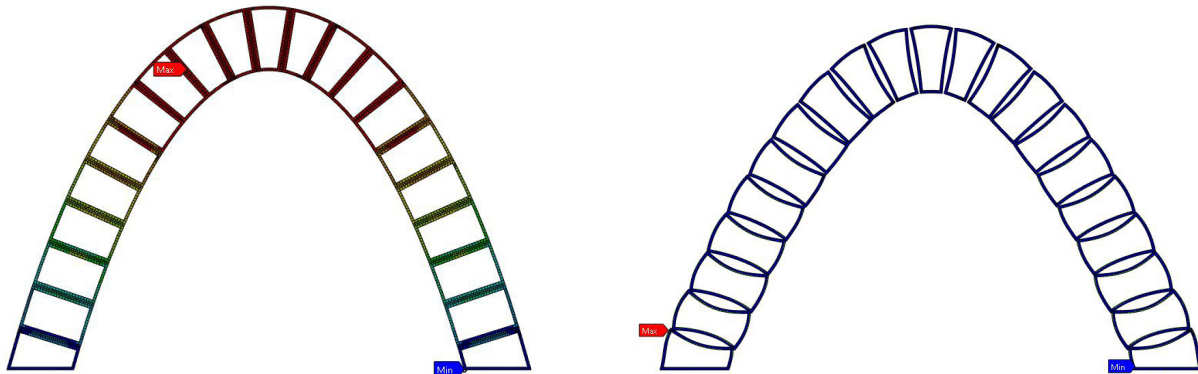


Figure 77: Hollow block arch 2D Total deformation and Tensile stress locations in glass

be varied for the 3D vaults.

A clear reduction in the total deformation is seen with the increase in young's modulus of interlayer; however, the deformation does not further significantly change with an interlayer with young's modulus above ~2000Mpa. Thus, the bounds of the property can be changed to better represent the design space for

optimization.

Figure 76 shows the relationship between the two input parameters with maximum tensile stress in glass. The coefficient of prognosis in this case is 71%- thus implying not a clear depiction of the response. It can be implied that too many input parameters have been selected in this case.



78 Figure 78: Parameter correlation Matrix

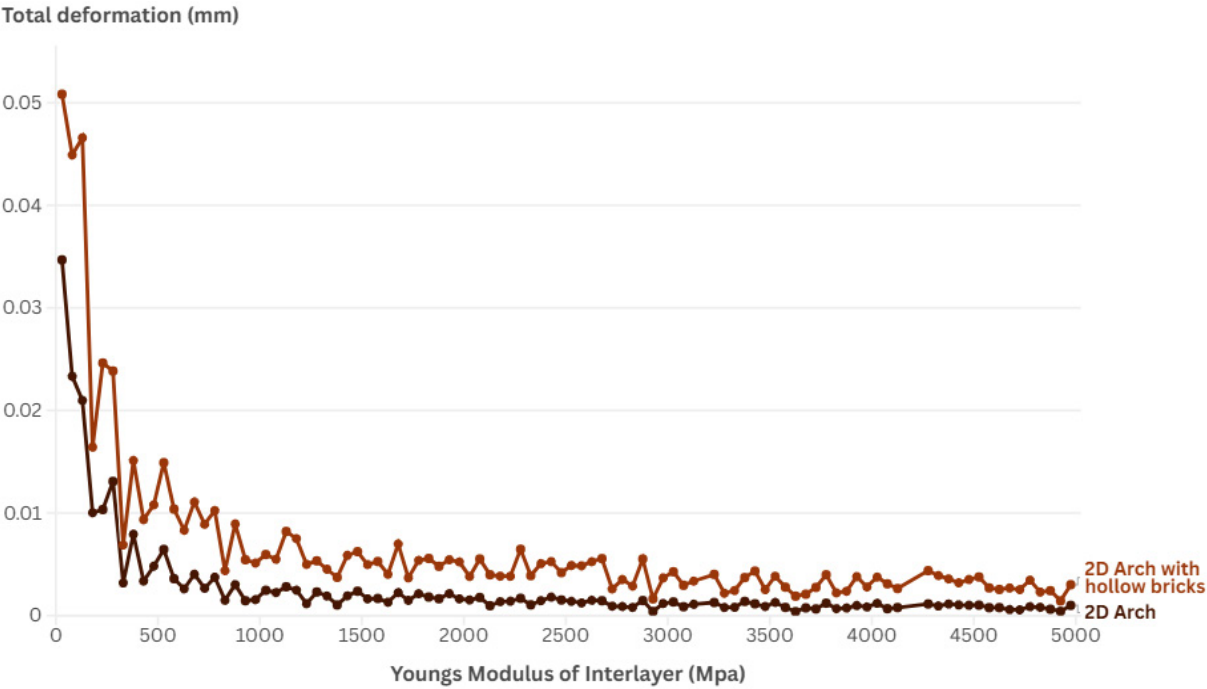


Figure 79: Total Deformation vs Young's Modulus of interlayer for the 2D Arches analyzed

Results:
ARCH 2- Hollow Bricks:

Similar results' trend was seen as compared to the solid blocks with approximated density; with a higher total deformation and higher tensile stresses in glass as expected due to geometry. This implied that the approximation of solid blocks is valid; however, a safety factor needs to be incorporated in case high stresses are expected.

Both the 2D arches were highly unstable under eccentric loading conditions since the contacts were not bonded. It is assumed that the osteomorphic form of brick and the compression only shape for the doubly curved vault would stabilize the structure. Nonetheless, eccentric loads as per Eurocodes are considered for validation in the following chapters.

Key take-aways

Deformation is minimum as the structure designed is a vault section. Therefore the outputs- stresses in glass as well as interlayer are to be monitored for responses to be set as objectives for the optimization process.

Interlayer thickness as well as arch thickness does not have a clear relation to total deformation or max. tensile stress in glass. Interlayer thickness will mainly affect the assembly process and thus can be set as constant for better control. A clear relationship with the stress in glass is not seen probably due to too many input variables.

For the interlayer, a youngs modulus of more than 2000Mpa does not further increase structural performance, and thus the bounds for youngs modulus maximum can be set to 2000Mpa for further analyses.

9.4 Optimizing the Catenary Vault

The designed catenary vault was used to create surrogate approximations with several loading conditions as shown in figure 80. The goal was to optimize the chosen parameters for the catenary vault under realistic loading conditions. However, it was observed that constant eccentric loading conditions have a complex relationship with the vault's varying geometric features which results in a very low accuracy of the coefficient of prognosis for the surrogate model and they cannot be used for optimization.

The loading conditions that were considered are mentioned in the table 7 alongwith the results for the surrogate created with the design samples selected within the bounds for the variable parameters. The loading conditions were considered as per Eurocode EN 1991-1-4 and EN 1991-1-1, and are elaborated in Appendix 2 of the report. This section of the report

presents the surrogate model for Load condition A: under Self weight only that is then used for optimization to find the range of young's modulus for the interlayer and the vault thickness to go with for best performance under self weight.

The analyzed result is then verified with FEA with same boundary and load conditions and also under eccentric load conditions to confirm its stability.

9.4.1 Variables and Sampling:

Parameters to optimize: Vault thickness (varied within a range of 100mm to 200mm) and Young's Modulus of the interlayer.

Sampling: Advanced Latin Hypercube(LHS) sampling

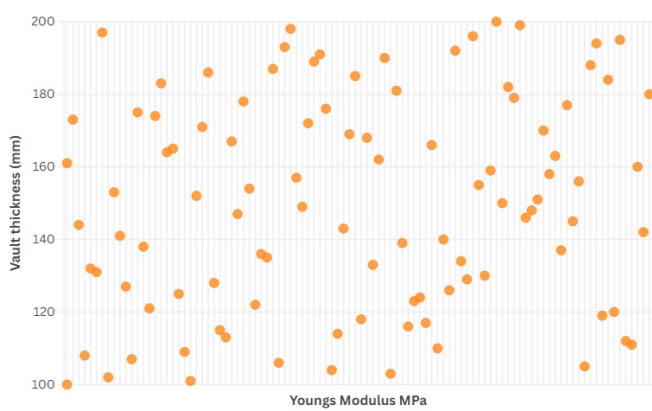


Figure 81: LHS sampling create Design Space with 100 designs



Figure 82: Boundary conditions

was done in optiSLang using the bounds of the Inputs in order to fill the design space with a 100 samples as shown in the scatter plot 81.

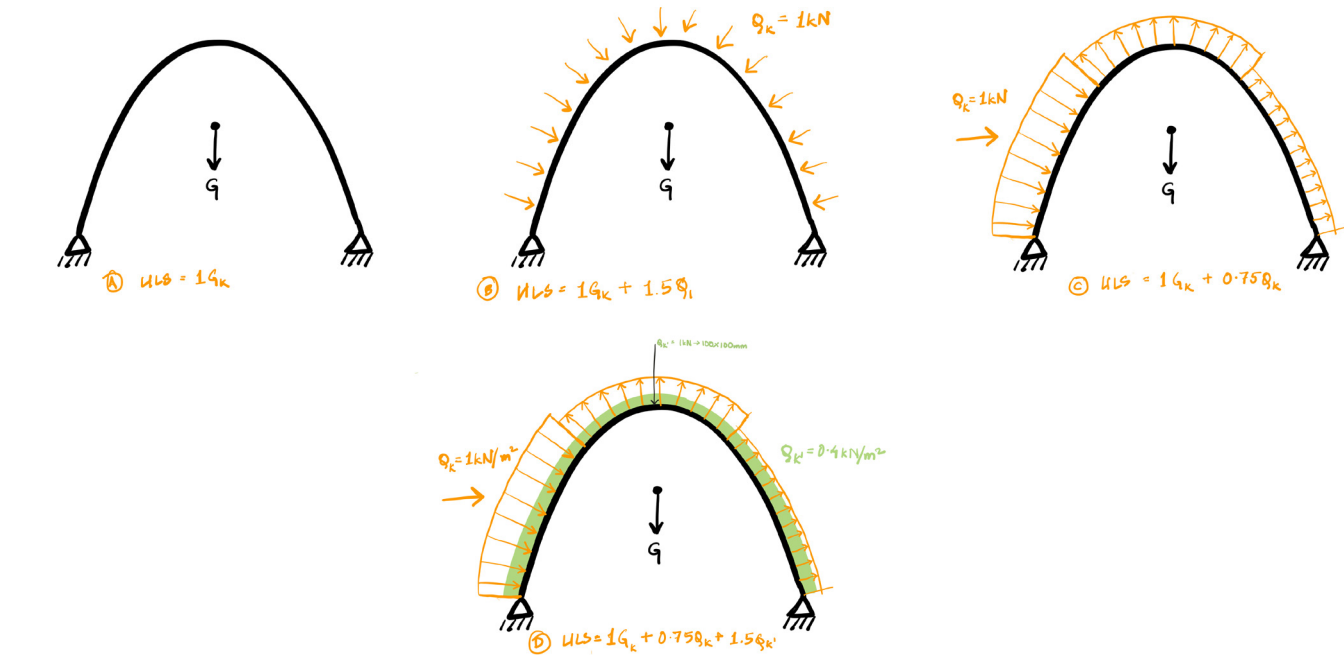
These sampled designs were then imported into grasshopper to export the geometries alongwith their labels as per the methodology discussed earlier.

9.4.2 Loads and Boundary Conditions:

Load Case A: Vault under self weight

Vault simplified to solid bricks with approximate density ~1403kg/m³ considering 12mm bead width and 6mm layer height for 3DP. Density of interlayer-1100kg/m³ as specified in section 9.2.1.

Boundary conditions: Fixed Displacement supports applied on the bottom mesh faces as shown in figure 82.
(The support detailing is done in chapter 12 of the report.)



80 Figure 80: Load conditions considered for design

Geometry	Design Points		Optimization	Surrogate Model	
	Load condition	Design samples	Objectives	Coefficient of Prognosis	Remarks
Catenary Vault	A. Self Weight	100	1. Minimize Tensile stress in glass	97%-99%	Clear relationship between input/output parameters
	B. Self Weight + Uniform maintenance load of 1kN/sqm	100	2. Minimize Total deformation	0-29%	Relationship between the inputs and
	C. Self Weight + Pressure load due to wind of 1kN/sqm on one side	100		0-62%	outputs not clear to be represented by a surrogate model.
	D. Self Weight + Pressure load due to wind of 1kN/sqm on one side + Uniform Maintenance load of 0.4kN/sqm + Maintenance Point load of 1kN over 100mm x 100mm area at the center of vault	200		3-11%	

Table 7: 3D scatter plot of designs for analysis of 2D arch

The model set-up for the Ansys Workbench is depicted in Appendix 2. Ansys Static Structural is used in this case to perform a non-linear FEA analysis. Symmetry option along two axis is used in this case since the conditions are symmetric.

9.4.3 Surrogate Model for Optimization:

OptiSlang's interface was used for the optimization process is depicted in Appendix 2. Following specifies the details of the optiSlang's Metamodel for optimal prognosis-MOP (surrogate).

INPUT: Youngs Modulus of the interlayer
Vault thickness

RESPONSES: Total deformation maximum of the Vault
Maximum Tensile Stress in Glass
Maximum Tensile Stress in Interlayer

Following are the approximation methods used for each response as best suited:

- A. Isotropic Kriging approximation - Total deformation maximum
- B. Isotropic Kriging approximation -Maximum tensile stress in glass
- C. Moving Least Squares approximation -Maximum tensile stress in the interlayer

The accuracies of the models are 97-99% and are depicted in figures 84, 85 and 86.

Inferences:

- A. Total deformation approximation (figure 84): Both fitting and prediction errors are very low. CoD (fitting) indicates very good fit to training data as well as CoP (prediction) indicates strong generalization to unseen data. Only a few outliers.
- B. Maximum Tensile Stress in glass approximation (figure 85): High CoD and CoP indicating strong fit and generalization. Mean error in prediction is

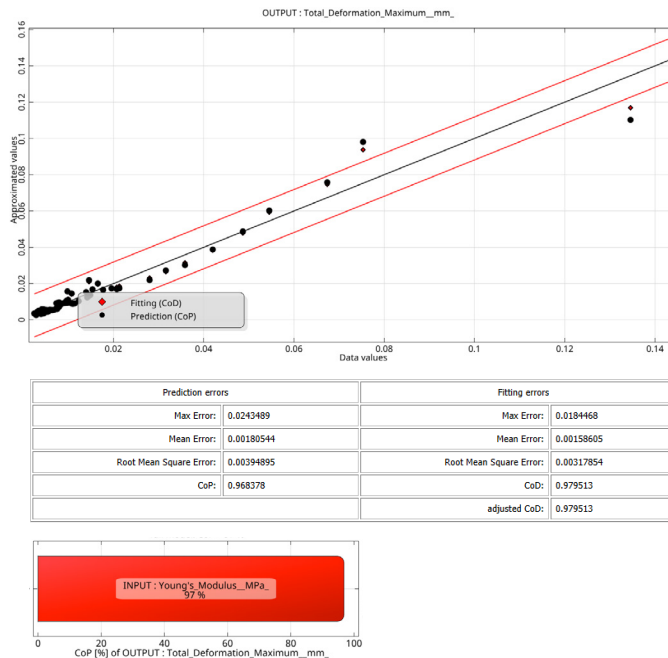
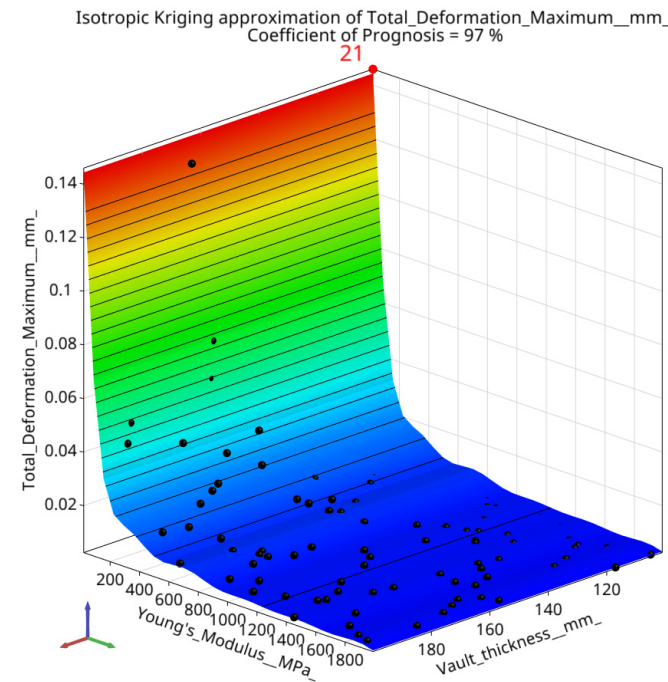


Figure 84: MOP- A. Total Deformation Maximum

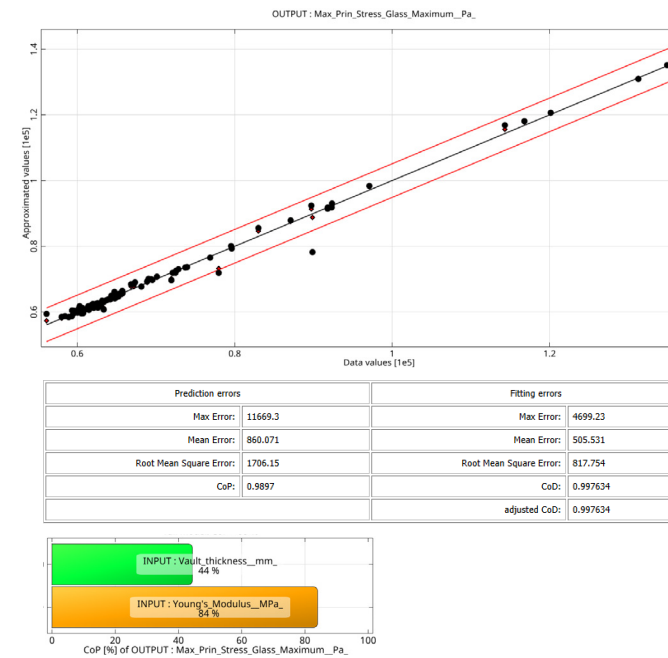
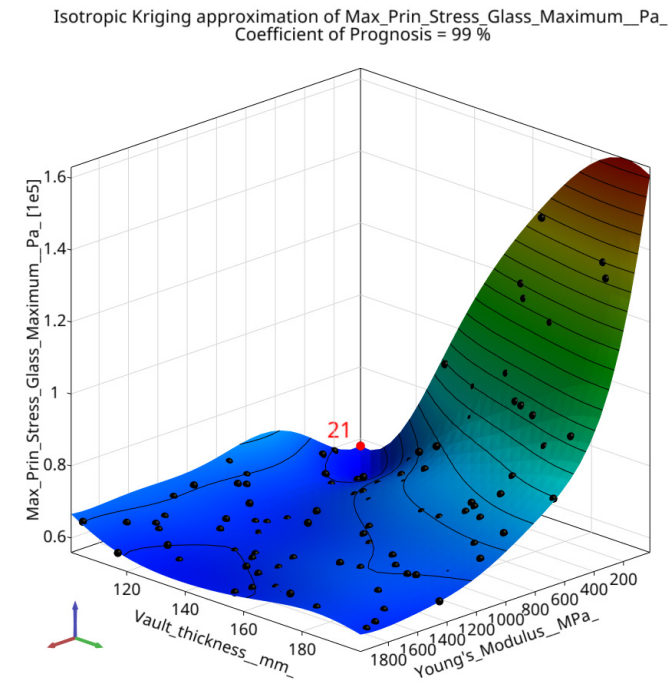


Figure 85: MOP- B. Maximum Tensile stress in glass

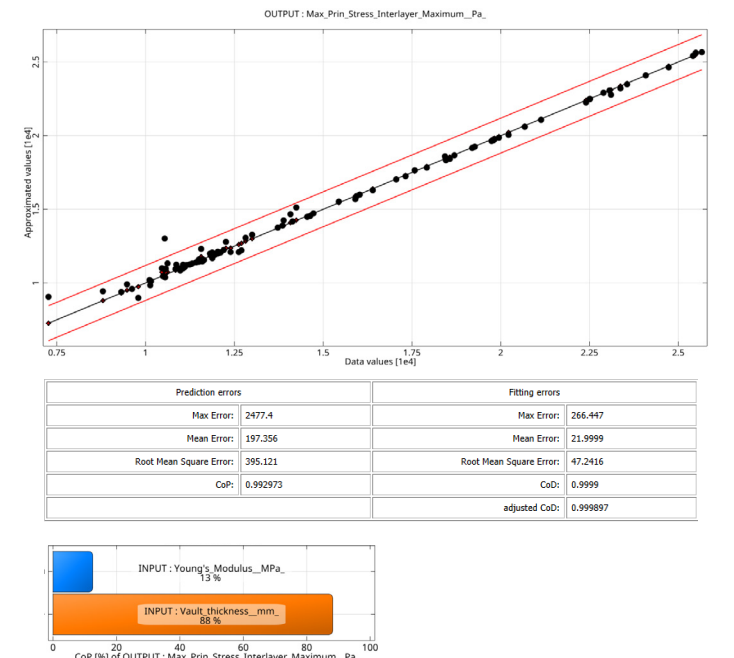
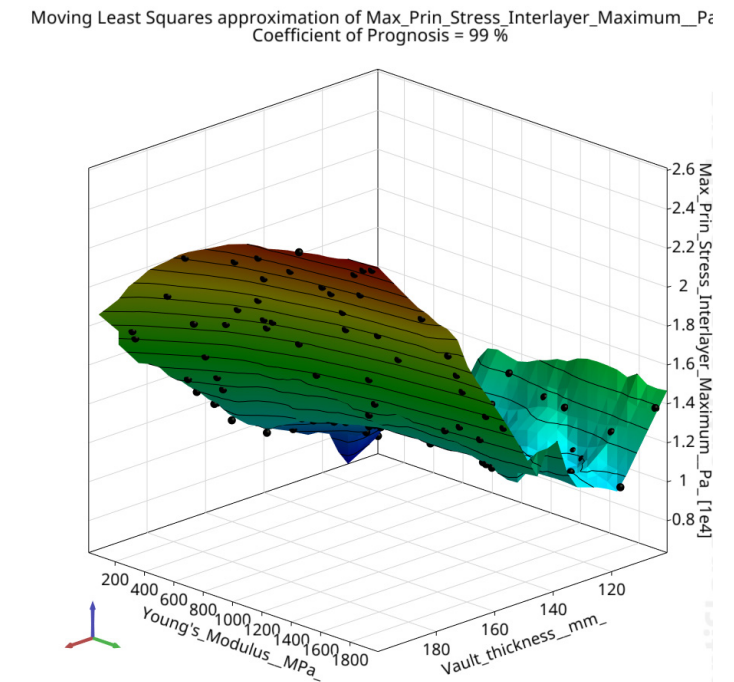


Figure 86: MOP- C. Maximum Tensile stress in interlayer

- 860Pa (slight increase on unseen data) which is acceptable.
- C. Maximum Tensile Stress in interlayer approximation (figure 86): Very accurate, and also generalizes well. Lesser outliers.

Fitness method: Pareto dominance

Criteria:

Objective 1: Minimize Total Deformation maximum

Objective 2: Minimize Maximum Tensile stress in glass

9.4.4 Optimization and Best Designs:

OptiSlang's Nature Inspired Optimization- **Evolutionary Algorithm** is used for the task with a maximum number of samples as 10,000 and a global search strategy.

Population size: 10

Start opulation size: 10

Maximum number of generations: 1000

Mutation rate: 50%

Results:

The Pareto front generated (figure 87) indicated two designs as seen in clear two clusters:

- Design A-features a very high Young's modulus, resulting in lower overall deformation. However, this comes at the cost of significantly increased stress in the interlayer as shown in figures 88 and 89, which compensates for the reduced stress in the glass. While structurally efficient, this solution

- may be unrealistic for practical implementation due to the extreme material properties required.
- Design B - presents a more moderate Young's modulus (around 200 MPa) and shows lower interlayer stress- as shown in figures 88 and 89, making it a more balanced and feasible option from both performance and material perspectives.

Filtering of results:

Two clusters of designs as from the Pareto front can be seen in figure 87. Figure 88 shows a comparison of % values of two designs selected from the two clusters.

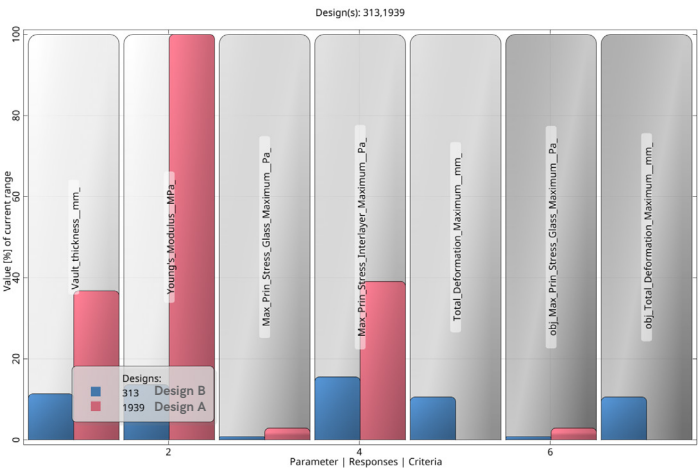
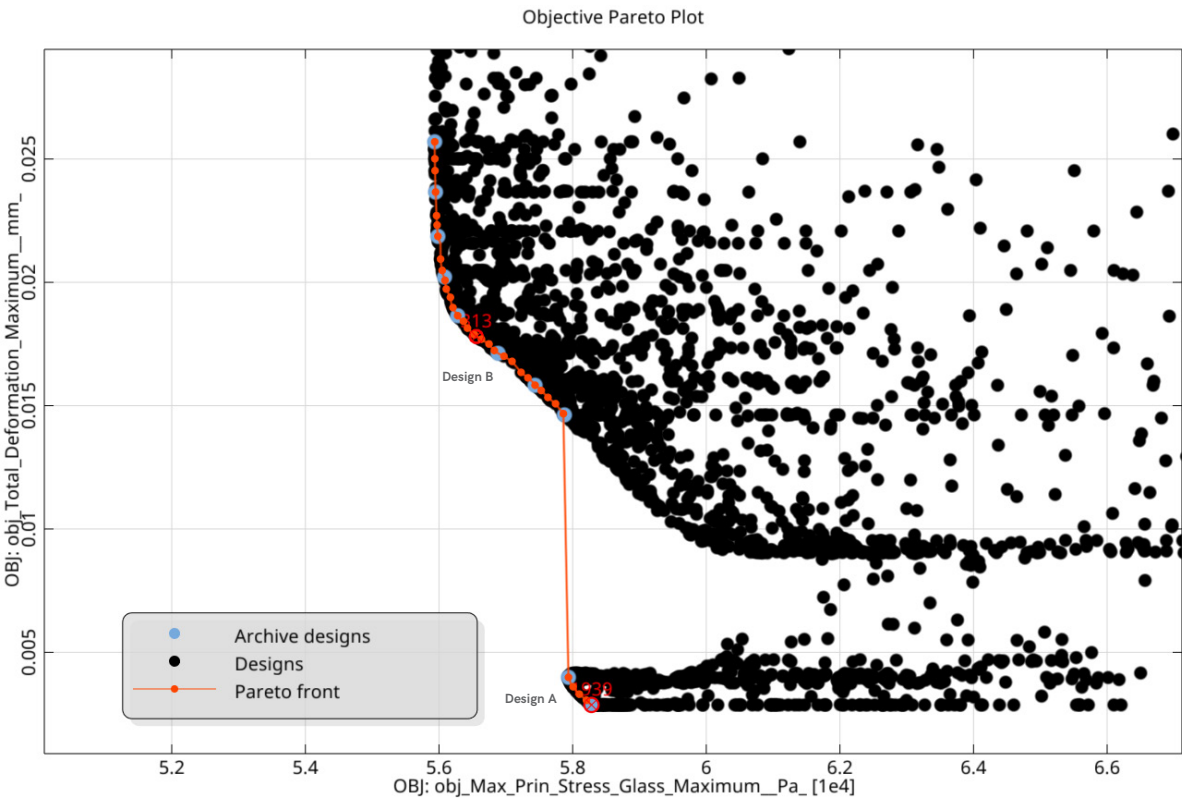


Figure 88: Comparison of the two design types



84 Figure 87: Pareto 2D plot- Tradeoff between objectives- minimize Total deformation and minimise maximum tensile stress in glass.

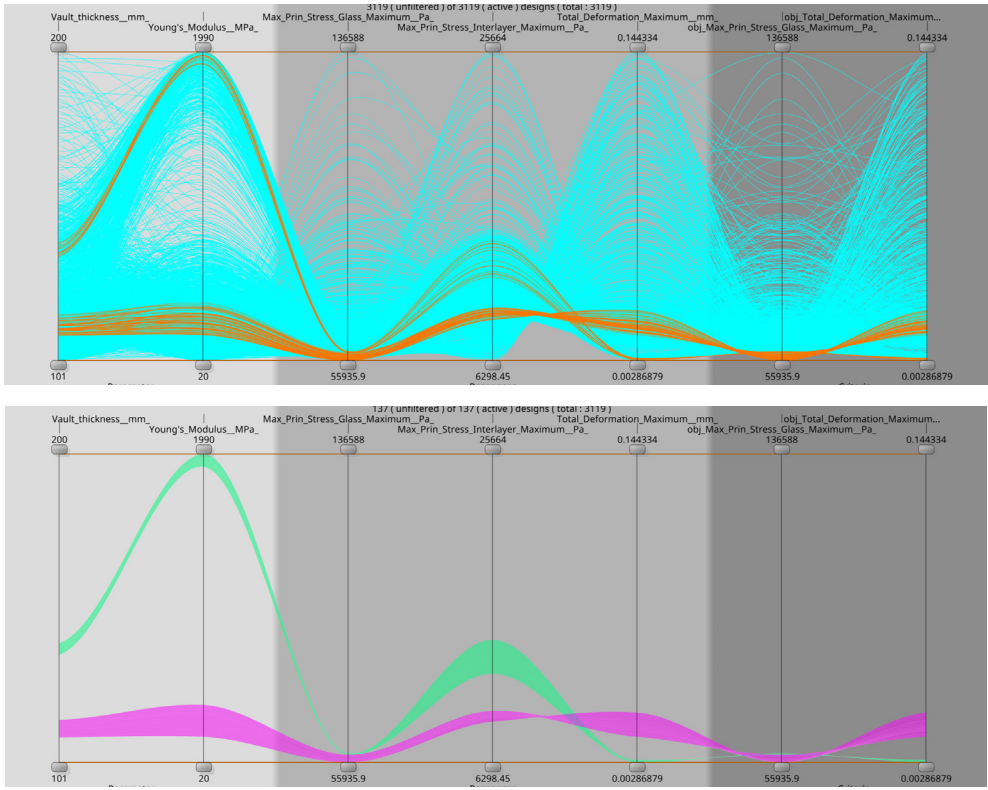


Figure 89: Two clusters of the best designs in the design space

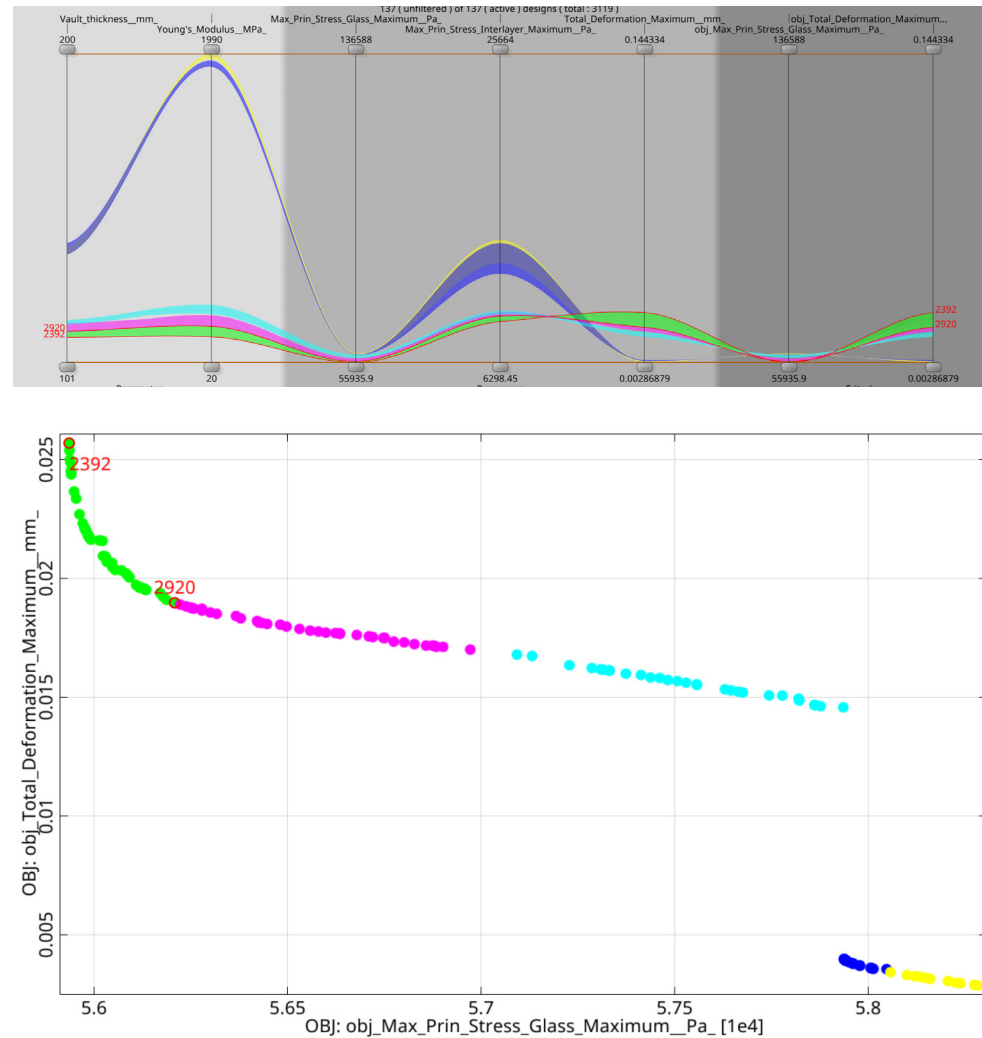


Figure 90: K-means Clustering of the Best Designs

9.4.5 Clustering of Best Designs:

The best designs were made into 5 clusters since the idea was to derive a stiffness range for engineering the interlayer in the next step. K-means clustering was used in this case as the objective was to make the clusters based on their values. The first cluster which causes the least stress in glass as seen in figure 90 was chosen as the range of Young's Modulus(E) for the

interlayer and vault thicknesses(t) to be considered. The two designs that define the range are:

Design 2392: E = 183.333MPa; t = 109.06mm

Design 2920: E = 250.493MPa; t = 111.086mm

9.5 Validation

The two designs that define the range of interlayer properties for the interlayer design along with their corresponding vault thicknesses were validated back in Ansys Mechanical with same boundary and loading conditions. Table 8 shows the predicted and FEA results.

Design Inputs			Responses	
Young's Modulus of the Interlayer(Mpa)	Vault Thickness (mm)		Total Deformation (mm)	Maximum Tensile stress in glass (MPa)
2392			Response Predicted	
	183.333	109.06	0.026	0.055936
	183	109	Actual (FEA)	0.015
2920			Response Predicted	
	250.493	111.086	0.018	0.056208
	250	111	Actual (FEA)	0.010

Table 8: Predicted and Actual results

Inferences:

Both the designs depicted a slightly lower deformation as well as tensile stresses in glass as well as in the interlayer. This is maybe due to the number of decimal places rounded off from optiSLang as more discrete values were considered for the geometry dataset.

The surrogate gives more conservative predictions in this case. Validation with FEA showed slightly lower deformation and tensile stress than predicted by the surrogate model within the mean errors, despite minor rounding of input parameters. This is likely due to small surrogate overestimations and nonlinear effects not fully captured in the model. The results remain within acceptable error margins.

The FEA presented better performance than predicted but within error margins, and thereby the range of designs- interlayer properties (Young's modulus 183-

250MPa) are considered for the interlayer engineering, but would need to be converted into stiffness in terms of mechanical behaviour as the obtained stiffness is in terms of young's modulus of a solid interlayer with density 1100kg/m³.

Performance of the vault under eccentric loading conditions:

Both vaults were analyzed under eccentric loading conditions in order to assess their performance with regard to global buckling under asymmetric loading.

Loads (figure#): Gravity loads with solid glass units (with equivalent with approximate density ~1403kg/ for hollow 3DP unit) and 10mm thick interlayer of 1100kg/cu.m.

Pressures on vaulted roofs due to wind as per Eurocode 1991-1-0 as shown in figure #.

A maintenance load as per Eurocode 1991-1-1, Dutch National Annex: uniform load of 0.4kN/sqm on overall shell, and a point load of 1kN applied on 100x100mm at the centre of the vault.

Boundary conditions: (Figure 92) Displacement

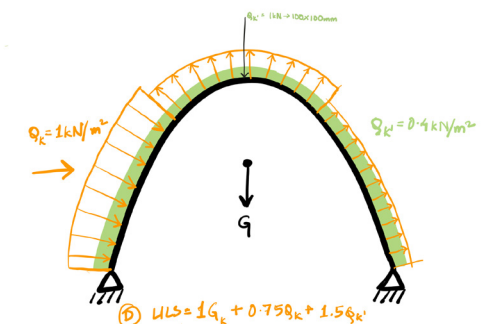


Figure 91: Loading conditions for Vault Performance

- A** Standard Earth Gravity: 9,8066 m/s²
- B** Wind pressure A: 600, Pa
- C** Fixed Support
- D** Displacement
- E** Wind pressure B: -900, Pa
- F** Wind pressure C: -300, Pa
- G** Maintenance load uniform: 400, Pa
- H** Maintenance point load: 1,e+005 Pa



Figure 92: Boundary conditions for Vault under eccentric load

supports at the free edges. Symmetry is used in one axis only since the vault is subjected to eccentric loading.

Results: The Vaults (as in table 8) are stable under these eccentric loading conditions only when the sides are supported with a displacement condition fixed at x and y directions as shown in figure 92. This suggests that edge restraints are probably inevitable in designing interlocking assemblies with glass when subjected to asymmetric loading.

Restraining edges lead to additional stresses in glass as seen in figure 93, and has to be carefully detailed out for application.

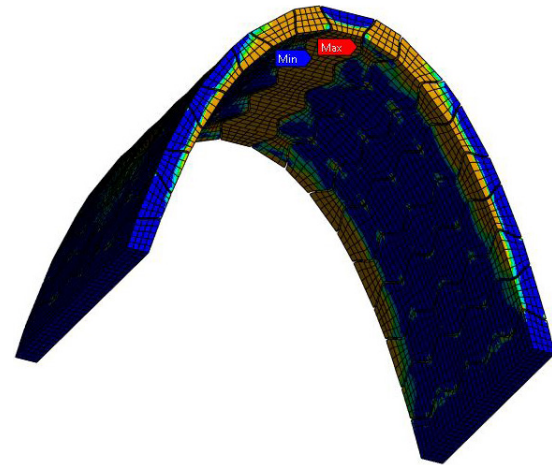
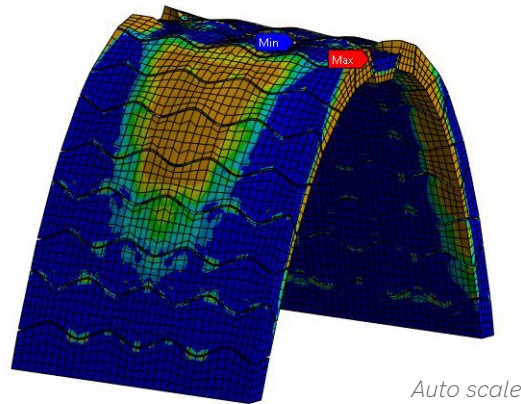
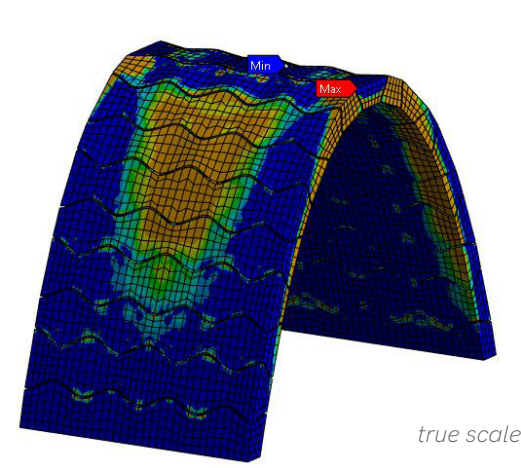


Figure 93: Stresses in glass maximum at restrained edges

Key take-aways

Catenary vault with input parameters of Vault thickness and Young's modulus does not have a clear relationship with the output performance criteria when vault is considered under constant loading conditions. This is because the output parameters are defined by a local maxima caused due to loading on the vault. Therefore it is considered to use a constant thickness in order to optimize with loading conditions.

The surrogate models presented had high accuracy and were robust as per the model qualities presented in chapter 9.4.3; however, the validation results vary slightly probably due to rounding off of parameters, and is overlooked in this case.

As inferred previously from 2D arch analyses with hollow vs solid bricks of low density, the hollow bricks depicted higher deformation and stress values. A final validation has to be done with hollow bricks to check the stress and deformation levels.

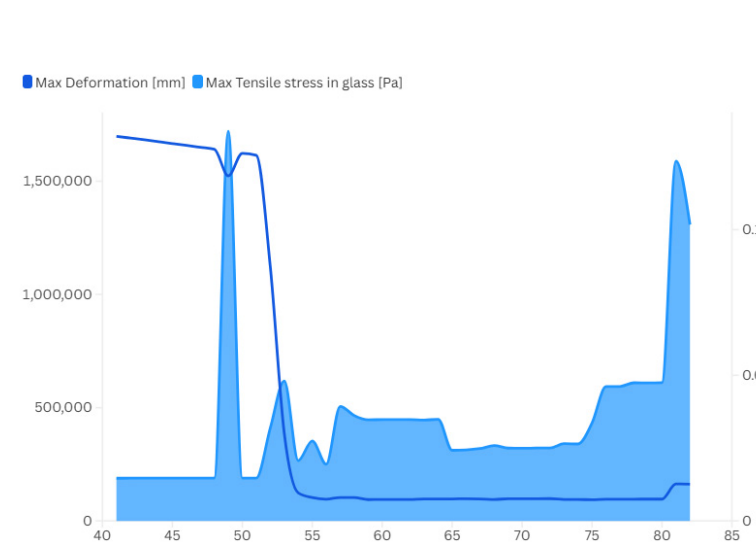
The required interlayer's young's modulus as inferred should be within the range of 183-250MPa. This is considering a solid interlayer of density 1100kg/m³ and has to be converted to stiffness range for the interlayer engineering presented in chapter 10.

Interlocking vault assemblies would likely require edge supports for a stable assembly under eccentric loading conditions.

9.6 Brick Amplitude

Since the amplitude of the osteomorphic unit was considered constant and assumed not to affect the overall total deformation as well as stress in glass, the amplitude had to be decided with a wall where lateral loads are applied. The amplitude of the unit will mainly help the bricks to interlock in place during assembly. However in case of a free standing wall, the amplitude would play a role in the total deformation when a lateral load is applied in one direction. This is considered as the standard bricks from the Catenary vault can be used to assemble a free standing wall as depicted in chapter 8.

The optimization process depicted for optimizing Catenary Vault parameters in the previous sections were followed for a free standing wall made using the defined standard blocks from the vault-
Wall Dimensions as per design (Chapter 8.3.2) : Length- 1m, Thickness- 110mm, Height- 2.5m
Boundary conditions: Fixed at the bottom
Displacement restricting x,y



90 Figure 94: Brick Amplitude vs Max deformation, tensile stress in glass

deformation.
Load applied: Self weight and lateral wind load of 0.5 kN/m^2 at ULS: $0.75 \times 0.5 = 0.375 \text{ kN/m}^2$ perpendicular to the length of the wall
Amplitude of brick (INPUT) : 40 to 82mm (as calculated for a 300mm brick with glass 3DP constraints in chapter 5.4.3.)
Interlayer properties as optimized in previous section.
Total design samples: $82 - 40 = 42$
Goal: to understand the relationship between the amplitude of the brick to total deformation for a dry assembled wall using osteomorphic brick units.
Response recorded: **Total deformation(OUTPUT) and max tensile stress in glass**

Results:

As seen in figure 94, there is a more complex relationship between the brick amplitude and the total deformation and maximum stress recorded. The deformation sharply decreases after 50mm brick amplitude but also is seen increasing after an amplitude of 80mm.

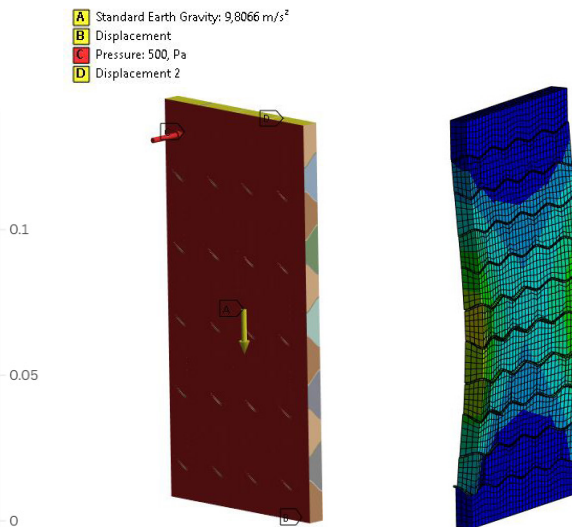


Figure 95: Boundary conditions, deformation at auto scale

It was observed from (Source: Oikonomopoulou et al., 2018) that increasing the amplitude enhances shear capacity by enlarging the contact surface, but at the same time, it raises the likelihood of shear-key failure a controlled and preferable failure mode that can serve as an early warning mechanism.

As per the FEAs, it was inferred that when the amplitude is increased over 50mm, slipping of bricks is reduced by the increasing shear capacity. When the amplitude is further increased over 75mm, the stresses in glass increase at the contact region (figure 96) when a lateral load is applied. Therefore, it is assumed safe to consider **~70mm amplitude** for the design.

Further simulations are required as to closely understand the behavior in order to optimize the amplitude of the block. This has to be further verified when the blocks are applied to the catenary vault under load conditions.

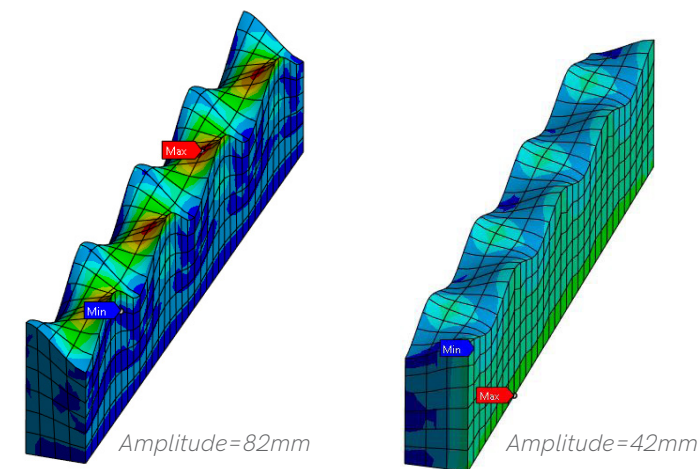


Figure 96: Stresses with high amplitude and low amplitude

9.7 Chapter Conclusions

This chapter detailed the development of a customized optimization workflow aimed at engineering the stiffness of a solid interlayer for dry-assembled glass vaults. By parameterizing both geometry and material properties, and integrating tools such as Grasshopper, Ansys, and OptiSLang, a robust and scalable method was established for evaluating the structural performance of different design configurations.

The focus was to identify a stiffness range for the interlayer that supports acceptable structural performance, particularly in compression-only systems like catenary arches.

The parameter sensitivity analysis confirmed that while stiffness is influenced by interlayer geometry (area and thickness) and material modulus, its impact on total deformation and tensile stress is not always direct or linear. This validated the need for surrogate modeling using methods like Polynomial Regression and Kriging to capture non-linear dependencies efficiently. The final selection of the Evolutionary Algorithm for multi-objective optimization was based on its robustness for handling complex, non-convex design spaces.

The required interlayer's Young's modulus as inferred from the simulations should be within the range of 183–250 MPa. The workflow developed in this chapter sets a foundation for more detailed optimization studies and supports the design of functionally graded or programmable interlayers in next chapters. It also emphasizes the importance of balancing computational feasibility with design flexibility in structural optimization tasks involving dry-assembled masonry systems.

10.0 | Engineering the kirigami interlayer

This chapter documents the process to reverse calculate the kirigami geometry (as chosen in section 7.3) parameters to achieve a given target stiffness.

Goal: To convert the obtained solid interlayer designs from the previous section to a kirigami geometry for application.

Assuming the interlayer as a simple linear spring with an area A under uniform load and deformation, the axial stiffness can be given by $k=EA/t$ as discussed in section 9. This equation is not valid for complex kirigami response. The stiffness of the designed kirigami geometry is can be determined with the following equation, when a pressure is applied on the kirigami thereby vertically pressing it down:

$$k = F_z/\delta_z$$

where F_z = Reaction force z component
 δ_z = Displacement in z direction

This kirigami stiffness would include bending, buckling, local geometry effects, cut patterns, out-of-plane motion, and therefore is not comparable to the theoretical axial stiffness $k=EA/t$ of a solid interlayer.

10.1 Defining the target stiffness range

As from the previous chapter, the target interlayer stiffness would be in the **range of the stiffness of a solid interlayer with young's modulus between 183Mpa and 250Mpa**. The effective structural stiffness of the solid interlayer at that E values is therefore determined using FEA. FEA was performed on solid interlayer sections with the same properties in order to derive their stiffness in terms of $k = F_z/\delta_z$. Table 9 shows the stiffness range converted from the young's modulus

range of the solid interlayer section having density 1100kg/m³. The target stiffness range for the kirigami is therefore between 315-415N/mm.

Solid interlayer range for selected catenary vault best designs			
Youngs Modulus [Mpa]	Density [kg/cu.m]	Thickness [mm]	Stiffness [N/mm]
E		t	
183	1100	10	315
250	1100	10	431

Table 9: Target stiffness range for the interlayer



Figure 97: Compression Test setup (Source: Fabrication-Integrated Design Lab MIT)

10.2 Target Stresses for the Kirigami

Initial compression tests on the kirigami structure were conducted at the Fabrication-Integrated Design Lab, MIT. The resulting stress-strain curve revealed a distinct linear elastic region prior to a plateau, which eventually led to structural failure. This pronounced elastic behavior indicated the potential for the kirigami to be used as a compliant interlayer, provided it operates within this linear regime.

For the intended application as an interlayer in a masonry vault, the goal was to utilize the kirigami within its elastic range. This ensures sufficient resistance to initial deformation while minimizing risks of buckling, creep, or long-term instability. To simulate this behavior, a linear transient structural analysis was carried out in ANSYS. The focus was on monitoring the reaction forces and deformation in order to record the stiffness, and also monitor the equivalent (von Mises) stress in the kirigami structure to evaluate the risk of yielding, using the material's known yield strength as a benchmark.

Other inferences from the activation of kirigami were taken into consideration for the parametric model for analysis as discussed in the section 10.4.

10.3 Material and Method

One of the key motivations for selecting kirigami as the basis for the interlayer design is its manufacturability from flat sheet materials, which are widely available and easy to process. This also presents a logistical advantage, as the inactivated kirigami can be transported in compact, flat form and only deployed on-site, reducing transportation complexity and cost.

Aluminum was chosen as the reference material for the

kirigami interlayer due to its mechanical compatibility with glass. It offers a similar Young's modulus and a closely matching coefficient of thermal expansion, thereby minimizing the risk of stress buildup from thermal mismatch in composite assemblies. Kirigami with Aluminum would also be easier to activate without using special equipments. While stainless steel was used for the initial physical prototypes at the Fabrication-Integrated Design Lab, MIT- primarily due to its availability in a variety of thicknesses- the material considered for the simulations in this thesis is aluminum. This selection supports the development of surrogate models based on material properties, with the understanding that final material selection may be revised during the prototyping phase.

Method:

The method used here can be outlined as follows:

- Defining the target stiffness in terms of N/mm from FEA on the solid interlayer
- Creating a surrogate model for the kirigami by performing FEA on varying geometry parameters of the selected kirigami- Tension Activated Kirigami (TAK). Inputs: geometry parameters and response: stiffness calculated from F_z/d_z .
- Perform an optimization with target stiffness range as calculated, with an objective to minimize stress in the kirigami as the idea is to stay within the elastic limit of the material.

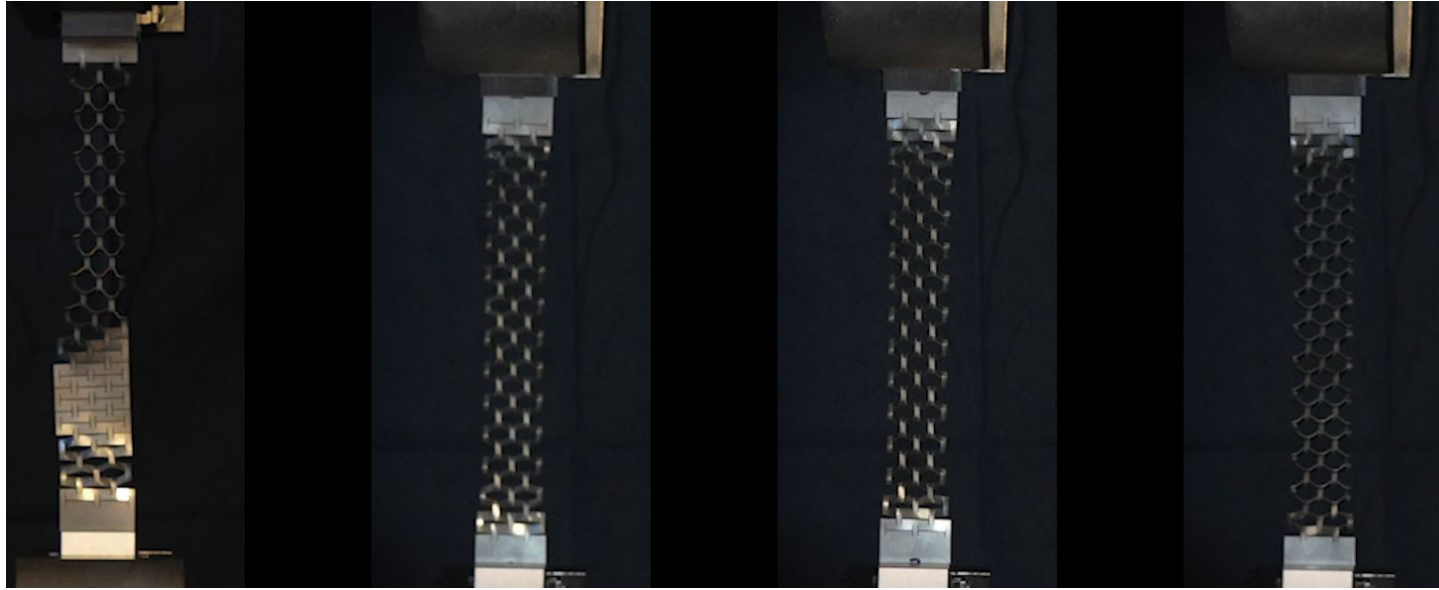


Figure 98: Activation of TAK samples (Source: Fabrication-Integrated Design Lab MIT)

10.4 FEA on kirigami geometry

10.4.1 Parametric model of Kirigami:

As inferred from the activation of TAK samples from MIT (Figure 98), following considerations and assumptions were made to parametrically model the same in grasshopper:

- The parameters L , H and W were considered from (Corrigan et al., 2023), as shown in the figure 96 which are used to define the cuts on the 2D sheet of material.
- As seen in figure 95 the vertical flaps tilt at a consistent angle from the vertical for a single sample. This angle depends on the parameters and thickness of sheet material chosen.
- There were anomalies of vertical flaps that activate in the opposite direction making the sample inconsistent after activation. This has been ignored in the parametric model.
- For simplification, activated kirigami pattern is parametrically modelled with the mentioned

parameters L , H , W , and two activation angles that defines the activated geometry as shown in the figure 99.

- The thickness is parametrized in Ansys Mechanical.

Kirigami is looked at as a metamaterial that can be tuned to achieve different mechanical properties, and further research is necessary to understand the relationship between the parameters and the activation angle.

10.4.2 FEA Analysis setup and workflow

To create the surrogate model and perform the optimization for the kirigami, the same workflow as used in section 9.1 for optimization of the overall design is used in this case in order to reverse calculate the kirigami geometry from the target stiffness. Since the kirigami has multiple modes for deformation and we will be using it in a dry assembly, Ansys tool Modal was used to consider the modal deformations at different frequencies as shown in figure 100. Ansys Transient was then used to derive the stiffness of the

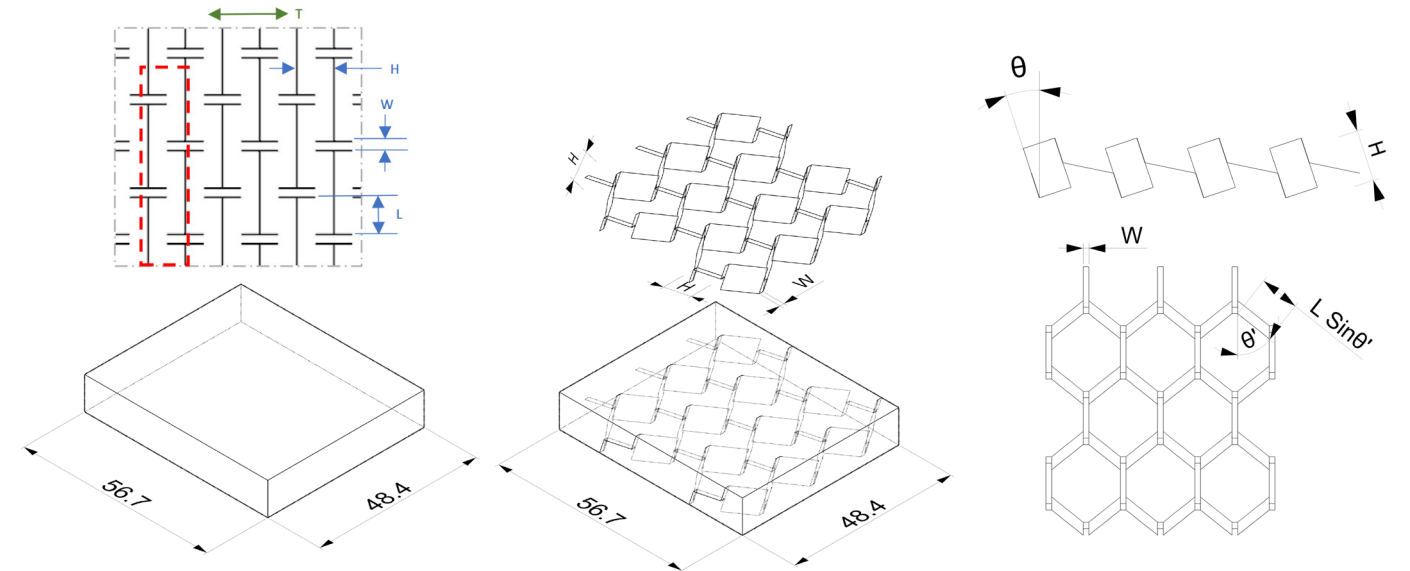


Figure 99: TAK parameters for activated kirigami model

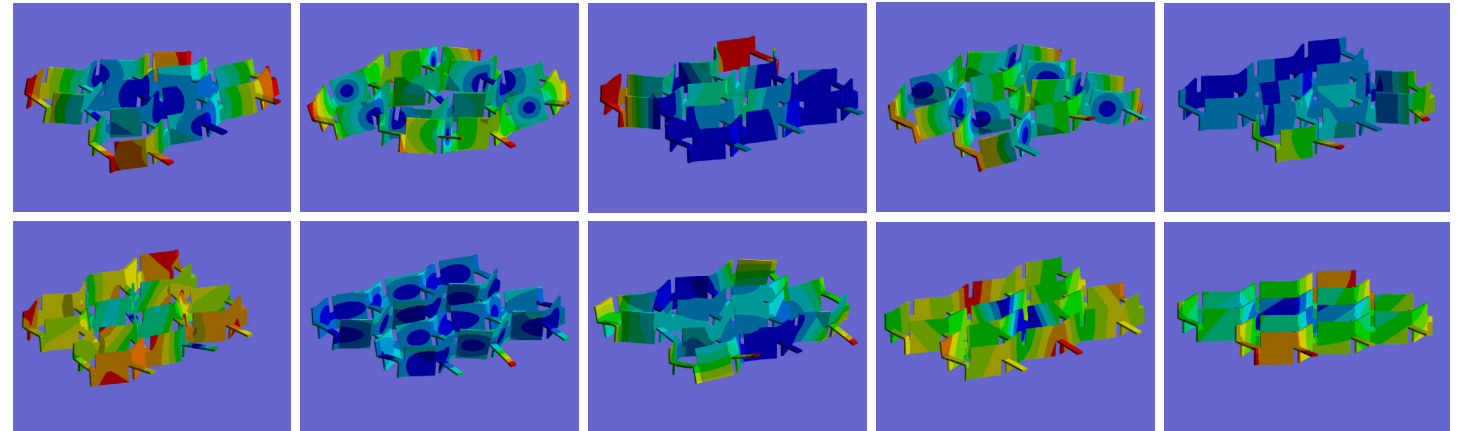


Figure 100: Several Modal deformations considered for FEA analysis

geometry when an incremental pressure is applied perpendicularly. Further description of the model setup has been documented in Appendix 2.

Boundary conditions: Pinned connection at the base since the vertical flaps can rotate as seen in the compression test (figure 97).

All parameters were not set to vary for this analysis. From (Corrigan et al., 2023) the parameter relation

was considered. The parameter W was kept constant at 1.2mm, since it only helps in activation and will not play a role in the stiffness. The parameters H and L were set to be equal as seen in (Corrigan et al., 2023) keeping the pattern uniform. The activation angles were also set as constant (refer Appendix 2).

10.5 Kirigami Surrogate Model

The desired input - stiffness of the kirigami was first calculated with the recored F_z and d_z in excel and Optislang's solver wizard was used to create the Metamodel for optimal prognosis-MOP (surrogate) for the kirigami. Following gives an overview of the created surrogate:

INPUT: Geometry parameter H and thickness of the sheet

RESPONSES: Stiffness of the interlayer, Equivalent stress in the interlayer

Following are the approximation methods used for each response as best suited:

- Linear Regression is used for approximation of Equivalent Stress maximum as well as stiffness.

The accuracies of the models are 99% and are depicted in figures 101 and 102.

Inferences:
Both the models CoD (fitting) indicates very good fit to training data as well as CoP (prediction) indicates strong generalization to unseen data. Only a very few outliers. The mean prediction and fitting errors for stiffness are around 19N/mm.

10.6 Reverse calculating the Kirigami geometry

Adaptive Response Surface Method(ARSM) is used in this case to create the surrogate model. ARSM is fast, there is only one input and 2 responses and a simple relationship is expected.

OBJECTIVE: Minimize equivalent Stress maximum

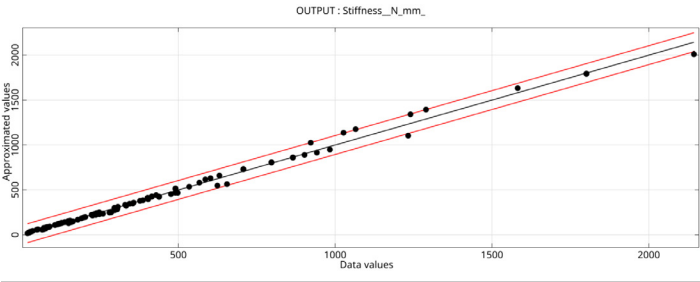
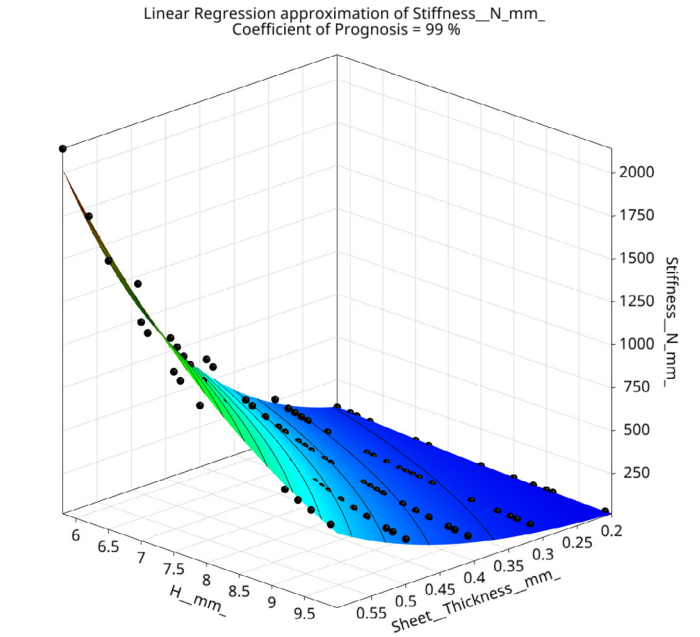
CONSTRAINTS: Target Stiffness between 315-431N/mm

Parameter H set to a constant oh 8.7mm which would result in an interlayer of 10mm thickness as per design. However, in case a sandwich interlayer is preferred, it can be tuned accordingly in order to achieve the stiffness target.

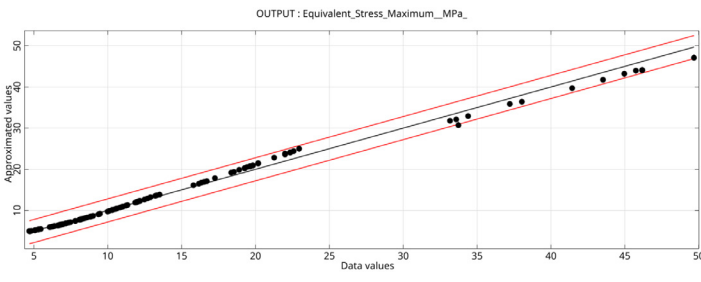
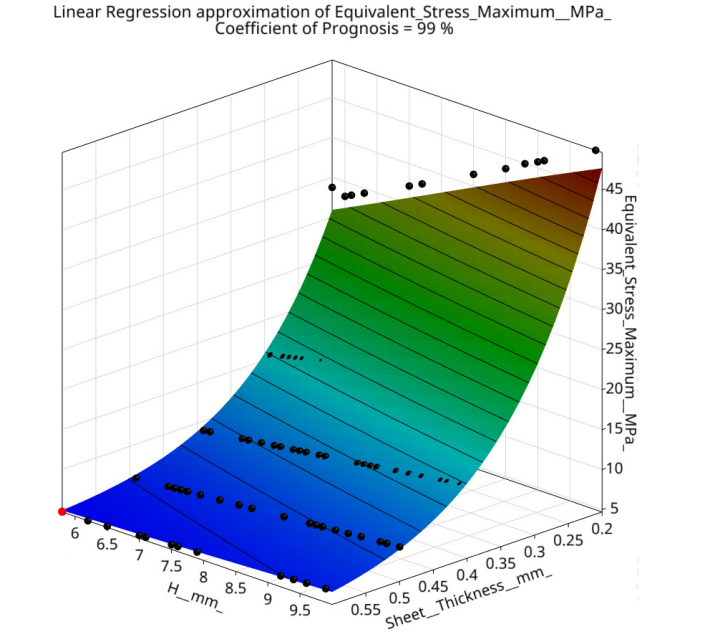
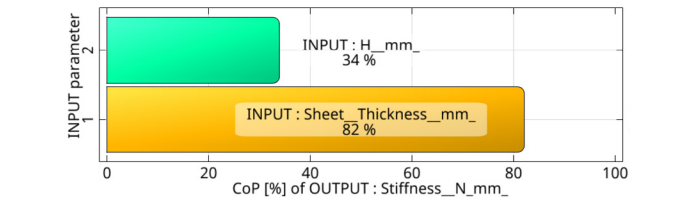
Inference:

The objective history plot as shown in figure 100 shows that objective stabilized within 25 iterations during the ARSM optimization, suggesting a relatively simple and smooth relationship between the kirigami geometry and its stiffness. The surrogate model based on linear regression was sufficient to capture the key trends, indicating that stiffness is primarily influenced by first-order geometric effects.

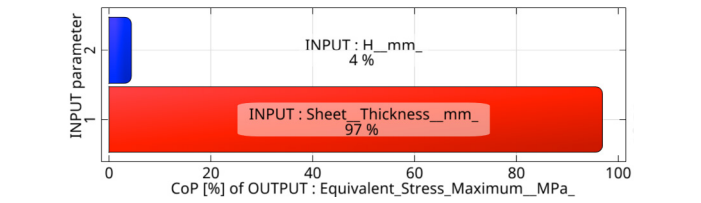
However, these results are expected to vary significantly when compared to physical test data. Therefore, the surrogate model should be calibrated with experimental results, and the optimized designs identified through ARSM can serve as candidates for physical sampling and validation.



Prediction errors		Fitting errors	
Max Error:	133.274	Max Error:	127.72
Mean Error:	19.1555	Mean Error:	19.0166
Root Mean Square Error:	35.05	Root Mean Square Error:	34.6225
CoP:	0.993016	CoD:	0.993186
		adjusted CoD:	0.992975



Prediction errors		Fitting errors	
Max Error:	3.02697	Max Error:	2.80773
Mean Error:	0.652077	Mean Error:	0.644075
Root Mean Square Error:	0.935202	Root Mean Square Error:	0.914968
CoP:	0.992901	CoD:	0.993205
		adjusted CoD:	0.992922



96 Figure 101: Stiffness MOP- Tension Activated Kirigami

Figure 102: Stress MOP- Tension Activated Kirigami

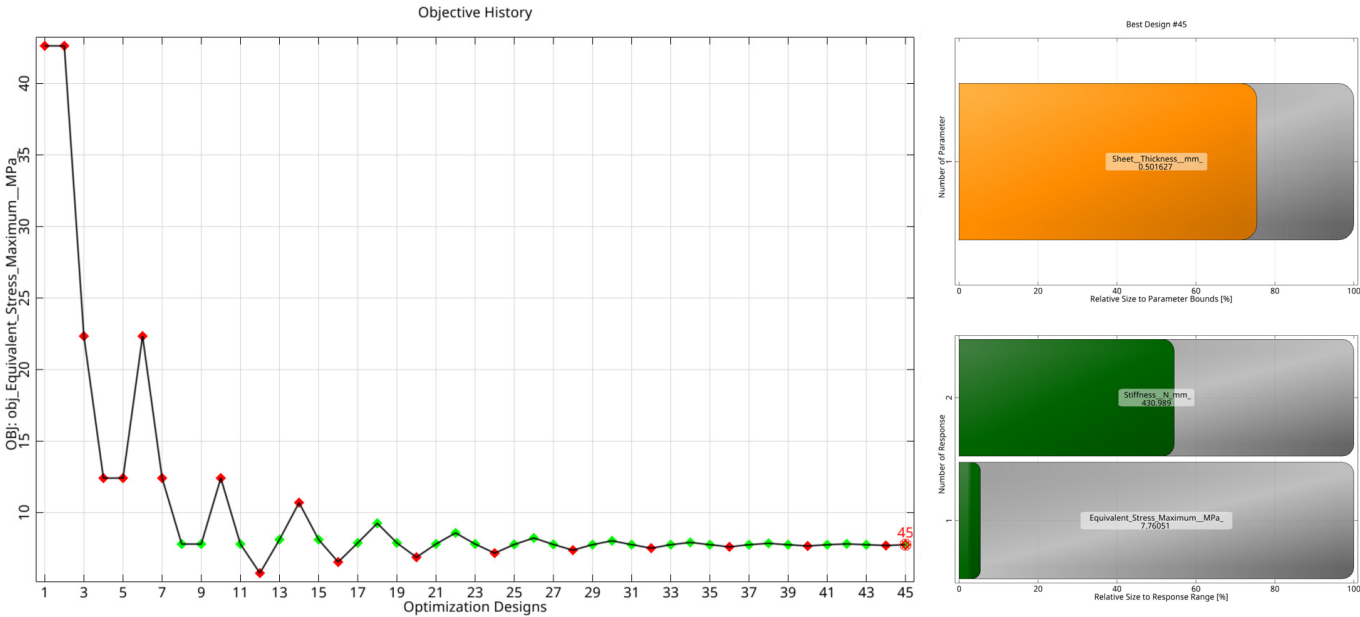
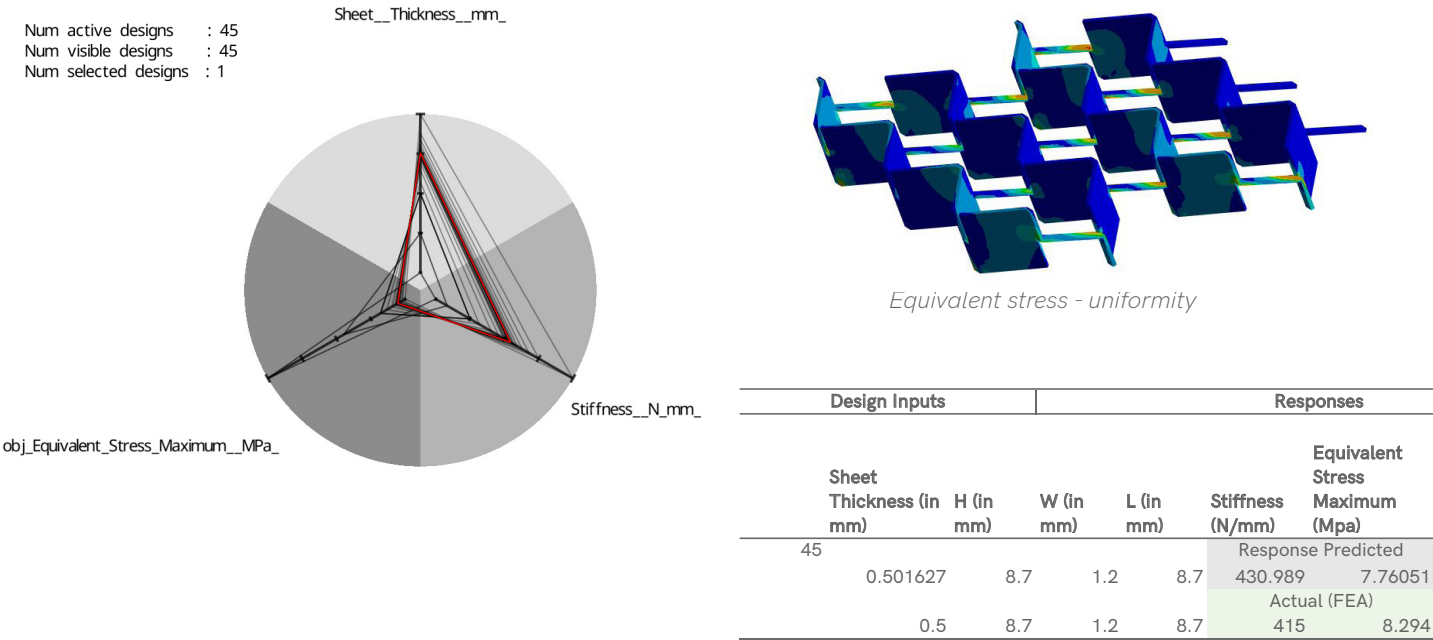


Figure 103: Objective History plot, and the best predicted design for kirigami



Design Inputs					Responses	
Sheet Thickness (in mm)	H (in mm)	W (in mm)	L (in mm)	Stiffness (N/mm)	Equivalent Stress Maximum (Mpa)	
45	0.501627	8.7	1.2	8.7	Response Predicted	
					430.989	7.76051
					Actual (FEA)	
	0.5	8.7	1.2	8.7	415	8.294

Table 10: Predicted results vs FEA results on best design

10.7 Validation

FEA was performed in Ansys Mechanical to validate the predicted performance of the best design selected. The sheet thickness was rounded off to 0.5mm due to material availability. The predicted and FEA results as shown in the table 10 validate the mean error of the surrogate model.

The stiffness of the kirigami as from FEA still lies within the stiffness range of the best designs of the catenary vault earlier specified. The equivalent stress as seen in the table 10 also shows that stresses are uniform, but it is assumed that this will not reflect in the case of osteomorphic shape, which has to be validated.

10.8 Kirigami Interlayer Performance

A 10 mm-thick kirigami interlayer was designed using the methodology outlined earlier in this chapter. Physical prototypes were fabricated to evaluate the performance of the kirigami interlayer in direct contact with glass. This testing aimed to identify a suitable interlayer material(s) and assess the contact behavior, particularly the potential need for a soft intermediate layer- such as neoprene- to mitigate localized stresses that could arise from direct contact between the metal interlayer and the glass surface.

Compression Test Set-up:

Three samples with same specifications were tested under compression using the setup shown in Figure 105. The specifications for the test components are below:

MDF: 2mm thick, 110 x 110 mm (as a buffer between glass and the compression machine head)
Glass: 8 mm float glass, 100 × 100 mm (wrapped with foil on one side only - the side towards the mdf)
Kirigami Interlayer: 10 mm thick, covering an area larger than the glass, with parameters: H = 8.7 mm,

W = 2.2 mm, L = 8.7 mm made with 0.5mm thick aluminum sheet.

Loading: 0.01mm/sec, the loading plate available was 6x12cm which was smaller than the glass(10x10cm). *The results here are considered as initial observations. It is therefore suggested to perform further tests with plates larger than the glass for a uniform loading.*

Multiple kirigami samples were produced to investigate the influence of the width parameter (W) on achieving a uniform activation pattern. These samples and corresponding observations are documented in Appendix 3. While the activation force and criteria for ensuring consistent deployment of Tension Activated Kirigami (TAK) fall outside the scope of this thesis, they are currently the subject of ongoing research at MIT.



Figure 105: (above) samples; (below) Compression test set-up

Compression Test Results:

The maximum capacity of the equipment available was 10kN. Following observations were made during the test-

- The glass did not crack with the applied load for all three samples.
- The kirigami interlayer deformed from state (a) to state (b) as seen in figure 107 for all three samples. The vertical flaps were close to 90 degrees vertical.
- Figure 108 shows the force vs displacement graphs of the three sandwich samples tested. A linear-elastic portion can be seen typically below 1mm displacement.

Further, to check the behavior with higher loading, another sample was tested using a manual load equipment setup as shown in figure 106. Above 10kN the kirigami interlayer was seen to buckle state (c) (figure 107). At around 19kN the test was stopped since the lower glass plate had already cracked- and the test was stopped. The glass cracked on the edge of the loading plate as illustrated in figure 106. **Three samples were further tested with a larger loading head which confirms the buckling of kirigami without damaging the glass and is presented in the Appendix 3.**

Stiffness of the Sandwich:

Displacement data for the three samples is filtered up to 1mm displacement and linear regression is applied to get the stiffness value (refer figure 108).

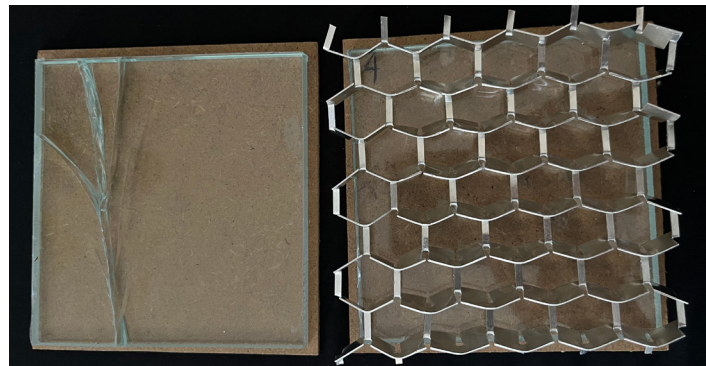
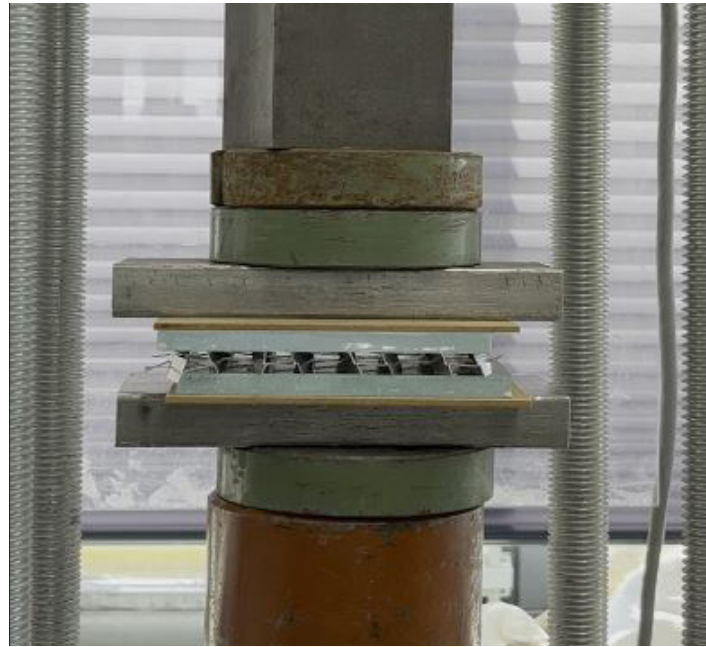


Figure 106: Sample 4 showing buckling of kirigami interlayer and glass failure due to experiment setup

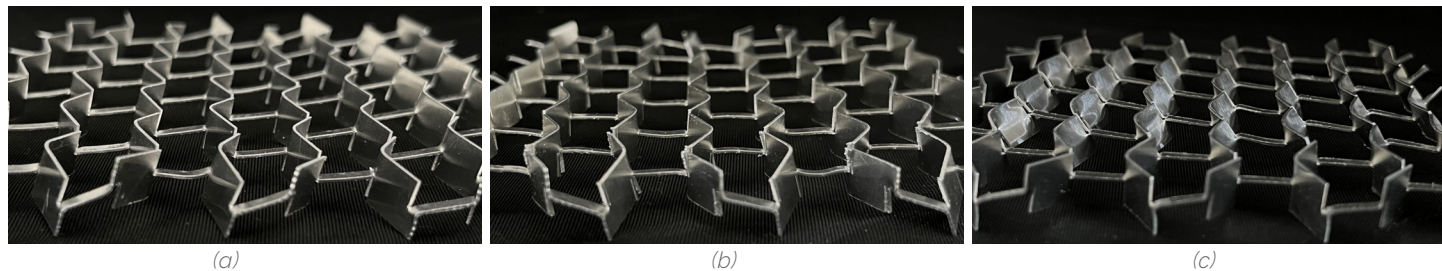


Figure 107: (a) Activated kirigami - vertical flaps at an angle; (b) Kirigami after 10kN applied force - vertical flaps almost 90 degrees vertical; (c) Kirigami after 19kN applied force- buckling of vertical flaps starts over 15kN

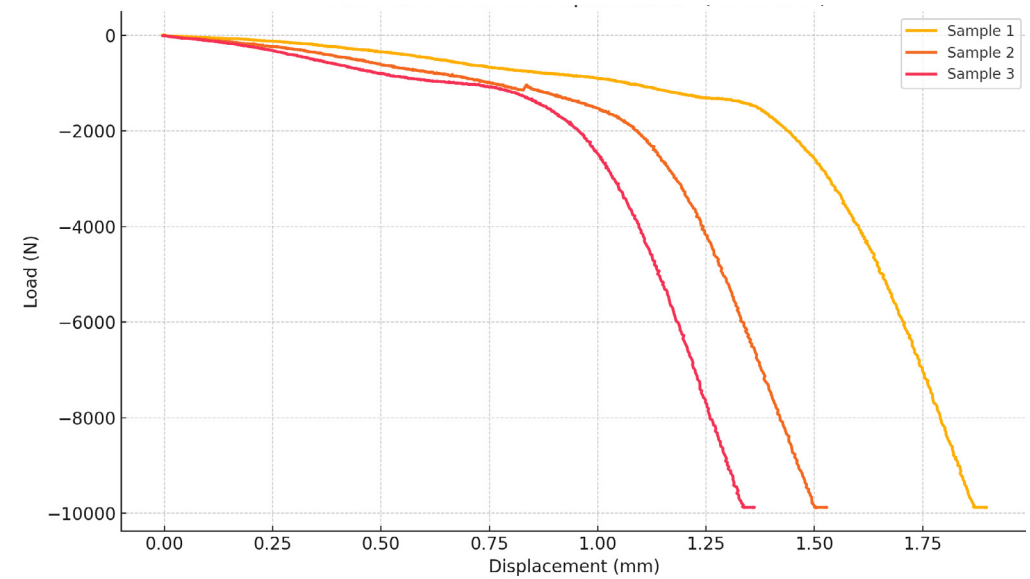


Figure #: Load-Displacement graph of the three samples

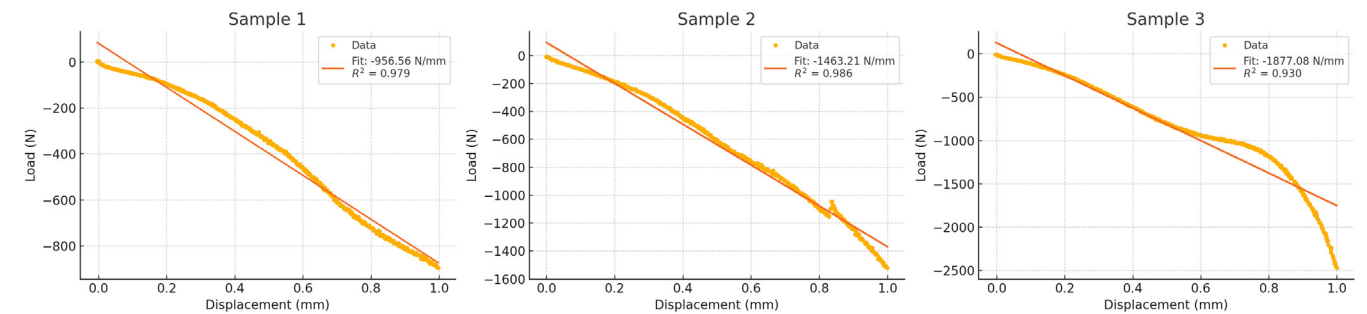


Figure 108: Initial Linear Region Fits (Displacement $\leq 1\text{mm}$)

Stiffness of the Kirigami interlayer:

To determine the kirigami aluminum interlayer's stiffness from the sandwich test, the stiffness of the other two materials were removed using the concept of series stiffness.

$$\frac{1}{K_{\text{total}}} = \frac{2}{K_{\text{MDF}}} + \frac{2}{K_{\text{glass}}} + \frac{1}{K_{\text{kirigami}}}$$

K_{total} = Total stiffness of the sandwich

K_{MDF} = Stiffness of MDF (2 layers considered)

K_{glass} = Stiffness of glass (2 layers considered)

K_{kirigami} = Stiffness of the kirigami interlayer

The stiffness of the 8mm thick float glass and 2mm MDF is determined by $k=EA/t$, assuming the young's modulus(E) of glass being 70GPa and that of MDF being 3GPa.

$K_{\text{MDF}} = 15,000\text{N/mm}$ per layer

$K_{\text{glass}} = 87,500\text{N/mm}$ per layer

Table # summarizes the stiffness values of the sandwich and the kirigami interlayer for the three samples. Because the MDF and the glass layers are much stiffer, their contribution to overall deformation is minimal. The stiffness of the kirigami is closer to 10^1

Sample	Sandwich Stiffness (N/mm)	Stiffness of the Kirigami interlayer (N/mm)
1	957	1125
2	1463	1896
3	1877	2656

Table 11: Calculated Stiffness of the sandwich and the kirigami interlayer

the stiffness of the sandwich. It is observed that the kirigami with parameters as calculated in the earlier chapter, in reality is much more stiffer than simulated on a parametric activated model of the geometry. All three samples show stiffness more than double of what is required and optimized for. Therefore we can say that more experimental research is required to tune the kirigami interlayer to the desired stiffness level to be used as an interlayer for the catenary vault structure.

Conclusions and Future work:

The tested kirigami samples turned out to be at least two times stiffer than the required optimized value for our interlayer application. This suggested that the activated kirigami parametric model does not resonate well with actual activated kirigami geometry. There are many more factors to be considered to fine tune the kirigami parametric model. A better suggestion is to simulate the activation in Ansys each time for an activated model instead of modeling the same parametrically on grasshopper. This process will take much more time to create the surrogate model as non-linear deformations need to be captured for the kirigami activation, but will result in a more realistic prediction model.

The suggested thickness of the interlayer needs to be reconsidered since 10mm thick interlayer needs to

accommodate for the surface deviations of the 3DP glass. Therefore, the kirigami interlayer can be 5-6mm so as to keep the glass elements at a safe distance from each other. Further detailing is necessary considering assembly of a designed interlocking masonry structure.

Key take-aways

The effective structural stiffness bounds were defined by performing FEA on a solid interlayer with optimized property range defined in the last chapter.

A parametric model of Tension Activated Kirigami (TAK) was made assuming uniformity in the activated geometry, considering factors of activation as seen from the physical tests done at MIT and parameters of the cut-pattern for manufacturing.

A surrogate model was created using Linear Regression approximation with a mean prediction error of 19N/mm in stiffness. The validated model gave expected results with actual stiffness lower than predicted, but is within the range specified for a best performing design.

These results differ from physical tests of the kirigami prototypes created using the same parameters which exhibited double the stiffness value, so the surrogate model should be calibrated experimentally based on more tests.

One major inference from the compression testing was that the aluminum kirigami interlayer buckles without causing a crack in the glass suggesting that such kirigami geometry in aluminum can be used as an interlayer between glass elements, however more experimental validation is required with different materials/ parameters of the kirigami geometry and 3DP glass surface.

10.9 Chapter Conclusions

This chapter outlined the process of reverse-engineering kirigami geometry to achieve a target stiffness range suitable for use as an interlayer in compression-only masonry vaults. Starting from a solid interlayer benchmark, finite element analysis (FEA) was used to determine equivalent stiffness values, which then served as the target for kirigami design optimization.

A parametric model of Tension Activated Kirigami (TAK) was developed, informed by physical activation behavior observed in earlier prototypes. Using a linear regression model, the relationship between geometric inputs - cut height and sheet thickness- and the resulting stiffness and stress was established with a mean prediction error of 19 N/mm. The optimization was performed using the Adaptive Response Surface Method (ARSM), with the goal of minimizing equivalent stress while meeting a stiffness constraint between 315–415 N/mm. The optimization quickly converged, indicating a smooth and well-behaved design space. The final design identified by the surrogate and ARSM framework is a **TAK interlayer with a sheet thickness of 0.5 mm, which achieves the upper target stiffness of 415 N/mm.**

Validation of the surrogate predictions confirmed performance within the required range, though deviations from predicted values emphasize the need for experimental calibration. The tested kirigami prototypes exhibited more than double the strength required for application as an interlayer- thereby suggesting a way to calibrate the kirigami surrogate model based on physical testing of kirigami samples. This remains in the scope of future work. Overall, this chapter demonstrates that kirigami, when treated as a tunable metamaterial, can be engineered to achieve structural stiffness targets- provided physical validation and iterative refinement are integrated into the design loop.

11.0 | Validation

This chapter documents the further validations performed using FEA on discrete models with the parameters optimized in the previous chapters to propose a final design.

Goal: To validate the results obtained with respect to the catenary vault design.

11.1 Stiffness of kirigami on an osteomorphic plane

Since the proposed asseblly of catenary vault uses osteomorphic units, the kirigami performance has to be validated for the same.

In this case, the model used for simulation was a kirigami geometry with the parameters inferred from the previous chapter onto an osteomorphic unit shape of the brick. A FEA was done by applying a pressure on the geometry vertically downwards which resulted in a stiffness value of 500N/m with irregular stresses as shown in the figure 103 *However, in case of the vault assembly, the pressure will act perperdicular to the osteomorphic surface and therefore the simulation needs to be performed with osteomorphic units/ surfaces on either side of the kirigami interlayer.*

The resultant mesh of the kirigami alongwith the interlayer has more than 10,000 mesh faces as seen in figure 104. This simulation was computationally intensive requiring over 250gb of RAM memory and could not be solved using Delftblue supercomputers. Further work is necessary in order to simplify and validate this using FEA. Physical tests are suggested to be performed in order to assess the performance of the kirigami interlayer on a 3DP osteomorphic glass surface.

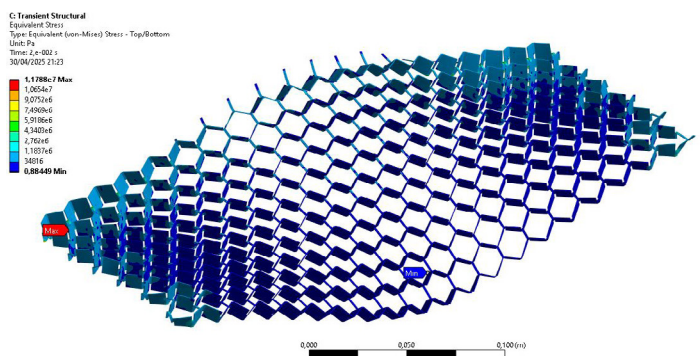


Figure 108: Stress distribution pattern in the interlayer when a vertical pressure is applied (2x)

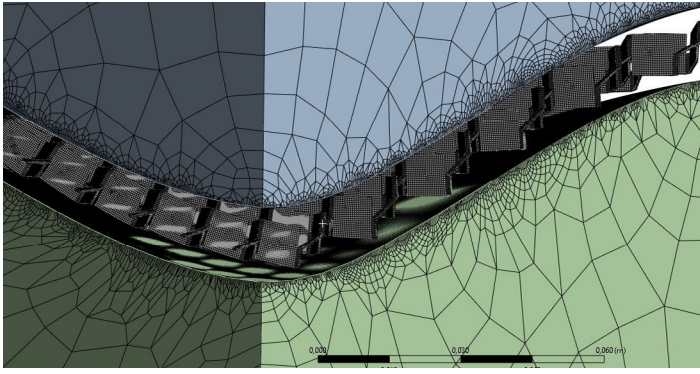


Figure 109: Meshing in Ansys Mechanical

11.2 Vault Design with 3DP units

The final Catenary vault proposed as shown in figure 111 to validate using hollow bricks with the optimized interlayer properties, and with eccentric load conditions. The vault design draws inspiration from the glass vault case study discussed in Chapter 2, particularly the use of stepped free edges- an approach derived from traditional barrel vault construction techniques. In this proposal, the stepped edge also facilitates the dry-assembly process by enabling a more stable and sequential placement of units discussed in chapter 12. Additionally, it was observed that under asymmetric loading conditions, the free ends of the vault require supplemental support to maintain structural stability.

In this section we validate the design with the optimized parameters, with more realistic eccentric loading conditions. We also compare the same if a soft interlayer is used, and the possibility to use a combination of 3DP and cast glass units.

Analysis 1- Eccentric loading on 3DP glass masonry vault with optimised interlayer

Loads: Gravity loads with hollow glass units (density 2450kg/cu.m) and 10mm thick interlayer of 1100kg/cu.m.

Pressures on vaulted roofs due to wind as per Eurocode 1991-1-0 as shown in figure 105.

A maintenance load as per Eurocode 1991-1-1, Dutch National Annex: uniform load of 0.4kN/sqm on overall shell, and a point load of 1kN applied on 100x100mm at the centre of the vault.

Boundary conditions: fixed at the bottom
Symmetry is used only along one axis since loading

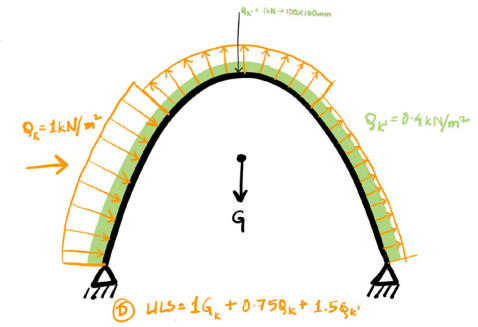


Figure 110: Loading conditions for Final Vault design

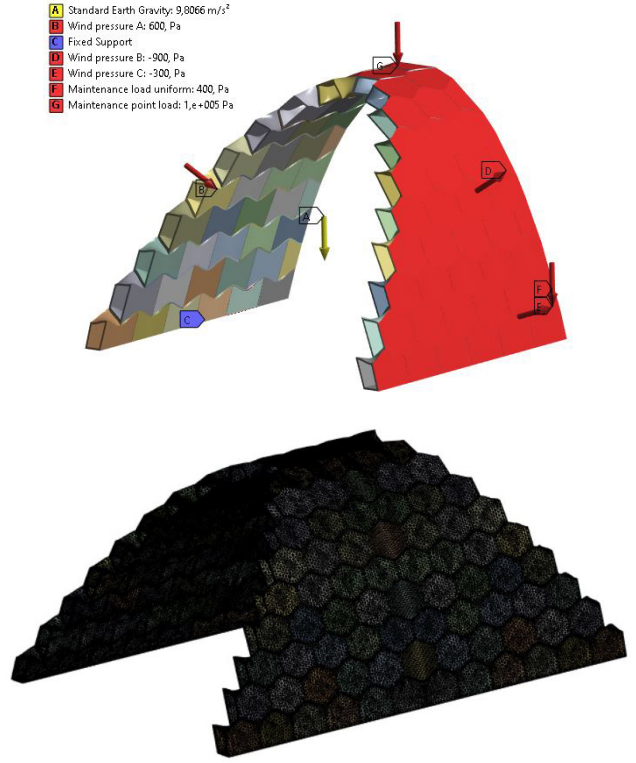


Figure 111: (above) Loading and Boundary conditions on stepped vault with symmetry; (below) Meshed vault

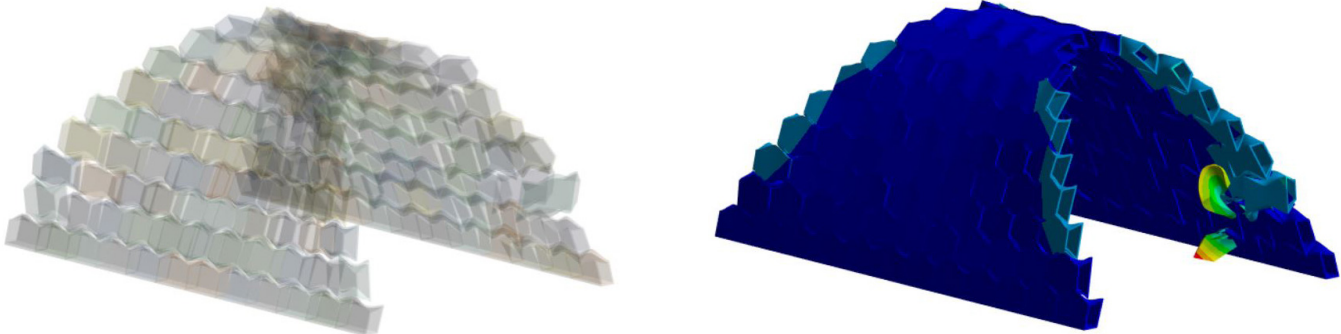


Figure 112: Unconverged solution for the stepped 3DP glass masonry vault design

conditions are eccentric.

Contacts: Frictionless contacts between glass-glass .
Frictional contacts between glass-interlayer with a frictional coefficient of 0.2

Results: Unconverged solutions- different friction coefficients (0.15, 0.2, 0.5, 0.8, 1.5) were tried but all designs failed to converge. Following observations were made-

- The masonry units at the free edge are only half interlocked- and therefore tend to slip out as seen in figure 112. *The stepped design therefore might not be a good solution for the interlocking mechanism*
- The vault tries to deform outwards indicating that its light-weight. *This suggests that optimizing the vault for lesser weight is not the possible solution when the vault is subjected to eccentric loading and edges are kept free.* Edges need to be restrained in such cases as discussed in section 9.5 earlier.

The meshing of the structure were found to be critical to achieve a stable solution since it is an interlocking structure subjected to asymmetric loading conditions. Several iterations of meshing strategies were used to simulate efficiently and have been demonstrated in Appendix 2 of the report.

Several strategies of edge constraints and increasing vault's weight using cast glass masonry units towards the top of the vault and the edges were then considered. The design options for a stabilized vault under these eccentric load conditions are presented in the next section.

11.3 Final Vault Design

The following table 11 depicts strategies to stabilize the designed vault under eccentric loading conditions. Stable solutions were achieved only after restraining the edges completely and refining meshing on ANSYS as depicted in Appendix 2. The solutions typically fail with abnormal behavior of the solid interlayer which could be a meshing issue. A higher friction coefficient of 0,2 was used in these analysis.

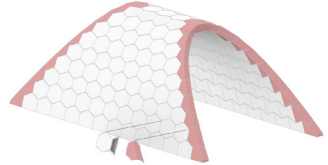
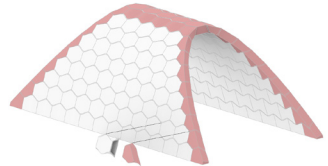
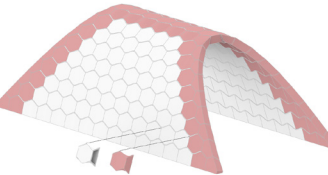
Design Strategy		Maximum Total Deformation (mm)	Maximum tensile stress in glass (MPa)
A	 Units added at the free edge- made out of cast glass and restrained in x, y, and z directions	0.09	7.8
B	 Units added at the free edge- made out of cast glass and restrained in x, y, and z directions + three rows at the top including the keystones considered as cast glass units	0.15	5.6
C	 2 rows of free edge units made out of cast glass and restrained in x, y, and z directions and three rows of units at the top considered as cast glass units for added mass	Did not converge to a solution due to extreme memory requirements	

Table 11: Design strategies for stabilizing the final vault design under eccentric loads

The vault can also be simplified to a simple catenary vault as optimised for and validated under these load conditions in section 9.5. *The friction coefficient is a crucial factor for the assembly yet to be determined by experimental tests. Another material can be used to achieve a higher friction coefficient on either side of the kirigami interlayer- with a clipping mechanism to the glass unit.*

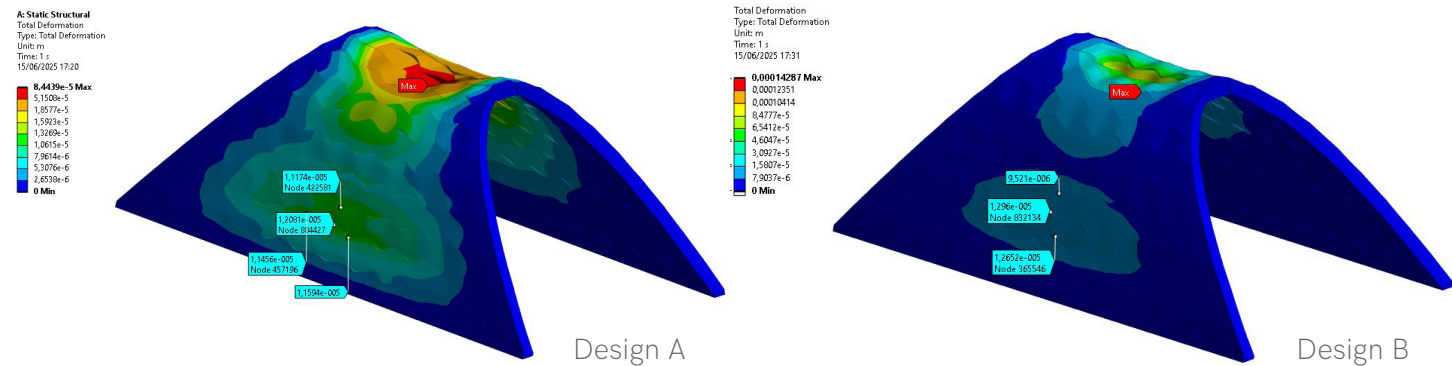


Figure 113: Deformation of designs A and B at AUTO-SCALE

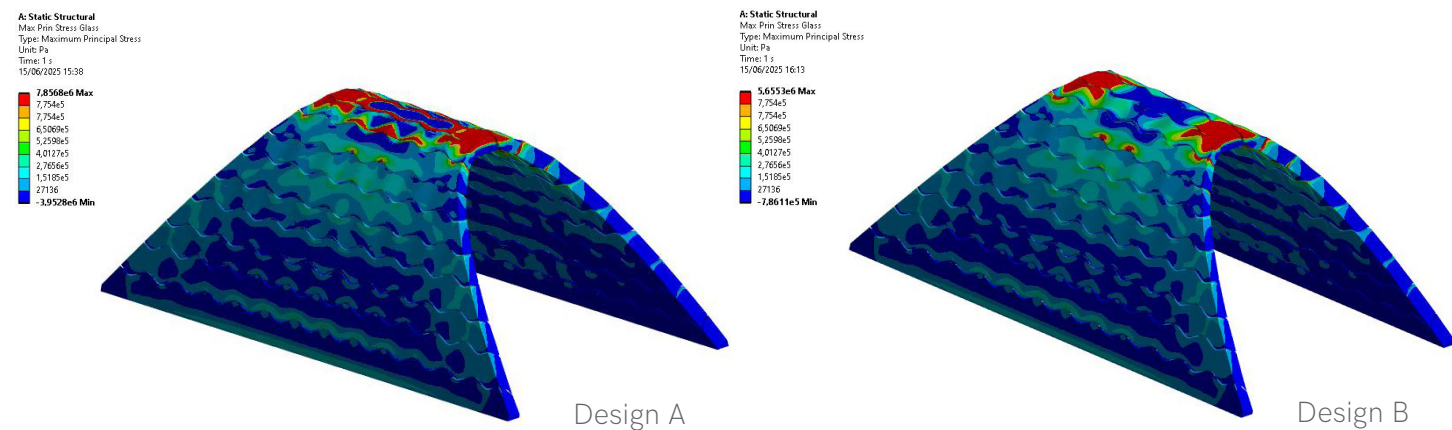


Figure 114: Maximum Tensile stresses in glass for designs A and B at true scale.

Inferences: As shown in Figure 113, both designs exhibit maximum deformation at the crown where the point maintenance load is applied.

Design B, which places heavier cast-glass units at the top, demonstrates improved interlocking. This is evident from the reduced lateral displacement under wind loading compared to Design A, which uses lighter 3D-printed hollow glass units. The lower side displacement in Design B indicates a more stable assembly. And at the same time, Design A showcases higher stresses in glass at the keystone area since the edges are now heavier.

trade-offs. As seen in Figure 114, it results in lower stress concentrations in the glass but it increases material usage and mass of the structure. While tensile stresses in both designs remain below the allowable tensile strength of glass, the increased weight only at the edges leads to greater internal forces with the 3DP hollow units next to them for design A, particularly near the fixed supports.

In summary, a heavier vault improves interlocking performance but increases material use and the mass of the structure overall. Although the inclined vault geometry helps reduce overall tensile stresses, it can compromise interlocking efficiency- highlighting the balance between structural performance, material

optimization, and assembly behavior. A more feasible design need to be selected based on the assembly detailing and re evaluating the interlayer to allow tolerances.

Key take-aways for design

A stepped design might not be a good approach for interlocking assemblies as edge units need to be restrained for a stable solution under eccentric loading.

Vault geometry (inclined shape) helps reduce tensile stress but may undermine interlocking.

Balance is required between material use, interlocking stability, and stress distribution.

Final designs explored combinations of 3DP and cast glass units for optimized structural behavior.

Kirigami interlayer- The performance of the kirigami on an osteomorphic surface is not determined, physical testing for the same is suggested considering the kirigami prototypes behave very differently than the parametric model as seen in the previous chapter. The kirigami surrogate needs to be replaced with physical test data instead of FEA data for more realistic predictions. An alternate could be to simulate the activation of kirigami within Ansys before testing compression behavior with FEA.

At the end, it all comes down to assembly detailing for the interlayer to select a possible design solution- by re-evaluating the design with an interlayer which would allow for necessary tolerances for taking care of the surface deviations of the masonry units as well as necessary friction for a stable assembly.

¹⁰⁸ This improved interlocking in Design B comes with

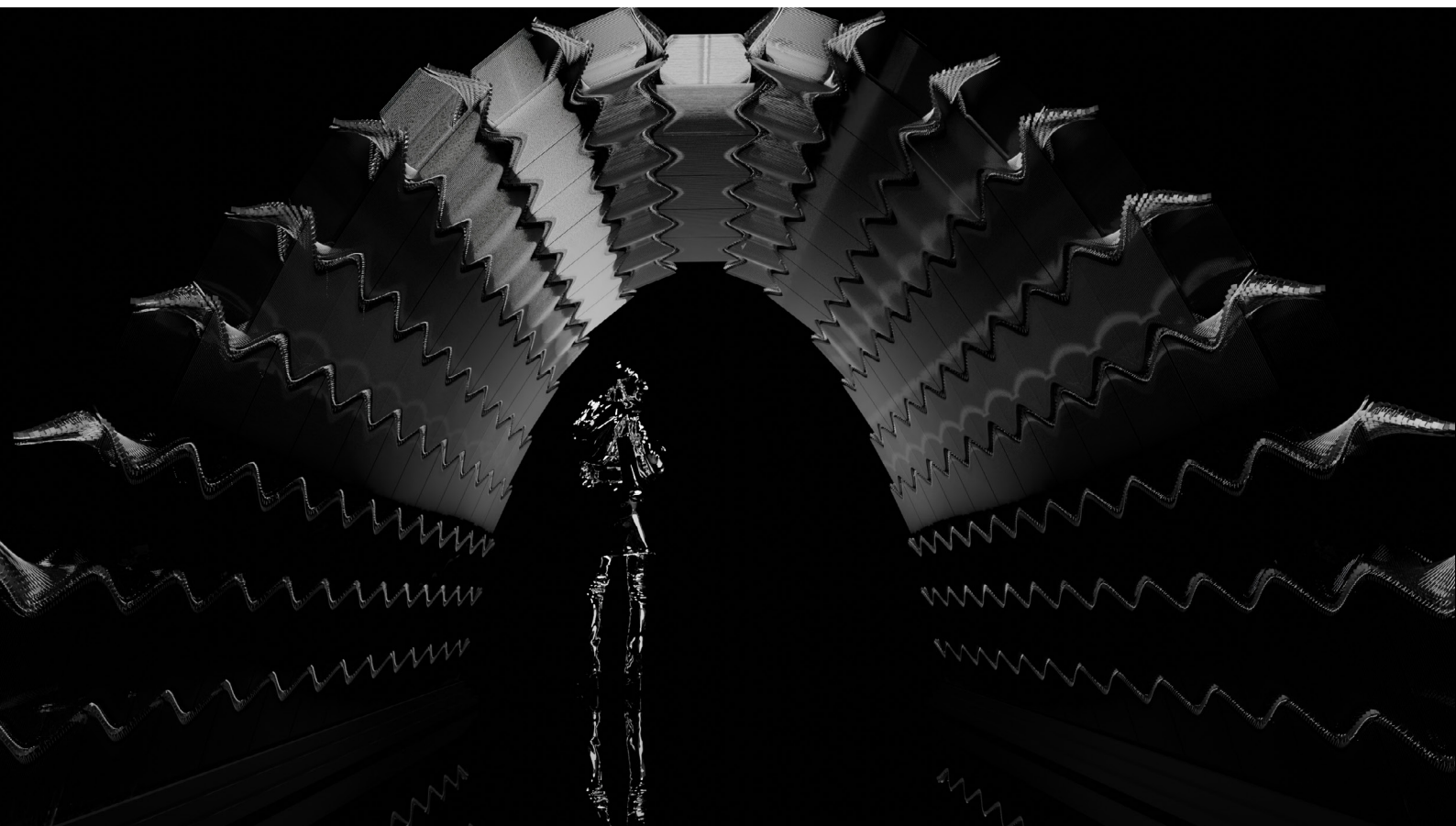


Figure 115: Impression of the designed vault

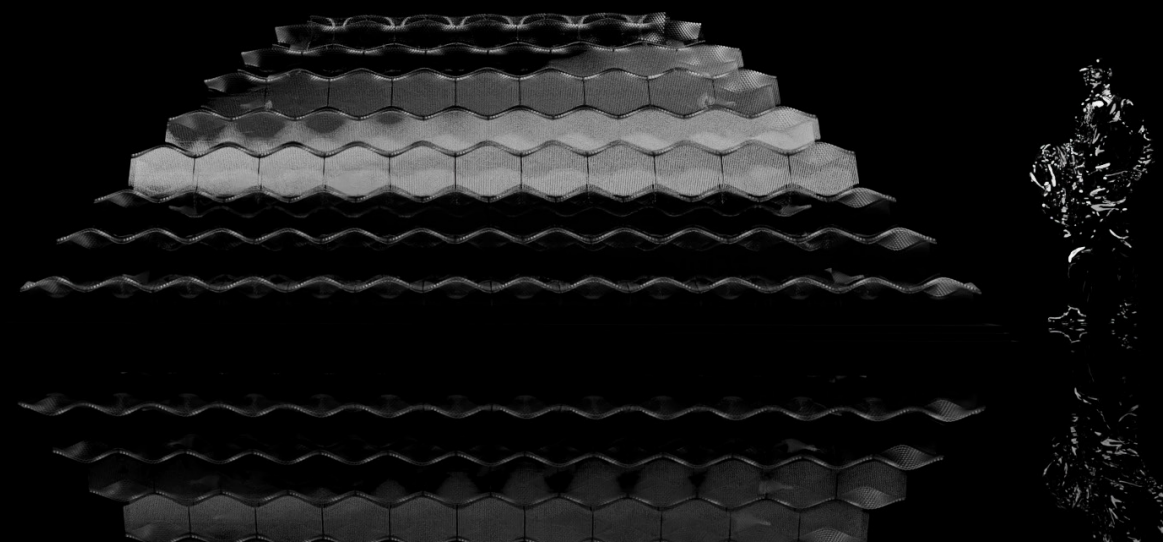


Figure 116: Impression of the designed vault

12.0 | Assembly and Detailing

The Assembly process would be very crucial in this case because- it is a complete dry assembly proposal using hollow glass 3DP units which need careful handling. The osteomorphic form chosen for the vault helps in placement of the bricks in their correct position by thereby interlocking them, but at the same time it would need larger tolerances in order to complete the vault with the keystone placement at the top.

Unlike adhesive-based systems as used in case study of the glass vault, each unit in this dry-assembly design must be individually supported during assembly. This necessitates a custom-designed formwork that not only accommodates each unit but also maintains stability throughout the construction. The scaffolding should be slightly oversized relative to the vault's intrados to account for tolerances. Once removed, the vault is expected to settle into its final compression-only state.

Currently, the interlayer properties have been optimized based on the geometry of the completed structure. However, this does not account for the potential stresses during construction—a factor that can only be evaluated through prototyping. It is therefore essential to re-engineer the kirigami-based interlayer, ensuring it can accommodate moderate stresses during assembly while maintaining its post-deployment performance.

12.1 Assembly process and formwork

An assembly method is suggested based on scaled models made during the process. Figure 118 demonstrates the assembly process.

- The scaffolding needs to be designed with precision in order to support each block during the assembly

process. The formwork should slightly exceed the vault geometry, allowing the structure- along with the interlayers- to shift into final position under compression once the support is removed. This remains in the scope of future work.

- Base support conditions require careful detailing and experimental validation, as peak stresses are expected here during unit placement. This aligns with findings from the dry-interlocking cast glass bridge by Aurik et al. (2018).
- To provide a robust and stable base, the first row of masonry units could be constructed using an alternative material (e.g., concrete or timber). A possible base detail sketch is shown in Figure 117.
- The stepped free edges assist with dry-assembly but remain vulnerable to slipping if not fully interlocked. The advised solution of edge constraints discussed in chapter 11 has not been further detailed in this thesis.

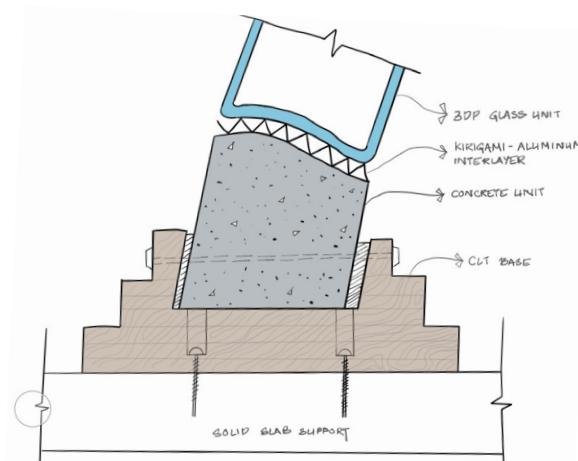


Figure 117: Foundation Detailing

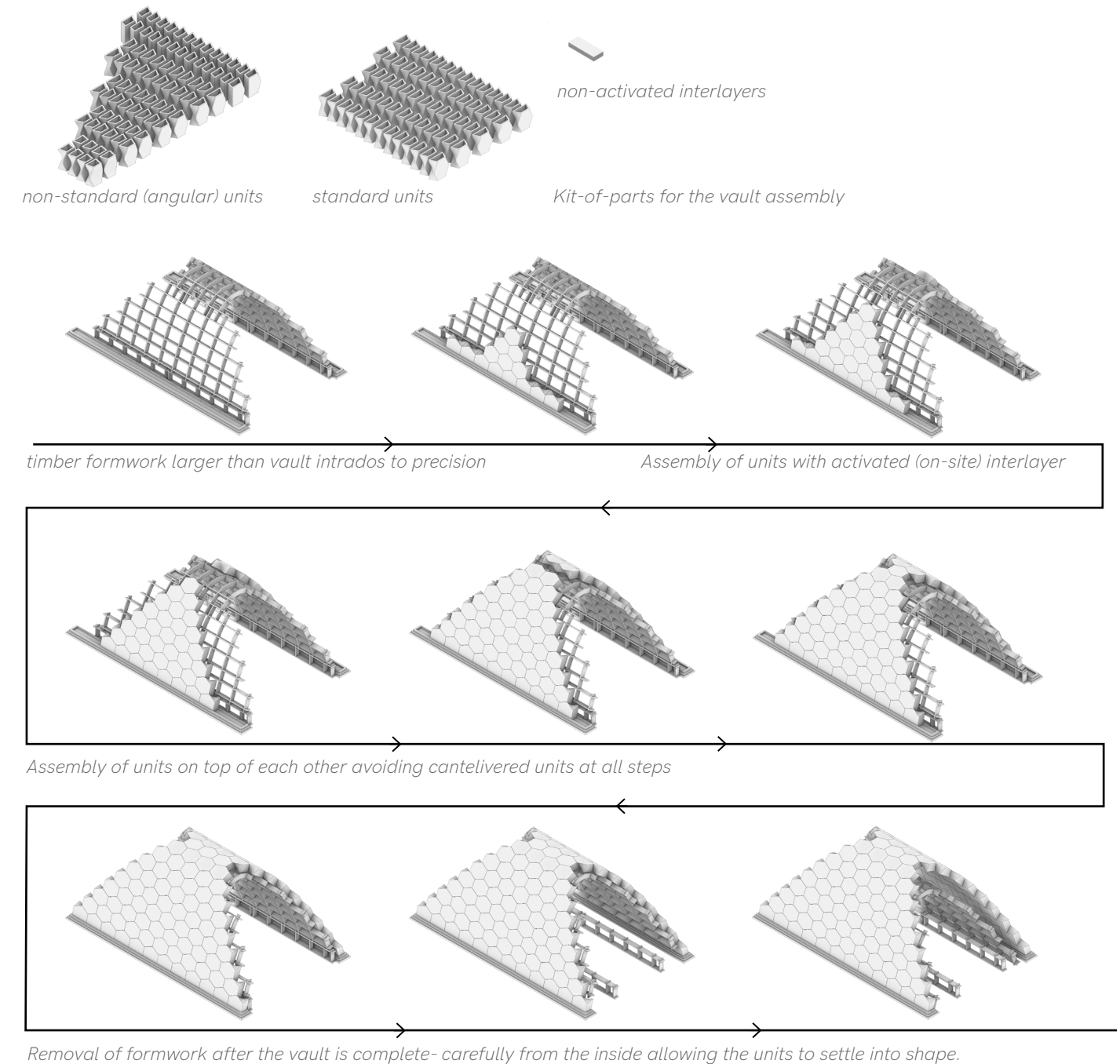


Figure 118: Assembly process

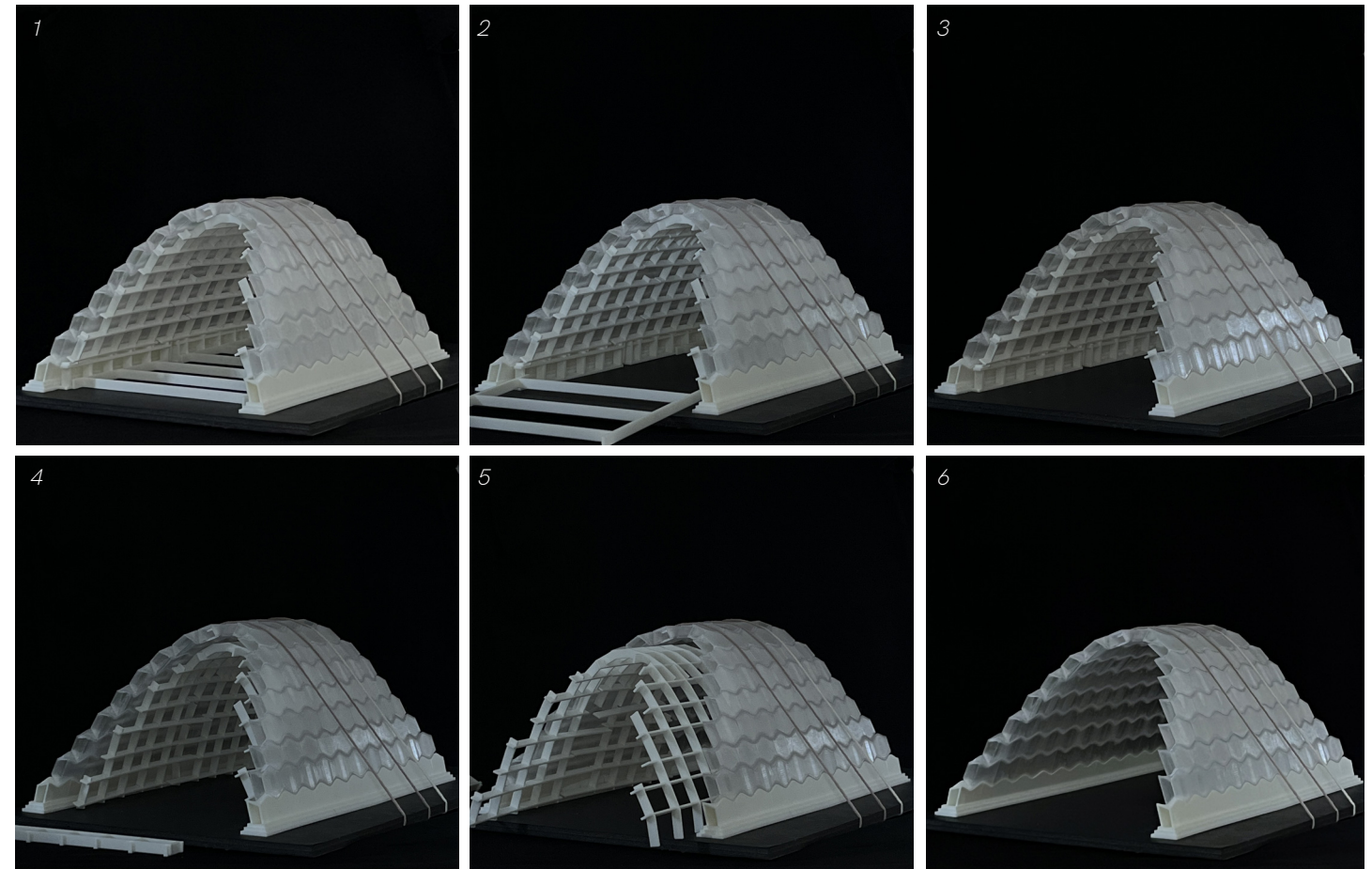
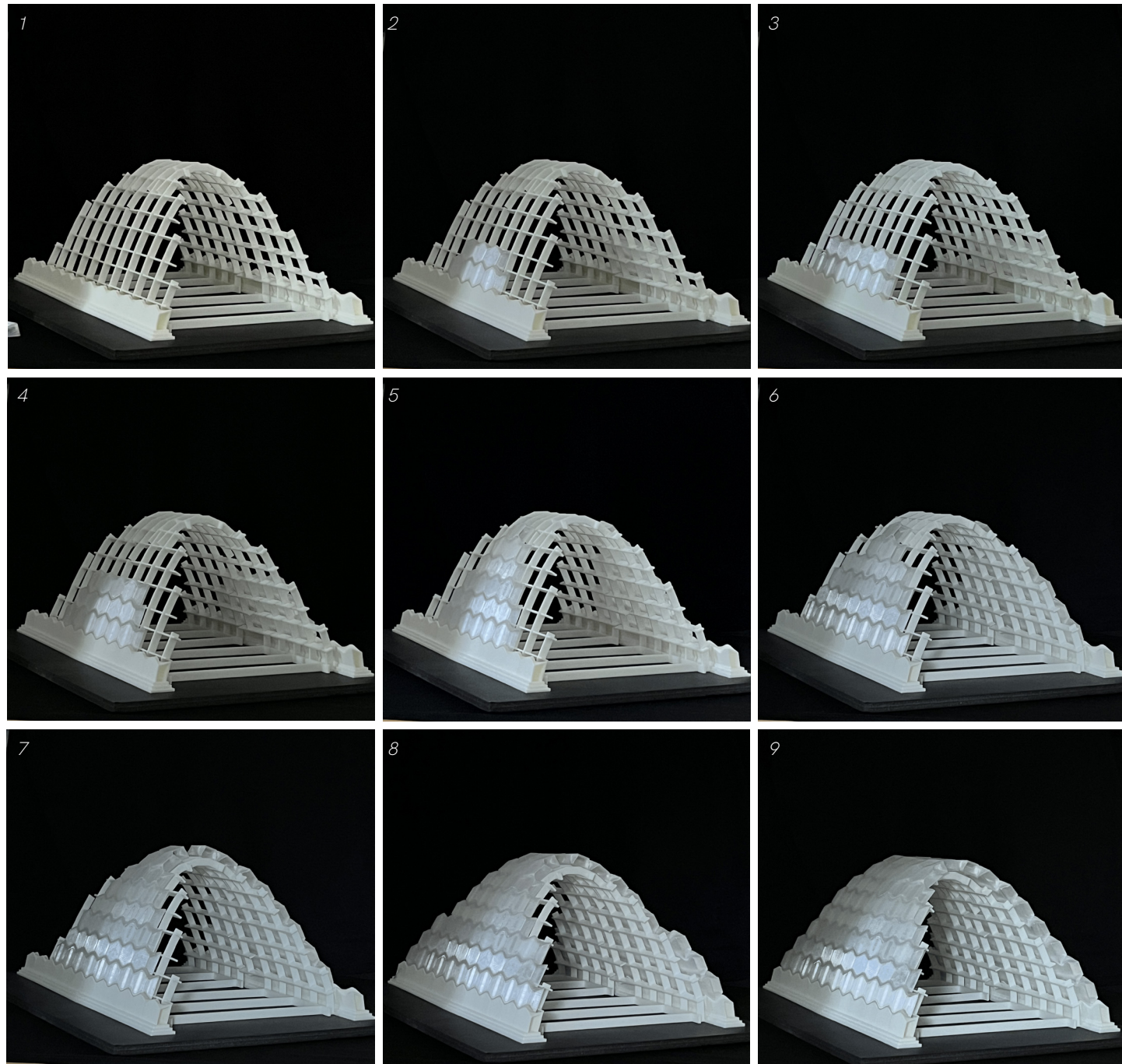


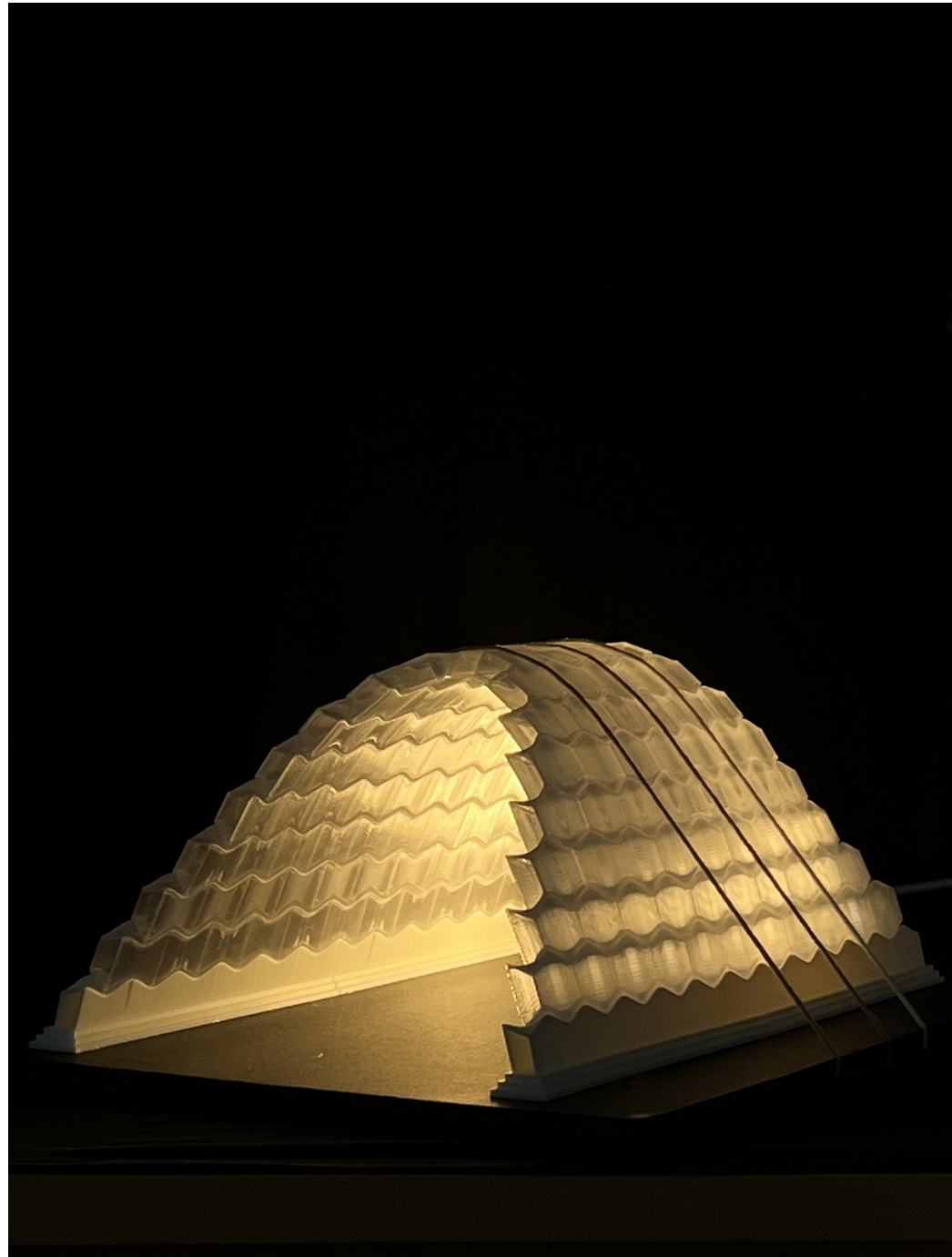
Figure 120: Removal of formwork with tension strings installed

12.2 Scaled model demonstration

The scaled model was fabricated using 3D-printed PLA for the base blocks and formwork, while PET was used to represent the 3D-printed glass bricks. In this model, the edge bricks and constraint strategies discussed in Chapter 11 were not implemented. Instead, structural stability was achieved by introducing tension strings across the center of the vault, as illustrated in Figure 120.

in this model, as they are not fully interlocked and are therefore prone to slipping. Additionally, because the vault is extremely lightweight- due to the hollow plastic construction of the units- tension strings were necessary to stabilize the structure prior to the removal of the formwork. The kirigami interlayers were not included in this scaled model.

The assembly process, shown in Figure 119, follows the same methodology previously outlined. The free stepped edges remain the most vulnerable components



116 *Figure 121: 1:10 Scaled model of the designed vault with tension strings - 3DP PLA and PET*

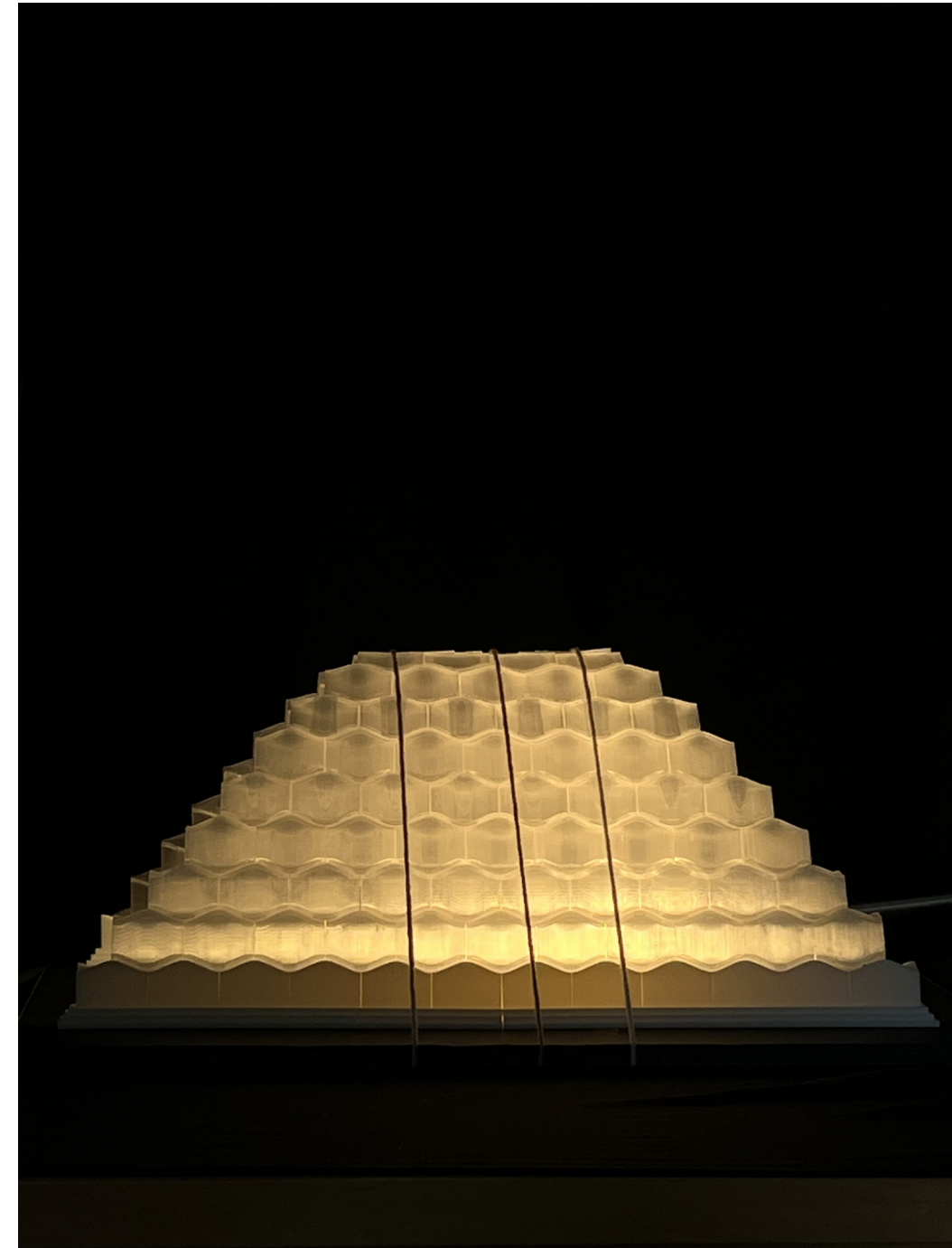


Figure 122: 1:10 Scaled model (side view) of the designed vault with tension strings - 3DP PLA

An abstract 3D geometric pattern composed of numerous small, dark gray cubes arranged in a grid-like structure. The cubes are slightly offset from each other, creating a sense of depth and movement. In the background, a series of thin, white, curved lines form a large, open, bowl-like shape, suggesting a dynamic, flowing structure. The overall composition is set against a solid black background, emphasizing the geometric forms and their interplay.

Conclusion

13.0 | Conclusions

13.1 Conclusion

This research set out to investigate masonry design methodology optimizing the properties of interlayer design in dry-assembled, compression-only masonry structures, with a case of a glass brick vaults. A comprehensive framework for evaluating and designing interlayer stiffness to ensure both structural and manufacturability performance was developed through a sequence of parametric models, simulation pipelines, and optimization protocols.

Three unique geometries- one freestanding wall, a catenary vault, and one form-found doubly curved shell- were explored in order to gain insight into geometric parameters' effects on assembly as well as behavior. Each was parametrized with manufacturing constraints with some variables (e.g., brick amplitude or wall height) and some constants (e.g., brick thickness), thereby allowing for optimization studies based on specific subsets of parameters.

One of the main contributions of this work was the development of an integrated design-to-analysis process using Grasshopper, Ansys, and OptiSLang to enable automated parametric exploration of interlayer stiffness and material properties. The analysis demonstrated that while parameters like geometry and material modulus govern the interlayer stiffness, the effect of the latter on structural performance metrics like deformation and tensile stress is in most cases non-linear. Such an outcome necessitated the use of surrogate model techniques, such as Polynomial Regression and Kriging, which were able to capture the subtle interdependencies in the system.

Evolutionary Algorithms, **identified an optimum value of interlayer stiffness between 183–250 MPa for the designed glass vault assembly.** This interlayer stiffness was then used as a performance target in the design of a novel Tension-Activated Kirigami (TAK) interlayer. Using a parametric model informed by prior physical models, a predictive model was created relating kirigami cut geometry and sheet thickness to equivalent stress and stiffness. Optimization using the Adaptive Response Surface Method (ARSM) led to a TAK interlayer design that met the target upper stiffness of 415 N/mm with minimal internal stress. However, physical prototypes of the same TAK presented double the stiffness value required for the interlayer application thereby suggesting the kirigami surrogate model to be fine tuned/ rebuilt based on physical test data.

Although the optimized kirigami structure proved to have acceptable performance based on the parametric model, the simulation also elicited problems in the modeling of pressure loads in a direction along curved osteomorphic surfaces and is yet to be validated.

In summary, this research presents a novel methodology to design programmable interlayers for dry-assembled masonry systems using data-driven and simulation-informed approaches. The proposed methods open up avenues for future exploration of programmable materials, machine learning-based surrogate models, and complex structural geometries. While issues remain- namely, in translating digital predictions to physical response- the results demonstrate that kirigami-inspired interlayers can be engineered to meet specific structural performance specifications

upon integrating them with a tightly coupled design-simulation-optimization loop.

13.2 Discussion and future work

This thesis demonstrates the potential of a surrogate-assisted, parametric design and optimization workflow for dry-assembled masonry systems. This workflow enables the development of multi-material or composite masonry (e.g., 3D-printed glass with cast glass or concrete bricks) where interlayers can be optimised to enhance performance and accommodate fabrication and construction tolerances.

Unlike current dry-interlocking masonry approaches, which demand extremely high precision (as seen in the work of Block Research Group, ETH), this research shows that a well-designed interlayer can mitigate such requirements. It opens a possible direction for introducing interlayers as functional and structural buffers in interlocking masonry structures, especially for glass masonry, improving constructability and resilience.

The optimised interlayer properties can be used to select any available interlayer material for the designed assembly. The kirigami-inspired interlayer is a tunable solution, capable of locally adjusting stiffness and adapting to complex geometries, though its full evaluation was limited by computational constraints. Surrogate models allowed rapid optimization, supported by automation, but their accuracy depends on the quality of training data. To improve reliability, future work should calibrate these models with physical tests and can integrate machine learning and detailing into a unified design-validation

loop. The activation of the kirigami can be simulated instead of using a parametric model. Furthermore, the physical samples showed extremely high stiffness value implying a major mismatch to the surrogate model developed. Further study must incorporate inferences from the currently ongoing TAK study at MIT. In addition, Physical testing is essential, both for short-term mechanical validation and long-term behavior, and will be key to refining the simulation workflow.

Despite strong digital performance due to compression-only geometry, the absence of tensile stresses in the model likely underrepresents real-world effects, such as local tension from imperfections, edge conditions, and assembly tolerances. It is observed that a 10 mm thick interlayer in a deployed state might not be a suitable solution and should be lesser. Assembly remains a critical factor, especially in dry construction. Even with digital planning, practical detailing, support conditions (Aurik et al., 2018), error tolerance, and reversibility require careful attention. The formwork must accommodate precise positioning with flexibility for in-situ adjustments. Moreover, end-of-life disassembly strategies are increasingly vital for meeting sustainability goals.

Finally, few limitations of this study could be addressed in future work:

- Optimising the vault weight with applied load for an efficient interlocking of the units as in this case the vault was optimized to be lightweight.

- Long-term material behavior (e.g., interlayer aging, creep) must be tested and incorporated into the workflow.

- Seismic performance of dry masonry vaults remains an open challenge

Reflection



14.0 | Reflection

My growing interest in the world of additive manufacturing led me to do a little research as a part of a course during the second quarter of MSc 1. I was fascinated by the innovation of Glass 3DP, and was very curious to explore more about its application possibilities in the built environment. Motivated by a subject that never ceases to engage me- and drawn to the opportunity to delve into both structural and computational design- I chose to focus on this area for my graduation studio. I feel privileged to collaborate with leading experts in glass innovation, and the experience so far has presented a steep yet rewarding learning curve. The following section offers a reflection on this journey.

Graduation process:

1. "How is your graduation topic positioned in the studio?"

My graduation topic, centered on the architectural potential of Glass 3D Printing, is closely aligned with the studio's emphasis on innovation at the intersection of material research and computational design. The studio deals with the expansion of technological boundaries and the discovery of new ways to integrate new technologies into the built environment, and therefore it is an appropriate setting for a topic that resists conventional approaches to both material use and construction.

Positioning with the Building Technology Graduation Studio:

- Computational Exploration: A significant part of the thesis is dedicated to computational design and automation. Through parametric modeling and custom scripting, I developed a digital workflow that enables the generation of multiple

design iterations and surrogate models. These tools support performance-driven design and allow for the exploration of structural optimization strategies, aligning with the studio's strong interest in computational design processes.

- Structural Optimization: My graduation thesis is guided by structural performance needs. By incorporating simulation and analysis within the design process, the research optimizes the geometry of 3D printed glass components for overall structural performance while considering manufacturing limitations. This performance-based approach lies at the core of the Building Technology track's emphasis on research that combines design with engineering precision.
- Innovation in construction: Although rapidly evolving, Glass 3D printing is a novel fabrication strategy that has not yet been seen in architectural applications. My project not only showcases the potential of this method of production but also suggests a novel engineered interlayer that is specifically engineered for desired performance outcomes. It explores the potential of the Japanese art of kirigami and depicts a method to engineer a sheet material to obtain certain desired properties. This addresses the studio's inquiry into the possibilities of material technologies and continued advancement in building materials.

- Construction Workflow and strategy: Beyond design and research process, the project reflects on how such parts that are digitally designed can be realized in the physical world. The thesis skirts construction process and methodology, engaging with the Building Products and Innovation sub-

discipline in investigating how such new systems can physically be developed, assembled, and potentially scaled within real architectural contexts.

2. "How did the research approach work out (and why or why not)? And did it lead to the results you aimed for? (SWOT of the method)"

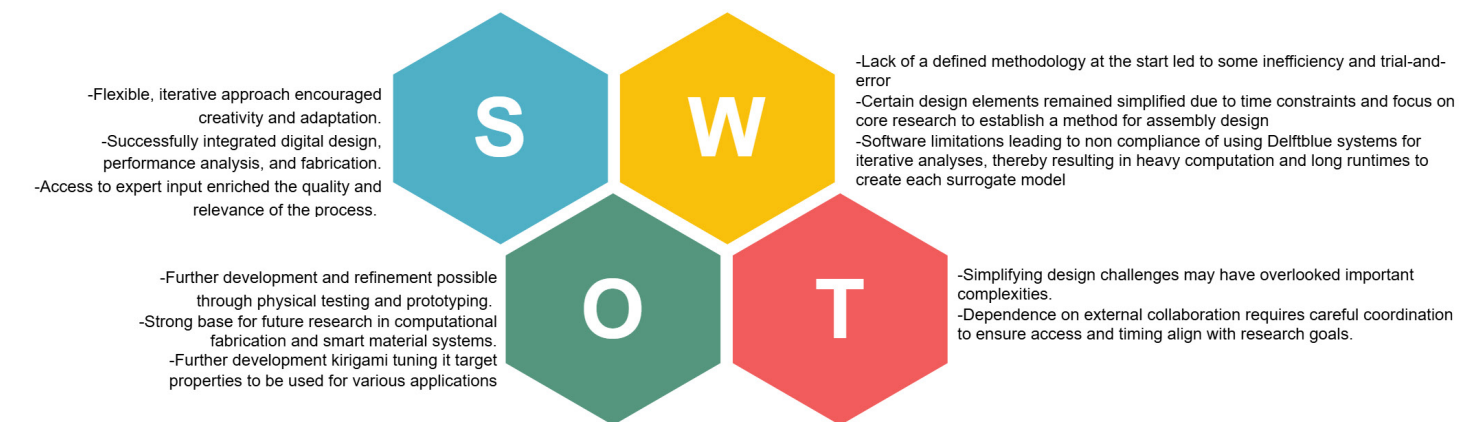
The research process eventually has proven to be successful so far, but it evolved drastically throughout the work. Initially, the process was not strictly defined- instead, it developed organically as I progressed with the research. It was mostly a *research-through-design* process, wherein exploratory iteration was a significant contributor to both the design and the direction of the research.

Early on, I had not recognized the need to narrow the scope and refine my objectives to remain focused and manage complexity, thereby spending more time in eventually doing so. This shift allowed me to concentrate

on the most critical aspects of the research- namely computational workflows, structural performance, and fabrication strategies. Some design challenges were simplified rather than fully resolved, in order to prioritize the areas that were central to my research questions.

Despite these trade-offs, the approach successfully met my intended learning outcomes. It provided a strong foundation in:

- Advanced computational design and parametric modeling.
- The integration and application of machine learning for performance prediction and optimization.
- A better understanding of structural engineering principles relevant to non-conventional materials
- Real-world insight into fabrication constraints and workflows, especially through collaboration with the design and fabrication lab at MIT.



3. "What is the relationship between the methodical line of approach of the graduation studio (related research program of the department) and your chosen method?"

This graduation thesis is well aligned with the methodical line of approach of the Building Technology graduation studio and the department's research programs, particularly in computational design, digital fabrication, and material innovation.

The studio's focus on the developing technologies in construction, material investigation, and computational practice is reflected in my work, combining parametric modeling, machine learning, and performance-based design with novel applications of 3D printed glass. The methodology also intersects with the department's general research project in Digital Fabrication and Building Products and Innovation, in particular in its emphasis on developing buildable systems based on computational and material research.

Therefore, my research not only is a suitable match within the parameters of the studio's methodological goals but also serves the department's ongoing exploration of how technology can redefine both the product and process of architectural design.

4. "How are research and design related?"

In my project, research and design are closely interrelated, with a continuous feedback loop between the two. It should, however, be noted that as much as they inform each other, design served as the controlling leader to question and validate the research goals.

Early design goals- such as the making of a compression-only glass vault- involved much research in structural behavior, form-finding strategies, and material constraints. Although this approach proved to

be convoluted and was later changed, it did help inform the scope and focus of the study. Upon realization that a number of design targets would lie outside the pragmatism of the research duration, the design was adjusted but not the fundamental research objectives.

By this process, design was simultaneously driver and testing ground for the research. It posed questions that the research sought to address, yet research paid back in modes and knowledge that informed more realistic or strategically trimmed design options. This mutually reinforcing relationship allowed the project to be kept close to application while still maintaining the methodological demands of the thesis.

5. Did you encounter moral/ethical issues or dilemmas during the process? How did you deal with these?

While I did not encounter direct moral or ethical conflicts, there were important considerations related to collaboration, authorship, and research integrity, particularly because my thesis is partially embedded within a broader ongoing research project led by the Fabrication-Integrated Design Lab (FIDL) at MIT. The research was to be part of their effort to create fully circular 3D-printed glass modules for the built environment as informed by kirigami-interlayers.

My initial plan was to use numerical test data generated by the MIT group as my input design. However, due to time and access constraints, those findings were not incorporated into my thesis. While this created a level of uncertainty and complexity, I was careful to be open and to make clear that any external knowledge drawn on in my work- i.e., visual observations, informal discussions, and meeting interactions- was duly qualified as qualitative reference points and not as formal data sources.

Fortunately, the kirigami geometry I selected for the development of my interlayer design was the same that they tested at MIT, providing some indirect validation for the direction I pursued. Still, I decided to limit the use of their work to general inspiration, maintaining an independent, self-created, and accountable design and verification process.

I believe the collaboration could have worked out better if our timelines for research matched and research outcomes were exchanged through the process.

Societal impact:

The broader objective of the Msc program AUBS at TU Delft encourages multidisciplinary practices, blending the knowledge and skills from design practice, from the physical and social sciences, technology and engineering, this programme explores innovative ways to create more sustainable development which is discussed further with the following questions.

1. "To what extent are the results applicable in practice?"

The results of this research suggest great potential for practical application, particularly in the formulation of the integration of 3D printed glass components into a reversible assembly design. The process involved a simulation and numerically verified method, with regards to given structural load conditions as well as the incorporation of early fabrication, handling, and assembly limitations. This assisted in ensuring the design investigation was not only conceptual but founded upon feasible parameters based on construction. Following can be drawn for the applicability in practice:

- Assembly and construction: An operational construction plan was put in place to think about

how these components might be made in practice, although further work must be done to adequately test and fine-tune this. The second most important step is physical prototyping and testing, which will enable the current assumptions to be refined and verified under actual conditions.

- Kirigami interlayer performance: As for the designed interlayer, the research went at it computationally to simulate its behavior within the entire assembly. However, due to limitations in modeling, certain material idiosyncrasies and real-world behaviors were oversimplified or not modeled. This means that while the simulation result is a good place to start, the real-world performance of the interlayer still needs to be tested and iterated on.

In summary, while the research is robust with empirical consciousness in practice terms, its full deployment shall be witnessed only through subsequent empirical testing and progressive refinement. This can be considered as a start point for 3DP glass assembly construction.

2. "To what extent has the projected innovation been achieved?"

The initially projected innovation- developing a way of designing reversible assemblies using 3DP glass units, and a strategy to design the interlayer for particular performance- has been achieved. The research demonstrates how digital design, simulation, and optimization can be combined to identify both the shape and behavior of such an element.

But within the realm of practical application, there is more to be worked out. Formwork design area, tolerance control, and logistics of assembly detailing are yet to be addressed in their entirety within this framework. Although the process itself can be done

and run, the final delivered design is still to fully counter all practical aspects of construction work.

In totum, the invention lies in putting down a conceptually working design and computational method, which sets the stage for further development and implementation.

3. "Does the project contribute to sustainable development?"

3DP- material optimised, minimal waste manufacturing

The project operates towards sustainable development by looking into the possibility of additive manufacturing (3D printing) in architecture, a tactic which is naturally favorable to sustainability by some significant advantages. Among them are material waste reduced, mass-optimized and structurally efficient forms, shortened lead times in development, cost savings, and enabling intricate shapes that would be impossible or challenging with conventional construction methods.

Circular Assembly with Glass- a fully recyclable material

By focusing on glass, a fully recyclable material, and interlayer engineering in a fully circular assembly in combination with optimization using computer simulations, the project contributes to the discussion about the efficiency and circularity of material use in building construction.

The thesis also acknowledges the limitations, namely the need for extensive pre-engineering, performance testing, and manufacturing control. All of these must be addressed before the maximum potential for sustainability in practice of 3DP assemblies can be realized.

4. "What is the impact of your project on sustainability (people, planet, profit/prosperity)?"

The project's environmental sustainability—material efficiency and circular potential, to be precise—is addressed in the previous question. Moreover, it promotes worldwide knowledge sharing and cooperation (people), encourages labour-efficient and resource-conscious design practices (planet), and explores how may lead to more efficient use of materials and fabrication processes in the long term (prosperity), although not yet cost-effective.

5. "What is the socio-cultural and ethical impact?"

I would say that this project is at the intersection of tradition and innovation- pushing how we build, with what we build, and who builds. In the working with 3DP glass, it touches on not only material innovation but also cultural shift in architecture- where automation, performance-based design, and sustainability start to supplant age-old conventions.

But while these technologies are exciting, they also raise ethical questions: Who gets to access these tools? Can such approaches be used outside of well-funded labs and studios? Although this project takes place within the high-tech space, it is still founded on the belief that efficiency and circularity shouldn't be an elitist privilege- their principles must be scalable and adaptable.

By its partnerships with recyclable materials and, as with the FIDL Lab at MIT, globally, the project encourages collaboration and mutual discovery. It's not trying to provide a finishing product, however, but open up a discussion as to what shape the future of construction should take- and how, maybe, it could be more productive, and responsible.

6. "What is the relation between the project and the wider social context?"

At its core, this graduation project is more than fancy glass and software simulations, -although the idea of 3DP glass and engineering a kirigami interlayer is fascinating, the project makes you rethink how we build fur the future. It makes you think about circular systems and dry assemblies for the built environment- designed for disassembly.

What if materials like glass- often seen as delicate or wasteful- could become engineered building blocks built with minimal wastage and can be reused again and again? This project lives in a simulated niche for now, but its a way forward to having fully circular glass assemblies in the built environment.

7. "How does the project affects architecture / the built environment?"

3D printed glass is still in its infancy, with fewer than a dozen printers worldwide and very limited architectural applications to date. This thesis completes one of the primary gaps by explaining how to assemble 3D printed glass into functional, buildable shapes. By its proposals for circular, demountable, and transportable assembly methods, it establishes the foundation for future uses- temporary pavilions, exhibitions, or sculptural works.

One day, we might see architectural components made entirely from 3D printed glass blocks- and this research attempts to mark a small but important step in that direction.

15.0 | References

3D Printing Technology for Glass

Baudet, E., Ledemi, Y., Larochelle, P., Morency, S., & Messaddeq, Y. (2019). 3D-printing of arsenic sulfide chalcogenide glasses. *Optical Materials Express*, 9(5), 2307–2317.

Inamura, C. (2017). Towards a new transparency: High fidelity additive manufacturing of transparent glass structures across scales.

Inamura, C., Stern, M., Lizardo, D., Houk, P., & Oxman, N. (2018). Additive manufacturing of transparent glass structures. *3D Printing and Additive Manufacturing*, 5(4), 269–283. <https://doi.org/10.1089/3dp.2018.0157>

Klein, J., Stern, M., Franchin, G., Kayser, M., Inamura, C., Dave, S., Weaver, J., Houk, P., Colombo, P., Yang, M., & Oxman, N. (2015). Additive manufacturing of optically transparent glass. *3D Printing and Additive Manufacturing*, 2(3), 92–105.

Maple glass printing. (n.d.). Retrieved from <https://www.mapleglassprinting.com/>

Massimino, D., Townsend, E., Folinus, C., Stern, M., & Becker, K. (2024). Additive manufacturing of interlocking glass masonry units. *Glass Structures & Engineering*. <https://doi.org/10.1007/s40940-024-00279-8>

Qaidi, S., Yahia, A., Tayeh, B. A., Unis, H., Faraj, R., & Mohammed, A. (2022). 3D printed geopolymer composites: A review. *Materials Today Sustainability*, 100240.

Stern, M., Townsend, E., Massimino, D., & Becker, K. (n.d.). Advancing sustainable 3D printing: The feasibility of recycled glass as a building material with additive manufacturing.

Zhang, D., Liu, X., & Qiu, J. (2021). 3D printing of glass by additive

manufacturing techniques: A review. *Frontiers of Optoelectronics*, 14(3), 263–277. <https://doi.org/10.1007/s12200-020-1009-z>

Cast Glass Assemblies

Aurik, M., Snijder, A., Noteboom, C., Nijse, R., & Louter, C. (2018). Experimental analysis on the glass-interlayer system in glass masonry arches. *Glass Structures & Engineering*, 3(2), 335–353. <https://doi.org/10.1007/s40940-018-0068-7>

Aurik, M. (2017). *Arched Glass Masonry Bridge*.

Oikonomopoulou, F. (2019). Unveiling the third dimension of glass: Solid cast glass components and assemblies for structural applications (PhD dissertation). TU Delft.

Oikonomopoulou, F., Bristogianni, T., Barou, L., Jacobs, E., Veer, F. A., & Nijse, R. (2018). Interlocking cast glass components: Exploring a demountable dry-assembly structural glass system.

Oikonomopoulou, F., Bristogianni, T. (2022). Adhesive solutions for cast glass assemblies: Ground rules emerging from built case studies on adhesive selection and experimental validation. *Glass Structures & Engineering*, 7(2), 293–317. <https://doi.org/10.1007/s40940-022-00178-w>

Oikonomopoulou, F., Ioannidis, M., & Koniari, A. M. (2023). Fabrication methods for topology-optimized massive glass structures.

Case Study- The Robotic glass Vault

Beghini, A., Miki, M., Walker, S., Han, I. X., & Parascho, S. (2021). Robotic construction of a self-balancing glass masonry vault: Design and tessellation.

Heyman, J., 1996. The stone skeleton: structural engineering of

masonry architecture. In *International Journal of Rock Mechanics and Mining Sciences and Geomechanics Abstracts* (Vol. 3, No. 33, p. 133A)

Parascho, S., Han, I. X., Beghini, A., & Miki, M. (2021). LightVault: A design and robotic fabrication method for complex masonry structures.

Parascho, S., Han, I. X., Walker, S., Beghini, A., Bruun, E. P. G., & Adriaenssens, S. (2020). Robotic vault: A cooperative robotic assembly method for brick vault construction. *Construction Robotics*, 4(3–4), 117–126. <https://doi.org/10.1007/s41693-020-00041-w>

Compression-only form, Tessellation, Armadillo Vault

Block, P. (2009). Exploring three-dimensional equilibrium.

Block, P., Rippmann, M., & Van Mele, T. (2015). Structural stone surfaces: New compression shells inspired by the past. *AD Architectural Design*, 85(5), 74–79. London: John Wiley & Sons.

Marmo, F., & Rosati, L. (2017). Reformulation and extension of the thrust network analysis. *Computers & Structures*, 182, 104–118. <https://doi.org/10.1016/j.compstruc.2016.11.016>

Miki, M., Igarashi, T., & Block, P. (2015). Direct application of Airy stressfunctionstoNURBSpatchesforcomputingcompressionshells.

Olivieri, C., Angelillo, M., Gesualdo, A., Iannuzzo, A., & Fortunato, A. (2021). Parametric design of purely compressed shells. *Mechanics of Materials*, 155, 103782. <https://doi.org/10.1016/j.mechmat.2021.103782>

Van Mele, T., Panozzo, D., Sorkine-Hornung, O., & Block, P. (2014). Best-fit thrust network analysis: Rationalization of freeform meshes. In S. Adriaenssens, P. Block, D. Veenendaal,

& C. Williams (Eds.), *Shell Structures for Architecture: Form Finding and Optimization*. New York: Routledge.

Veenendaal, D., & Block, P. (2012). An overview and comparison of structural form finding methods for general networks. *International Journal of Solids and Structures*, 49(26), 3741–3753. <https://doi.org/10.1016/j.ijsolstr.2012.08.008>

Kirigami

Corrigan, T., Fleming, P., Eldredge, C., & Langer-Anderson, D. (2023). Strong conformable structure via tension activated kirigami. *Communications Materials*, 4(1), 31. <https://doi.org/10.1038/s43246-023-00357-4>

Eidini, M., & Paulino, G. H. (2015). Unraveling metamaterial properties in zigzag-base folded sheets. *Science Advances*, 1(8), e1500224. <https://doi.org/10.1126/sciadv.1500224>

Muñoz-Barron, B., Sandoval-Castro, X. Y., Castillo-Castaneda, E., & Laribi, M. A. (2024). Characterization of a Rectangular-Cut Kirigami Pattern for Soft Material Tuning. *Applied Sciences*, 14(8), 3223.

Sun, Y., Ye, W., Chen, Y., Fan, W., Feng, J., & Sareh, P. (2021). Geometric design classification of kirigami-inspired metastructures and metamaterials. *Structures*, 33, 3633–3643. <https://doi.org/10.1016/j.istruc.2021.06.072>

Wang, J., Roveroni, M., Meneghetti, G., & Hao, G. (2024). Parametric design, simulation, fabrication, and test of an Origami-core-based sandwich composite material. *Mechanics Based Design of Structures and Machines*, 52(9), 6011–6032. <https://doi.org/10.1080/15397734.2023.2266833>

Appendix 1 - Form finding, Tessellations

1.1 Doubly Curved forms using Kangaroo

Initially, Kangaroo was explored for form exploration-with the hypothesis that an inverted tensile-only structure would be purely compressive. The load applied in Z-direction was calculated from the self weight of the shell made with 3D printed hollow blocks. It was observed that load was not the main driving factor for the shape of the membrane. By changing factors like weighing and amplitude, the vault was tuned to a desired shape similar to the glass vault studied as a case study. By changing the 'length factor' the vault edges sagging were controlled as seen in figure 1.

Initially the intention was to formfind the compression only shape as in the glass vault, however, the obtained shape from kangaroo didnot result in a compression only shell when analyzed using Karamba plugin in grasshopper.

As seen in figure 2 the shell from kangaroo has peak stresses in the extrados and intrados while nearly 0 stresses in the central area. This implies a bending moment occurs in the shell cross section with extreme stresses on either sides of the shell. The shell is therefore not compression only. It was further noted that letting the edges sag in kangaroo by not applying the load at edges results in a more compression only form. Therefore the free edges need to be restrained or stresses there should be within limits. *In the case of the glass vault case study, the bricks were bonded together and stresses were kept within acceptable limits, making the chosen form executable. However, the form itself does not appear to be a pure compression-only thrust network, and it seems likely that it was post-processed to achieve the desired shape.*

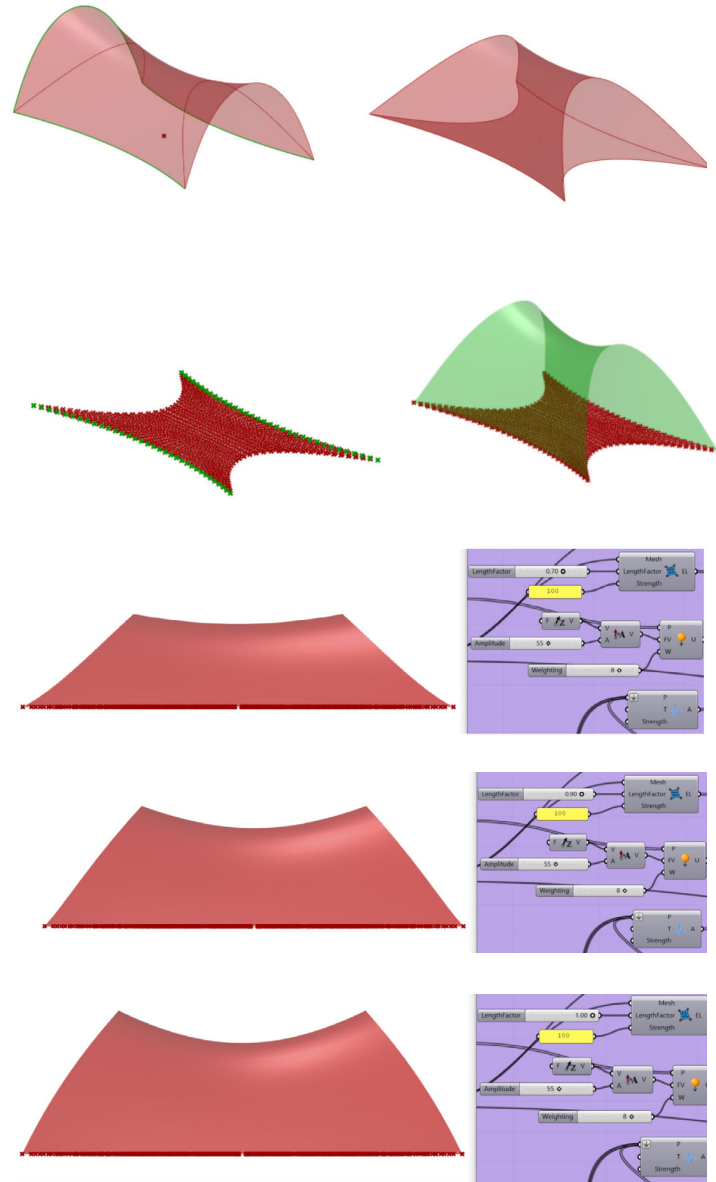
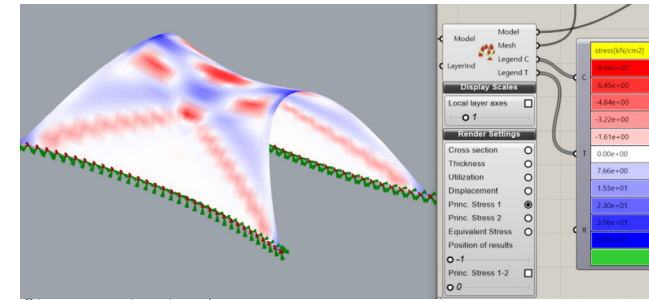
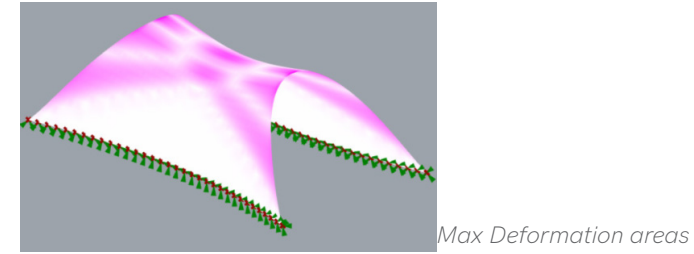
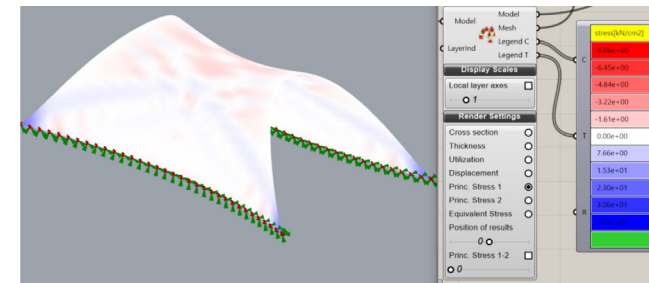


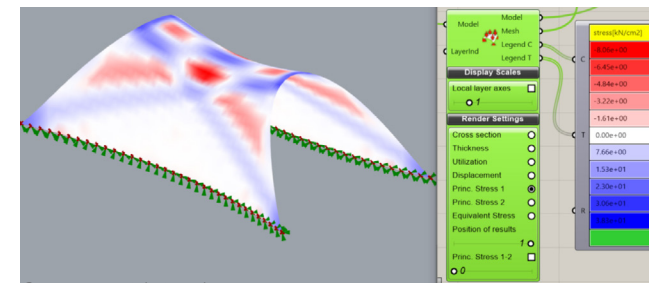
Figure 1: Kangaroo exploration to recreate the glass vault shape



Stresses at extrados

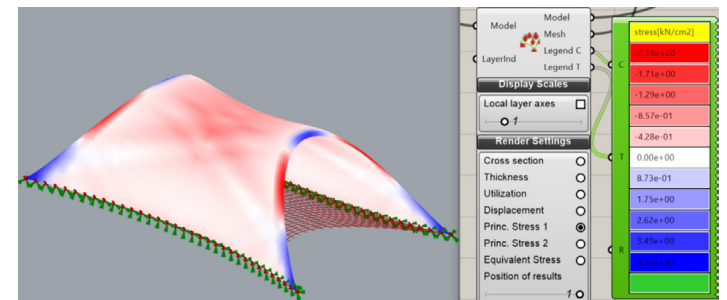
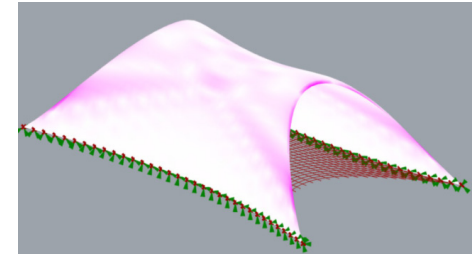


Stresses at center

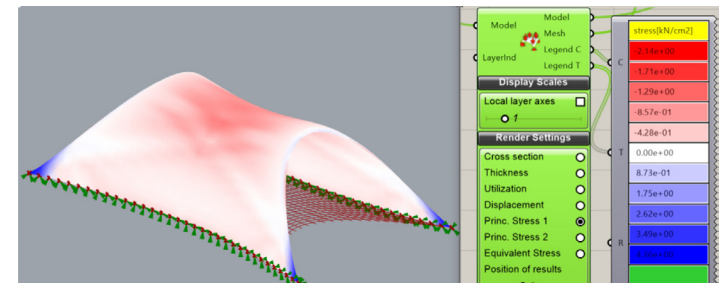


Stresses at intrados

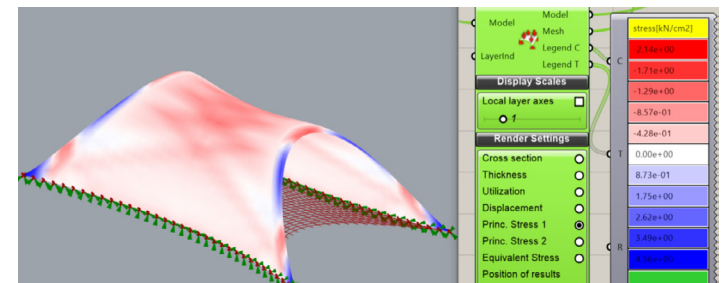
Figure 2: Karamba analysis of the kangaroo shell



Stresses at extrados



Stresses at center



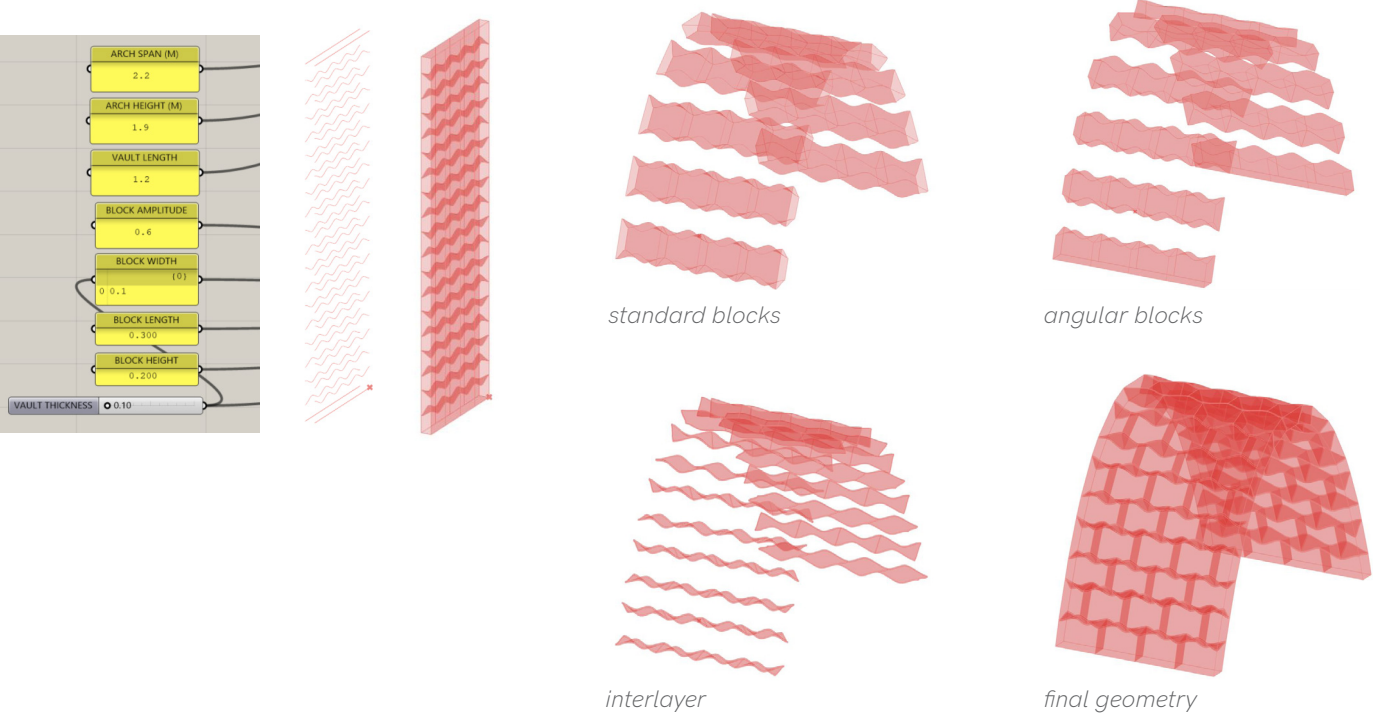
Stresses at intrados

Figure 3: Karamba analysis of the kangaroo shell with sagged edges

1.2 Catenary arch Tessellations

Since the tessellation design on a doubly curved shell considering the limitations of 3DP glass bricks and considered osteomorphic form of units were a major challenge that required greater amount of time, the vault was simplified to a singly curved vault- a catenary shape that follows an ideal load path for compression vaults.

Different tessellation patterns were tried on the vault as shown here in figure 4. It was observed that horizontal divisions are closer together towards the top of the arch due to more curvature, thereby resulting in unique course of unit typologies. They were therefore decided to be standardized as presented in the report.



1.3 Compression-only arch Tessellations

The aim is to depict a way to assemble a doubly curved compression only shell using dry 3DP glass masonry units. The main reference here was the Armadillo vault by the Block Research group and their methods about tessellating doubly curved forms using a structured mesh. Modelling the form founded doubly curved shell from Rhino Vault discretely incorporating 3DP constraints was a challenge.

Deriving a thickened shell with the thrust network using Airy's stress function as developed by Oliveri, 2021

was the ideal way to approach the problem but was not looked further into as that was not the main goal for the thesis. As seen in the figures 5, the shell offset creates a further distorted mesh you cannot work with. The sagging free edges in the thrust network had a smaller mesh network.

The shell offset therefore used was much thicker than intended so as to safely contain the thrust network withing the shell thickness and to incorporate lesser curvatures.

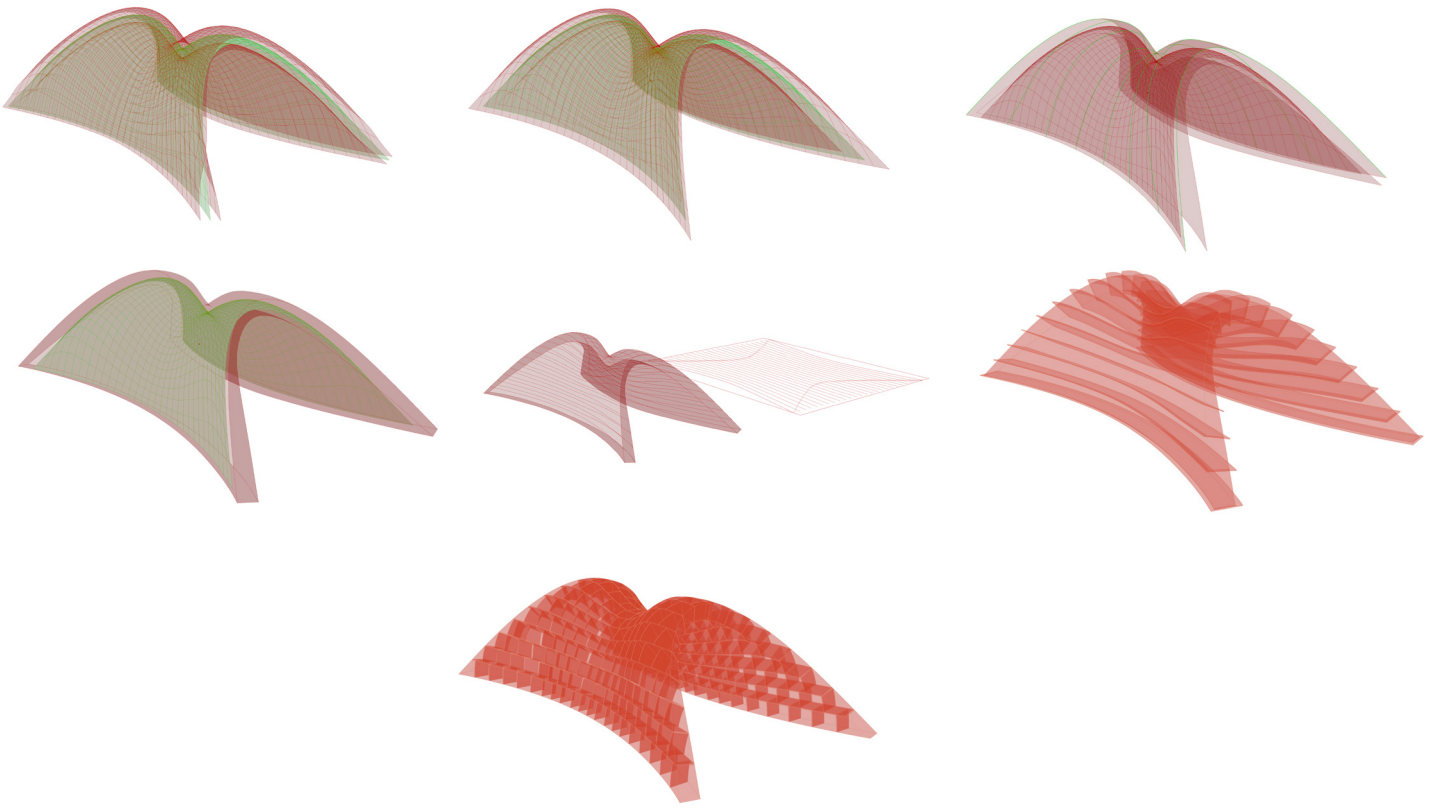


Figure 5: Tessellating a doubly curved shell

1.4 Kirigami parametric model

As discussed in chapter 10, the activation tests done at the Fabrication-Integrated Design Lab, MIT gave insights on the activated kirigami pattern which were observed in order to create the kirigami parametric model for analysis.

For the current surrogate model few things regarding the activated pattern were considered- and will be tuned based on the physical tests in the upcoming month.:

- The activated kirigami used as an interlayer will be uniform- no anomalies in pattern during activation is considered
- The tilt angle at which the vertical flaps tilt are constant with changing height of the vertical flap
- The kirigami is activated with a constant force that results in the desired hexagonal configuration modelled for with an angle of 60 degrees.
- The parameter dimensions are inferred from Corrigan et al., 2023, the values are parametrized proportionately so as to maintain the hexagonal uniformity in the pattern as proposed in the literature

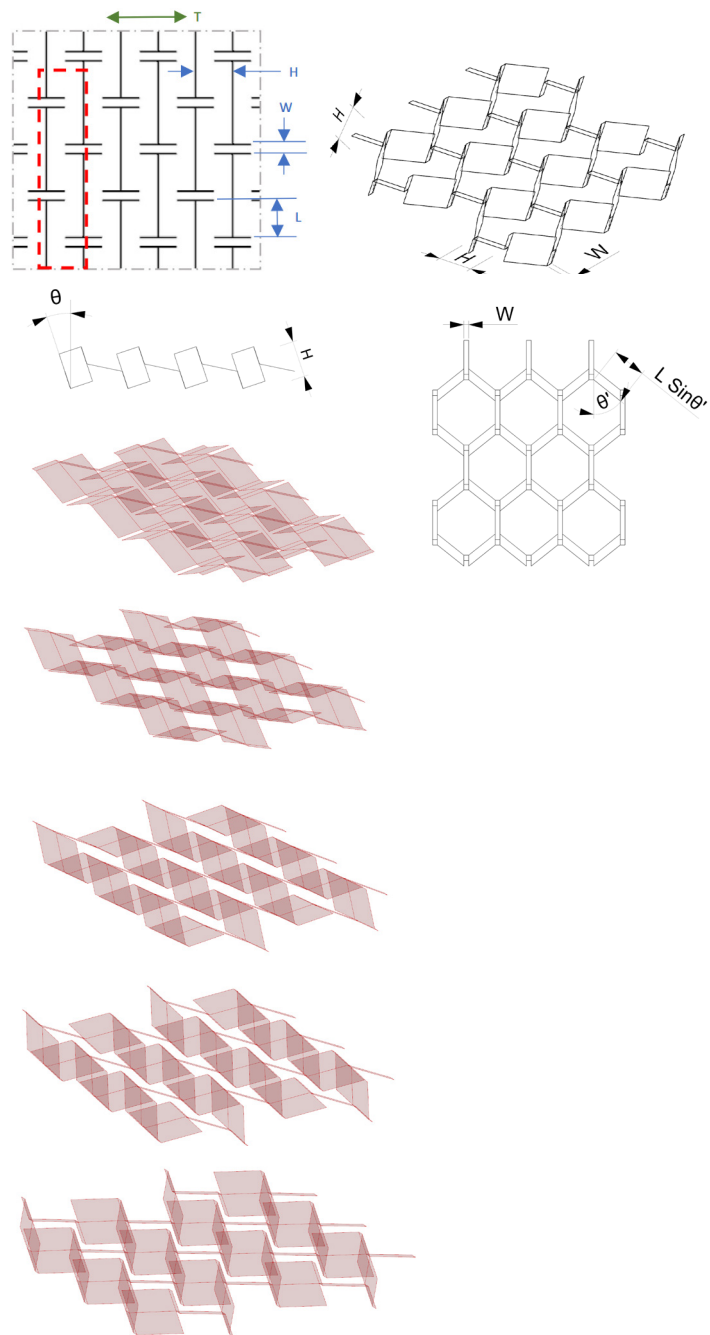


Figure 6: TAK parametric model

1.6 Geometry dataset from Grasshopper

Figure 7 shows the grasshopper- collibri and python setup for exporting geometries from sampled designs to create the designspace for surrogate creation

1.7 Simulating Catenary glass vault without interlayer

The initial FEA simulation was to see what happens in case no interlayer is used for the catenary arch assembly. This was also used as a means to getting acquainted with Ansys software interface and understand structural boundary conditions, loads etc in the application.

Inferences:

- The solution fails to converge as shown in figure 8. Iterative solver is used with GPU acceleration, and with non-linear material behaviour.
- Since glass-glass contact is not frictional, and the osteomorphic surface is not modelled with double curvature, the vault collapses.
- It is inferred that the local stresses due to glass-to-glass contact would be so high that the units would fracture before the vault collapses.

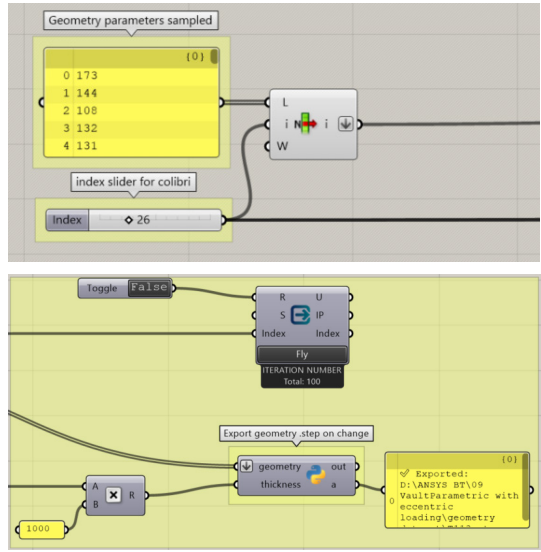


Figure 7: Geometry export from grasshopper

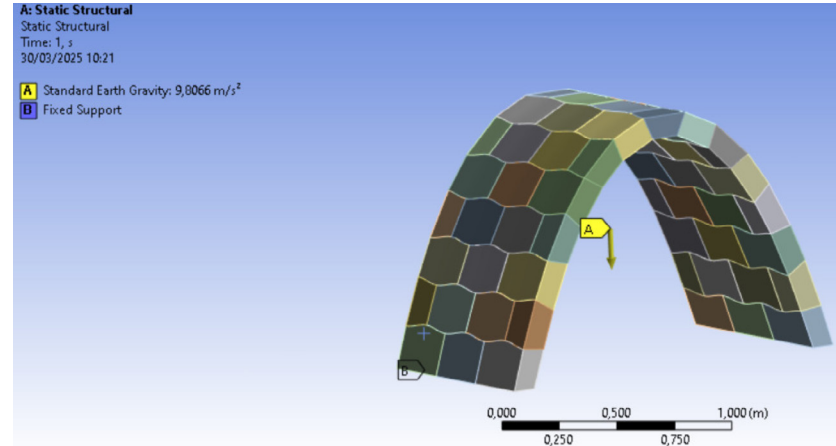
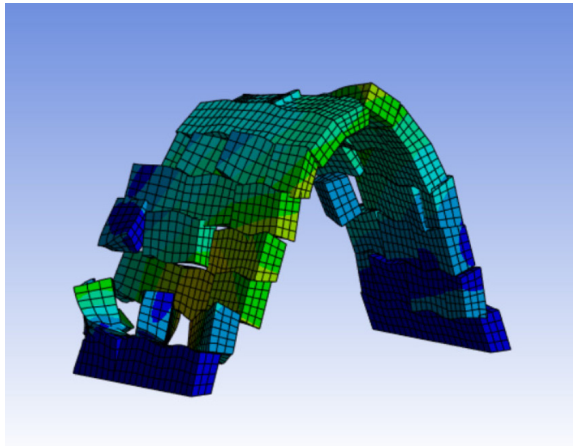


Figure 8: FEA - Vault with no interlayer



Appendix 2 - Structural analysis

2.1 Ansys Model Setup for parametric Global FEA of discrete masonry model

Initially Ansys Design explorer, and optiSLang components were used within the Ansys workbench. However, since results needed post processing it was found better to use optiSLang interface which has many more tools.

All analysis done consider non linearities in material, and global performance of the structure. Since the structure is a dry assembly system, global stability with load conditions are crucial for its overall buckling behavior.

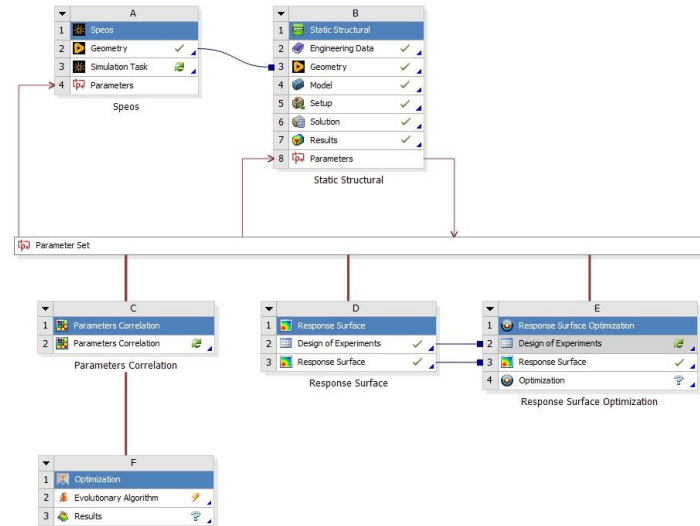
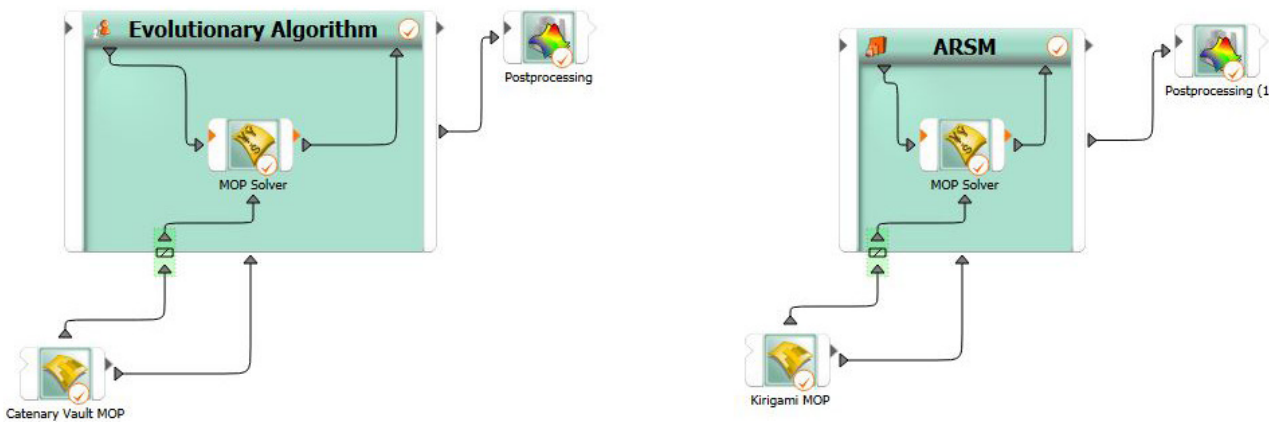


Figure 9: Ansys Workbench Interface for Structural Analysis

2.2 OptiSLang interface for both optimization tasks

The main drawback of using optiSLang was its handling of continuous parameter values—there was no control over the number of decimal places. Additionally, other challenges included dependent parameters, such as stress in the kirigami model, which had to be pre-processed in Excel before being imported into optiSLang’s Solver Wizard.



2.3 Ansys Model Setup for parametric FEA of Kirigami

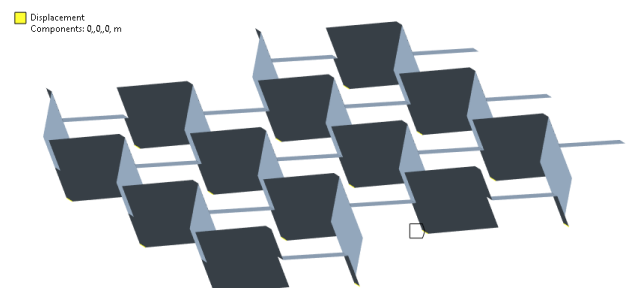
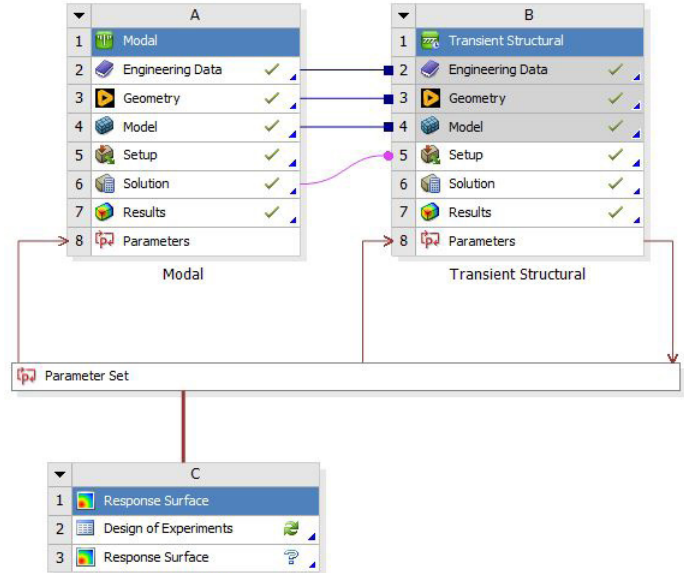


Figure 11: Boundary conditions for Modal deformations

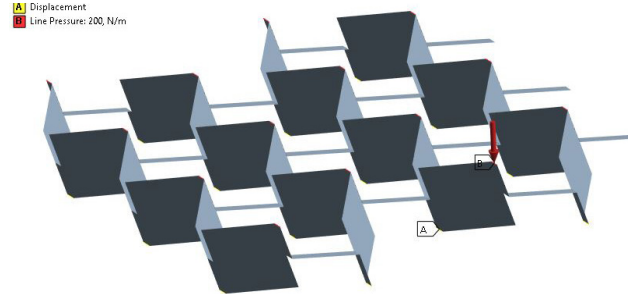


Figure 12: Boundary conditions for FEA

2.4 Parameter Sensitivity Analysis for 2D Arch

Two overly simplified 2D arches were initially used to verify the developed workflow as presented in the report, and they also allowed insights on the parameter sensitivity.

Since number of geometric parameters mean a larger design space to choose the samples from and would require more number of samples for the surrogate model accuracy, the idea was to keep them to a minimum considering the given time frame of this thesis.

As seen in the parallel charts below, the young's modulus was varied considering a very soft interlayer of 10Mpa to a very stiff interlayer of 5Gpa. The goal

was to see the relationship of the interlayer property to overall structural performance.

Effect of Interlayer property:

A non-linear response is seen in this case with the 2D arch- where a very soft interlayer leads to the highest deformations and a high stress in glass since the interlayer squeezes to make the glass come in close proximity to contact. The arches with soft interlayer still converged to a solution without slipping since a high friction coefficient was considered.

Effect of Vault thickness:

The vault thickness although has a non polynomial/ non linear relation with stresses in glass in this case as seen

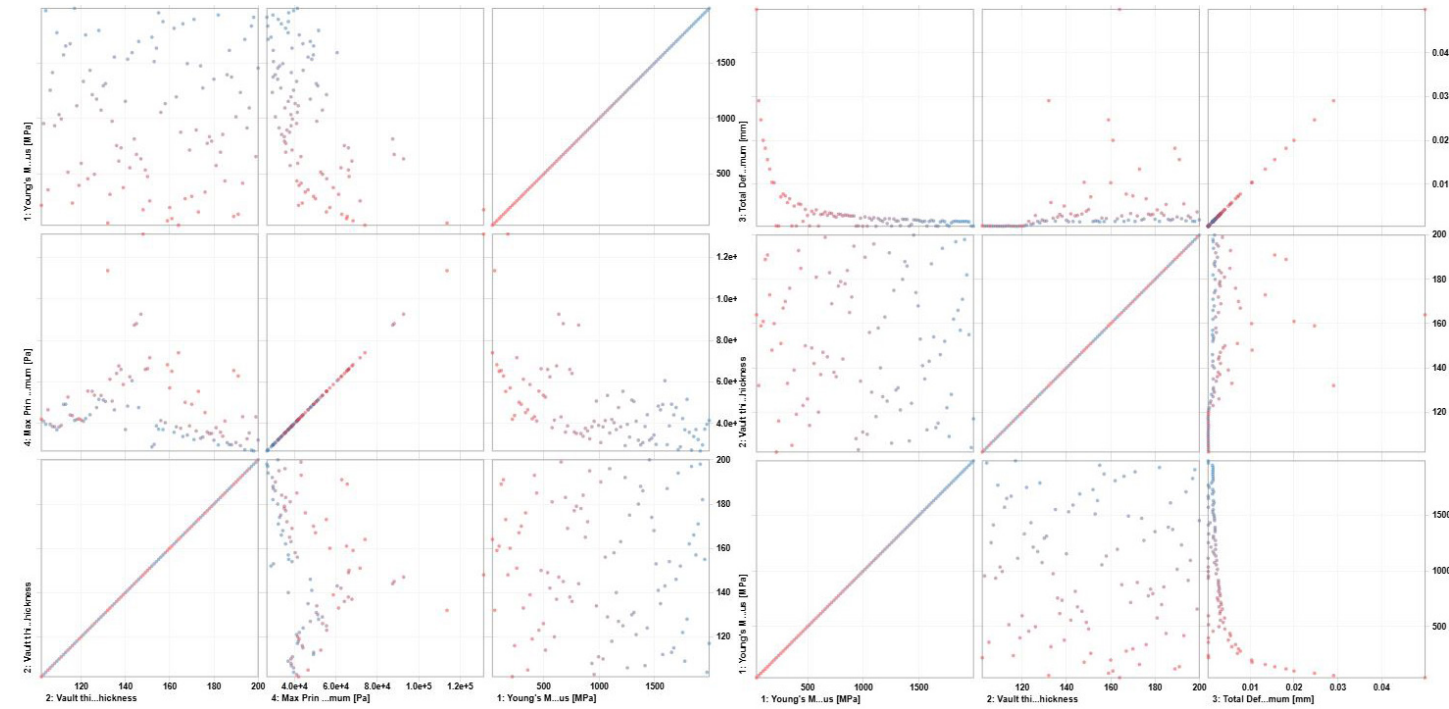
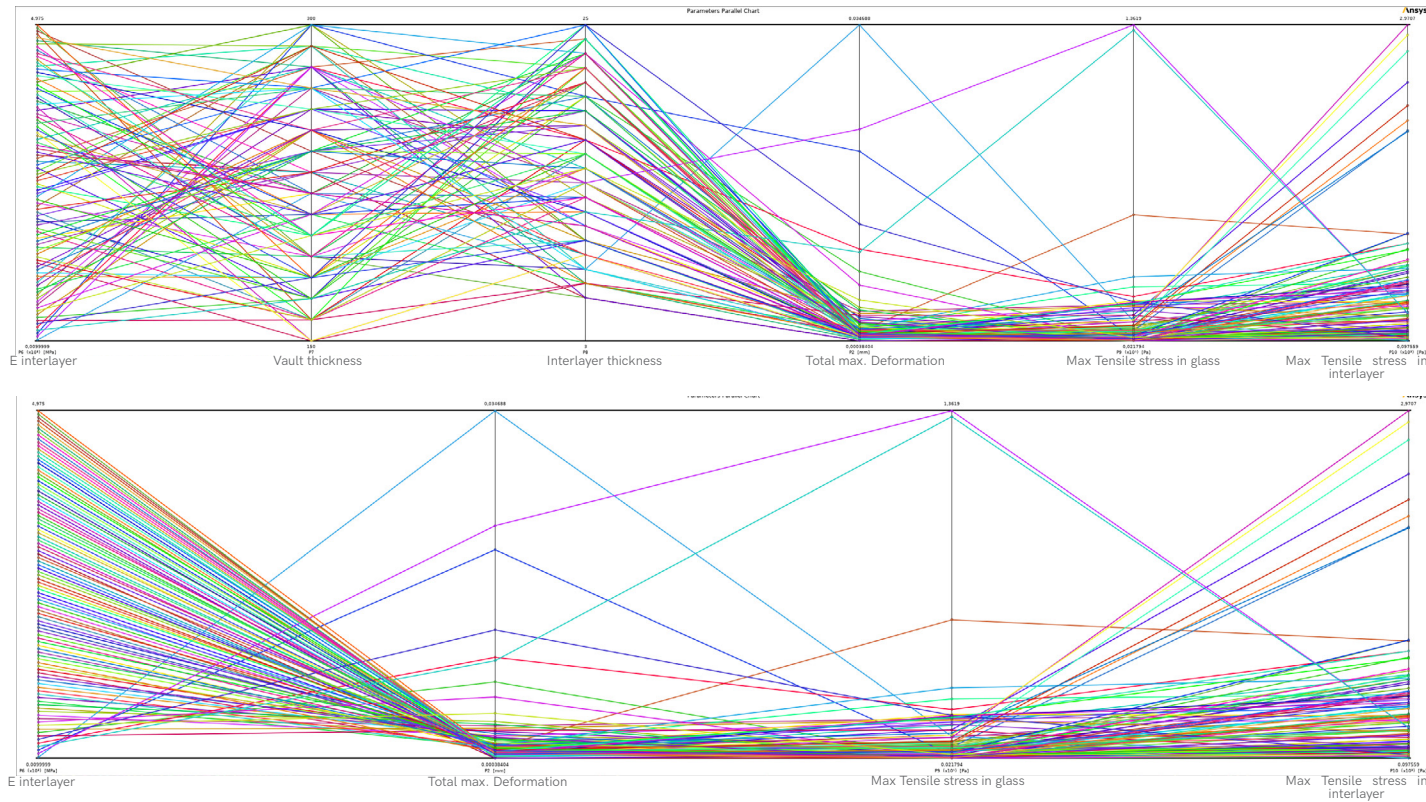


Figure 14: Input parameters vs Maximum tensile stress in glass

in figure 14, it was observed that this was due to the combined reaction of how stiff the interlayer is and how thick the vault is- for eg. a stiff interlayer would cause stresses in glass irrespective of the thickness, but thicker the vault- more the self weight and therefore more stress developed.

Effect of Interlayer thickness:

The performance with respect to interlayer thickness is also related to how stiff the interlayer is. The thicker the interlayer, the more stiff it has to be in order to not squeeze in. In this case as shown in figure 14 and 15, a non linear response is seen in total deformation and maximum tensile stress in glass- unclear as there are too many input variables in this case.

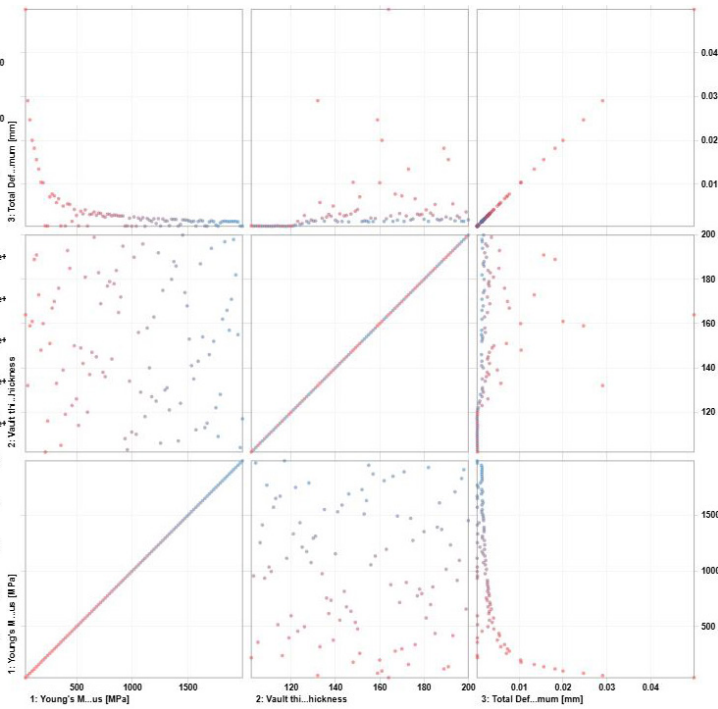


Figure 15: Input parameters vs Total deformation

In order to make the relationship better, the input variable of interlayer thickness is removed- since it will majorly influence the assembly detailing as discussed in chapter 14. A constant thickness also gives us the control to engineer the kirigami interlayer as discussed in our design goals for this thesis.

Further simulations were not done to truly understand how the performance is affected when the interlayer thickness varies, or the block height and subdivision varies in the vault but can be done in future works using the established workflow and parametric model defined in this thesis.

2.2 Optimizing for dry assembled Catenary Vault under different loading conditions

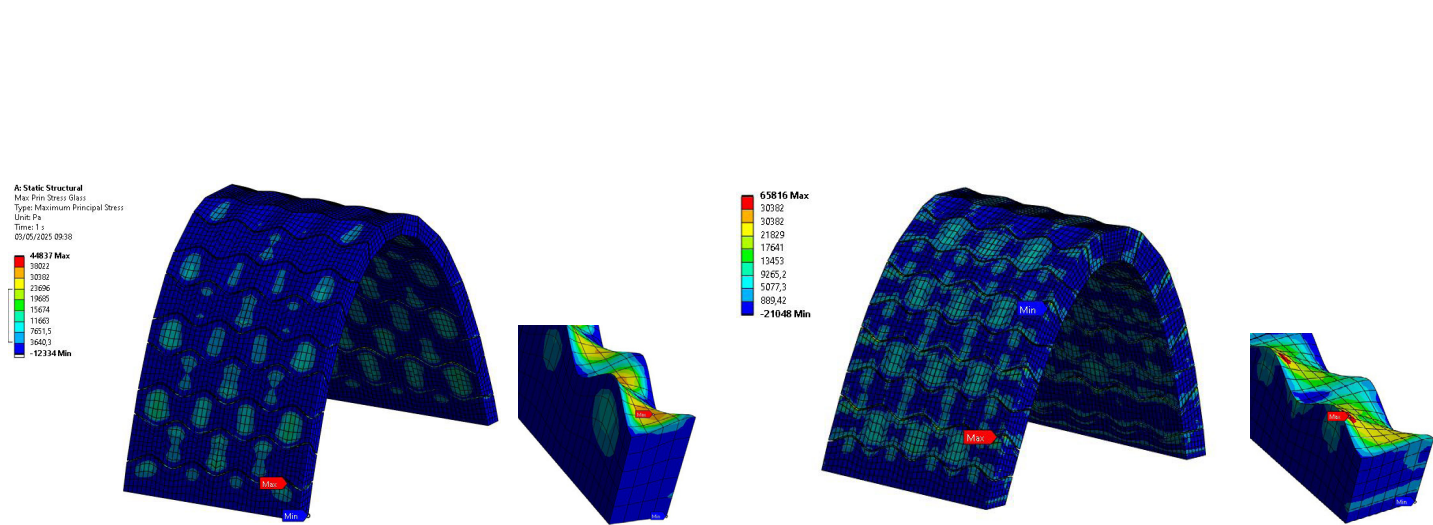
LOAD CONDITION A: Vault under self weight only

Optimizing for this load condition has been documented in detail in chapter 9 of the report which was finally used for determining the interlayer target stiffnesses. This section demonstrates factors that were observed during analysis with varying parameters.

PARAMETER SENSITIVITY

Boundary conditions: Fixed supports at the base. Symmetry conditions used on both x and y axis as the vault and its loading conditions are symmetric.

Inferences:
A change in peak stress location is seen with the increase in thickness of the vault- the optimised result tends to keem peak stresses towards the center of the osteomorrphic surface as seen in figure 16



142 Figure 16: Thin Vault with a stiffer interlayer (as optimized)

Figure 17: Thick Vault with a soft interlayer

LOAD CONDITION B: Vault under self weight and a maintenance load applied as pressure local to mesh surface.

Boundary conditions: Fixed supports at the base. Symmetry conditions used on both x and y axis as the vault and its loading conditions are symmetric.

Bounds: Vault thickness varied from 100mm to 200mm
Youngs Modulus of Interlayer varied from 20Mpa to 2000Mpa
Load: Maintenance load of 1kN/sqm(maximum as per Eurocodes 1991-1-1 for maintenance loads on Category H roofs) with a safety factor of 1.5 applied perpendicularly local to the mesh faces in the extrados of the vault.

Number of samples for the design space: 100

Surrogate model methods: Linear Regression(auto selected) for objective- minimise total deformation

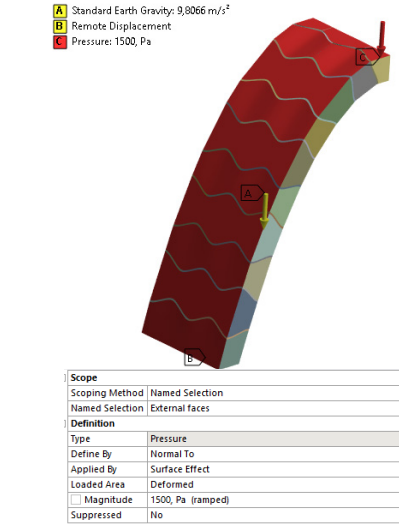


Figure 18: Boundary conditions

Linear Regression(auto selected) for objective minimise maximum tensile stress in glass

Key observations:
When a uniform (inward) pressure is applied on the the exterior surface of the vault, it stabilizes the vault and therefore can be used as a design intent incase certain eccentric loading conditions/ impact load is expected.

The surrogate model as seen in the figure 19 did not result in an approximation of the design space, since total deformation as well as stress in glass was very low for all designs (with random outliers) no matter the interlayer is soft or stiff.

Optimization was not done in this case. We only infer that stability of the vault under an external inward pressure can be achieved by using tension cables externally to stabilize and keep the vault in place in case of heavy impact loads or high eccentric loading that could destabilize the vault otherwise.

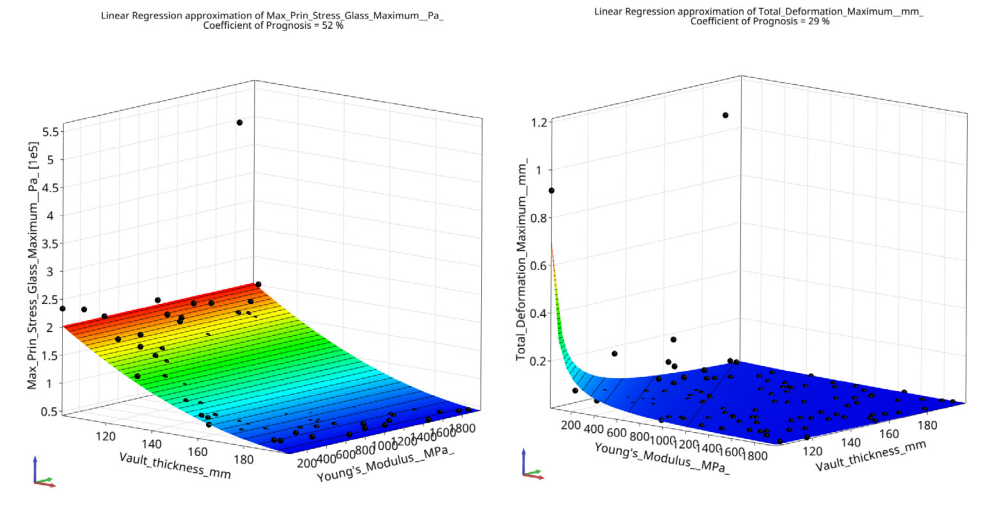


Figure 19: MOP with a low coefficient of prognosis

LOAD CONDITION C: Vault under self weight, pressures created due to wind on one side of the vault.

Boundary conditions: Fixed supports at the base. Symmetry conditions used on both x and y axis as the vault and its loading conditions are symmetric.

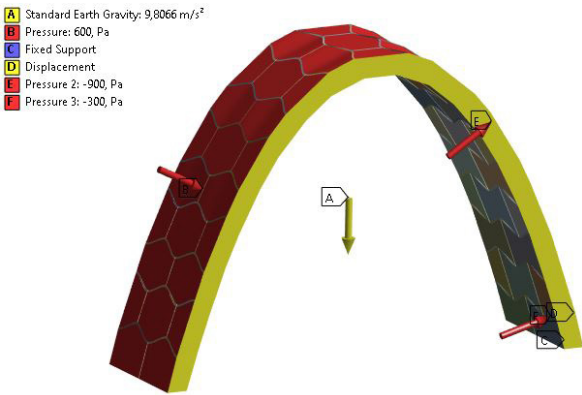
Bounds: Vault thickness varied from 100mm to 200mm
Youngs Modulus of Interlayer varied from 20Mpa to 2000Mpa

Loads: Gravity loads with densities considered for approximated hollow glass units- 1403kg/cu.m and 10mm thick interlayer of 1100kg/cu.m.

Pressures on vaulted roofs due to wind as per Eurocode 1991-1-0 as shown in figure 21. Safety factor of 0.75 is considered in this case for wind loads.

Number of samples for design space: 100
Surrogate model methods: Krigging for objective-minimise total deformation

Polynomial for objective minimise maximum tensile stress in glass



Key observations:
The surrogate model in this case did not achieve accuracy levels as compared to load condition A.

The output factors- total deformation maximum and stress in glass is governed by a local maximum because the vault thickness changes while the loading remains constant.

Eccentric loads were found to be more crucial for monitoring, since the vault is dry assembled.

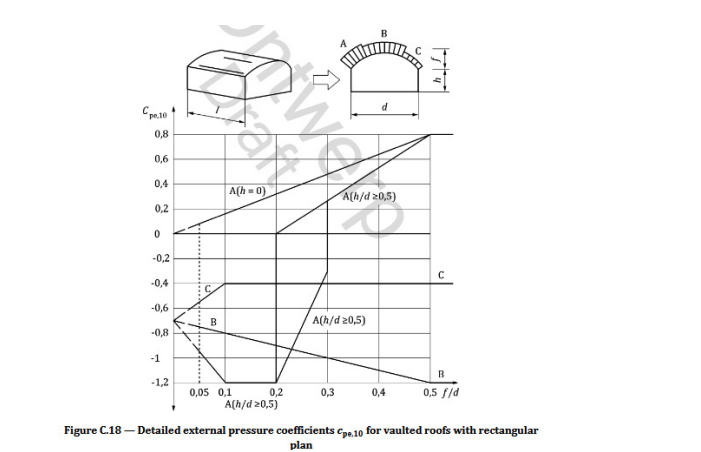


Figure 21: Wind loads from Eurocode 1991-1-0

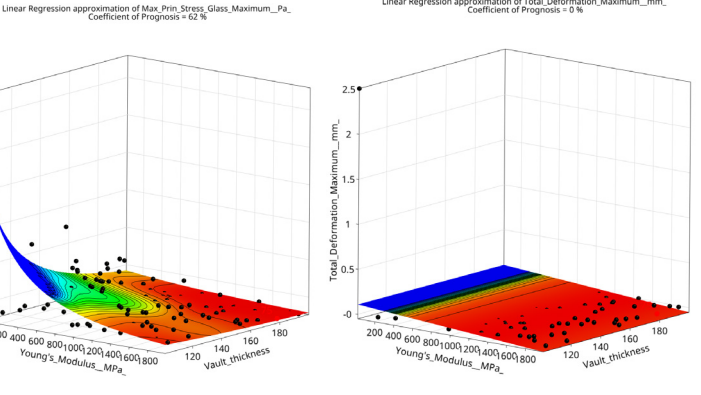


Figure 22: Ansys Model tree and setup

LOAD CONDITION D': Vault under self weight, pressures due to wind on one side, and maintenance loads

Boundary conditions: Fixed supports at the base. Symmetry conditions used on both x and y axis as the vault and its loading conditions are symmetric.

Bounds: Vault thickness varied from 100mm to 200mm
Youngs Modulus of Interlayer varied from 20Mpa to 2000Mpa

Loads: Gravity loads with densities considered for approximated hollow glass units- 1403kg/cu.m and 10mm thick interlayer of 1100kg/cu.m.

Pressures on vaulted roofs due to wind as per Eurocode 1991-1-0 as shown in figure 22.

A maintenance load as per Eurocode 1991-1-1, Dutch National Annex: uniform load of 0.4kN/sqm on overall shell, and a point load of 1kN applied on 100x100mm at the centre of the vault.

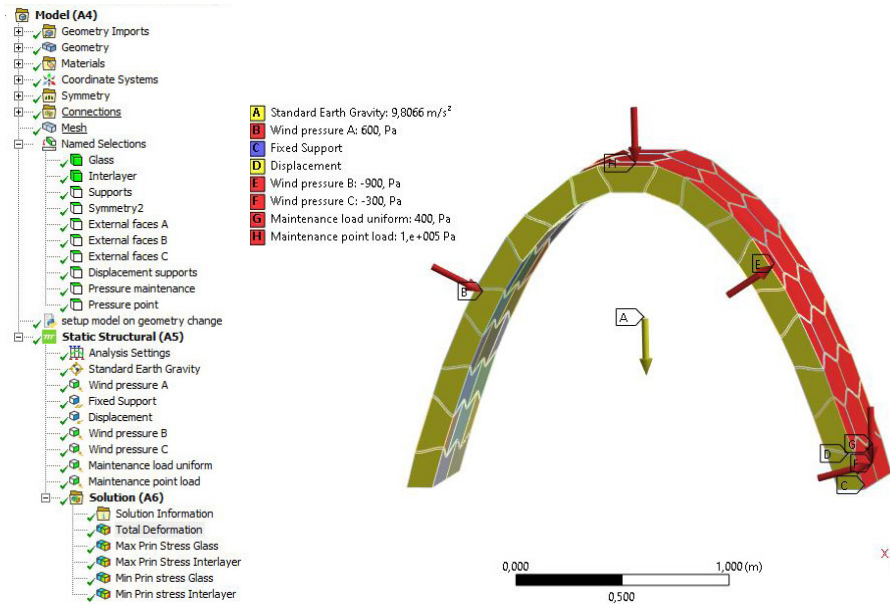


Figure 23: Ansys Model tree and setup

Safety factors not considered in this case
Number of samples for design space: 200

Surrogate model methods: Krigging for objective-minimise total deformation
Polynomial for objective minimise maximum tensile stress in glass

Optimization: Evolutionary Algorithm

Key observations: (same as load condition C)

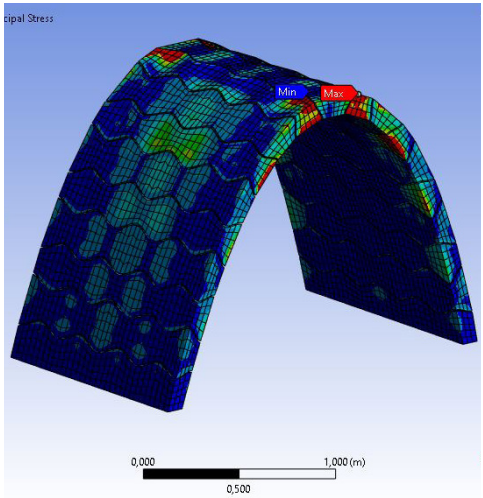


Figure 24: Local Stresses defined due to load

2.3 FEA of Final Design

Performing a FEA on a discrete model of the designed vault depicting hollow 3DP bricks, even though they were already simplified and the interlayer considered as a solid material of the equivalent stiffness. This was because a more fine mesh had to be used for the non-linear analysis, and the vault was comparatively larger with symmetry condition applied in only one axis. These simulations were done on compute p2 nodes of Delftblue supercomputers.

The Meshing: The meshing of the vault was found to be the most crucial factor for the analysis to converge to a solution without a geometry getting extremely distorted in the process. Iterative solvers were used so that the problem could be identified and this takes lesser memory for the solving process.

Figure 25 shows some of the quality of the meshes that were used for analysis in one of the design cases. The goal is to keep the element quality of the mesh closer to 1 and avoid really low values- lower than 0 which is likely to cause issues during analysis. Several meshing methods were explored, and **Patch conforming method** was found to be the most effective in this case.

Figure 26 shows unconverged solutions indicating issues in meshing, the interlayers are seen to slip in an abnormal way without causing the blocks to slip. Figure 27 shows the meshing level suggested for a stable analysis. Figure 28 shows a converged solution- with edges restrained and friction coefficient increased.

It is also beneficial to be aware of considering computer storage since each result range between 7 to 15GB.

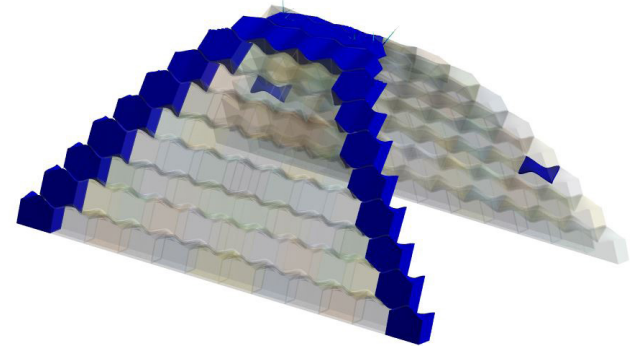
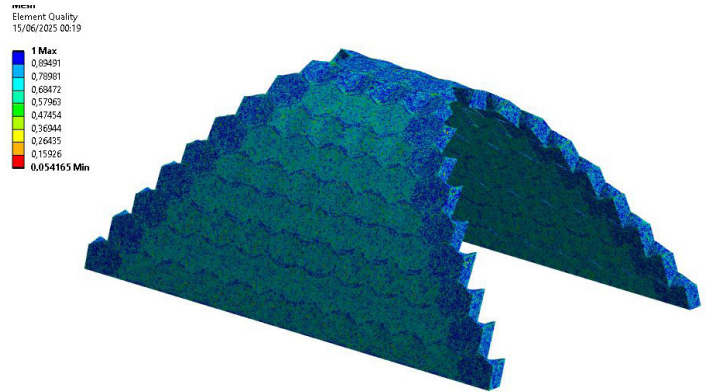
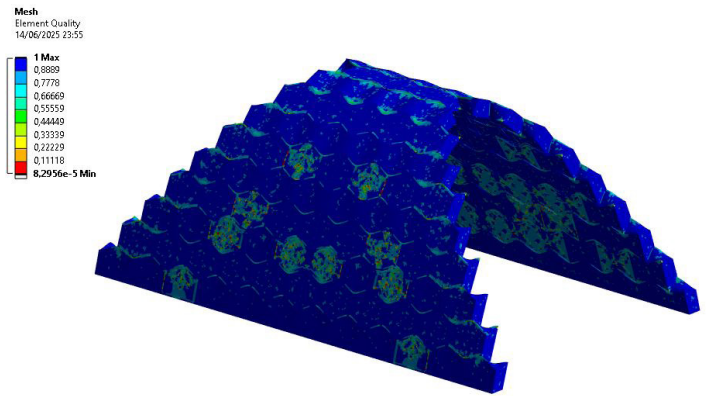
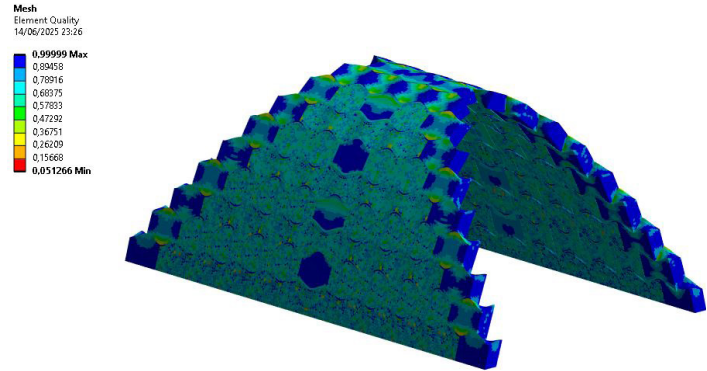


Figure 26: Unconverged solutions due to meshing

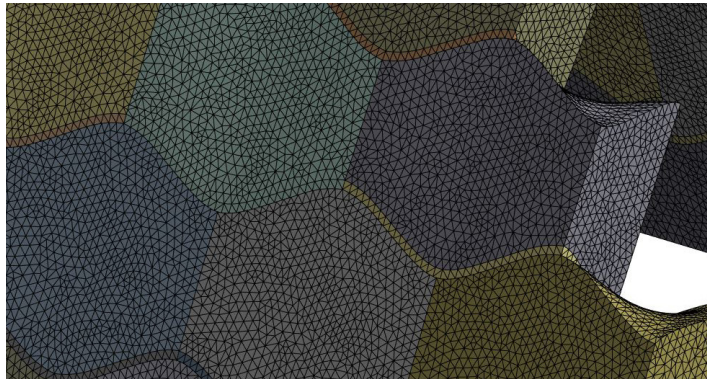


Figure 27: Suggested Meshing level

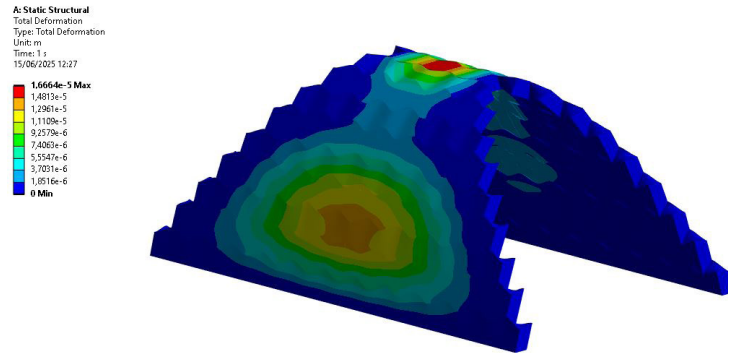


Figure 28: Converged solution after restraining the edge units

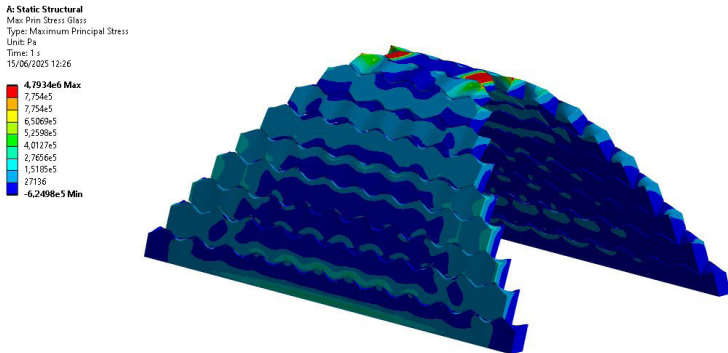


Figure 25: Meshing the vault

Appendix 3- Kirigami prototypes

3.1 Kirigami activation

The chosen kirigami geometry TAK is also an ongoing study at MIT, from which certain initial observations were considered to model the kirigami parametrically. The activation force and further parameter influence on the structural performance were not a part of this thesis and remains as a scope for future research to fine-tune a kirigami interlayer for application in an interlocking masonry design. A brief study was done as to understand the parameters of the TAK geometry-wise. It is observed that the parameter 'W' which is the width of the horizontal strip that pulls the vertical flaps upright are crucial for activation of kirigami and depend on material strength. Figure 29 shows an initial study of varying 'W' in samples created using 3DP PLA, since it was available at hand for rapid prototyping-where the thicker 'W' samples were found to be easier to activate with application of lesser force.

Several samples of varying 'W' parameter were made with 0.5mm thick aluminum sheet as shown in figure 30.

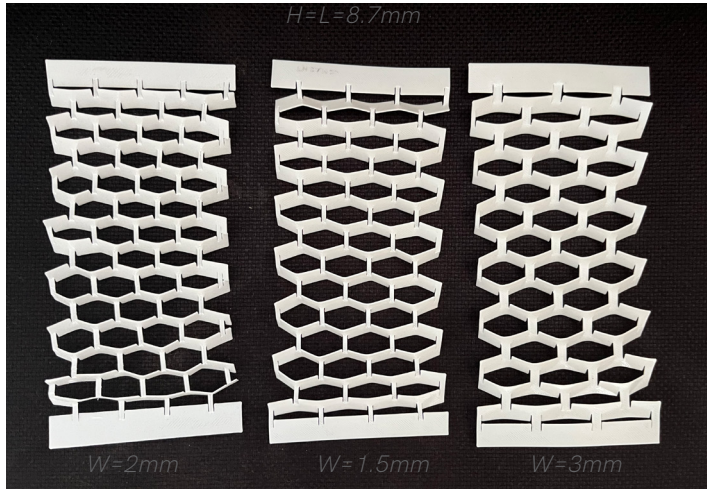


Figure 29: Prototyping TAK parameter variations

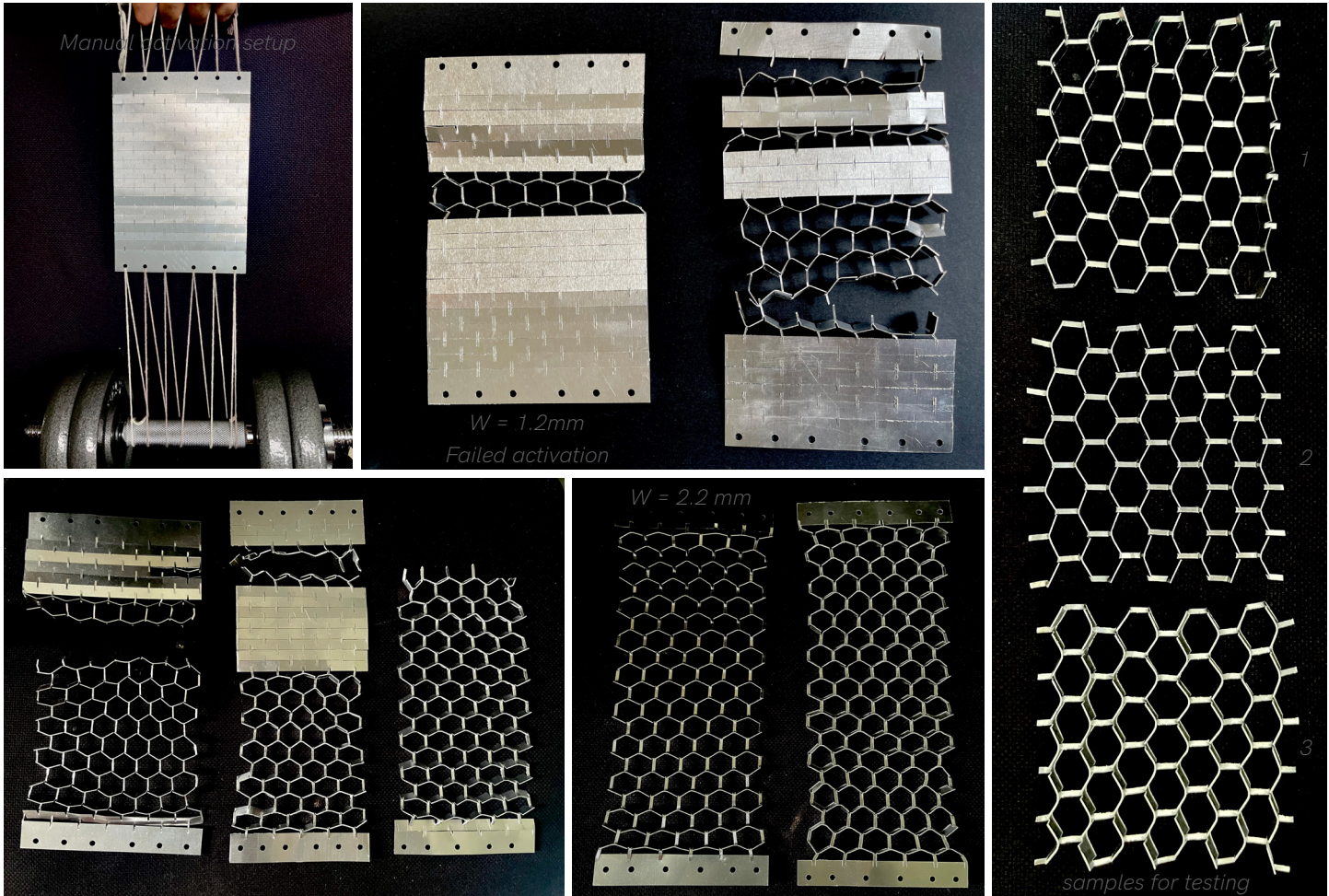


Figure 30: 0.5 Aluminum TAK prototype manual activation

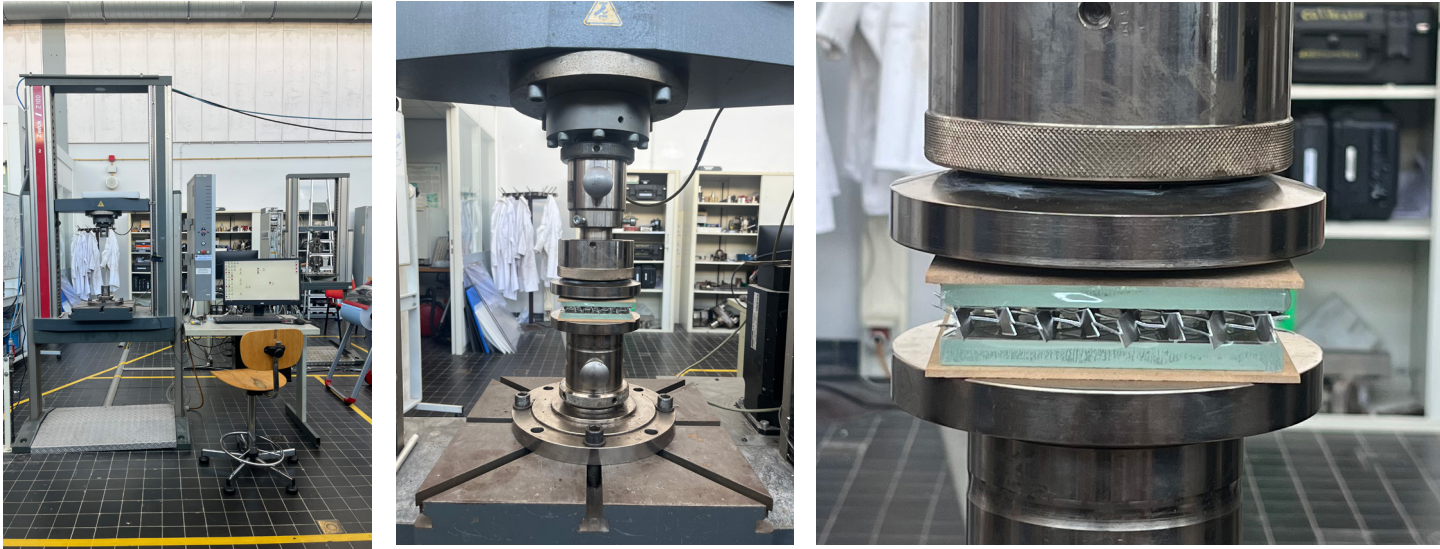
3.2 Kirigami Sandwich compression test

In order to test the composite behavior between the glass and the kirigami interlayer, several compression tests were done. 4 samples tested from which kirigami interlayer stiffness was calculated are presented in section 10.8 of the report. This section presents results from three samples under a different equipment setup with higher load capacity and larger loading plate which was not available earlier.

Experiment set-up:

Figure 31 shows the experiment setup with a loading plate of 15mm diameter. Loading- 1mm per minute. Tests were stopped at 4mm displacement since the kirigami interlayer had already buckled.

Figure 32 Shows the three samples used for testing. All of the samples follow the same configuration mentioned in section 10.8.



Results:

Initial low-force region is seen in the force-displacement graph (figure 34). This likely corresponds to initial settling or seating of the different layers- especially in a dry-assembled system with no bonding. The load is not yet fully transferred through the entire sandwich.

All three specimens then exhibit a much steeper, linear rise in force with displacemen depicting the elastic region. The kirigami may be contributing significant resistance here because its structure initially resists out-of-plane buckling. This suggests a stable load-bearing phase without damage to the glass. The kirigami interlayer is also seen buckling (figure 33) without causing any damage to the glass. This suggests that it can be directly used as an interlayer.

However as demonstrated in the final design validation, the friction coefficient and the performance of the kirigami interlayer with 3DP glass surface is yet to experimentally tested.

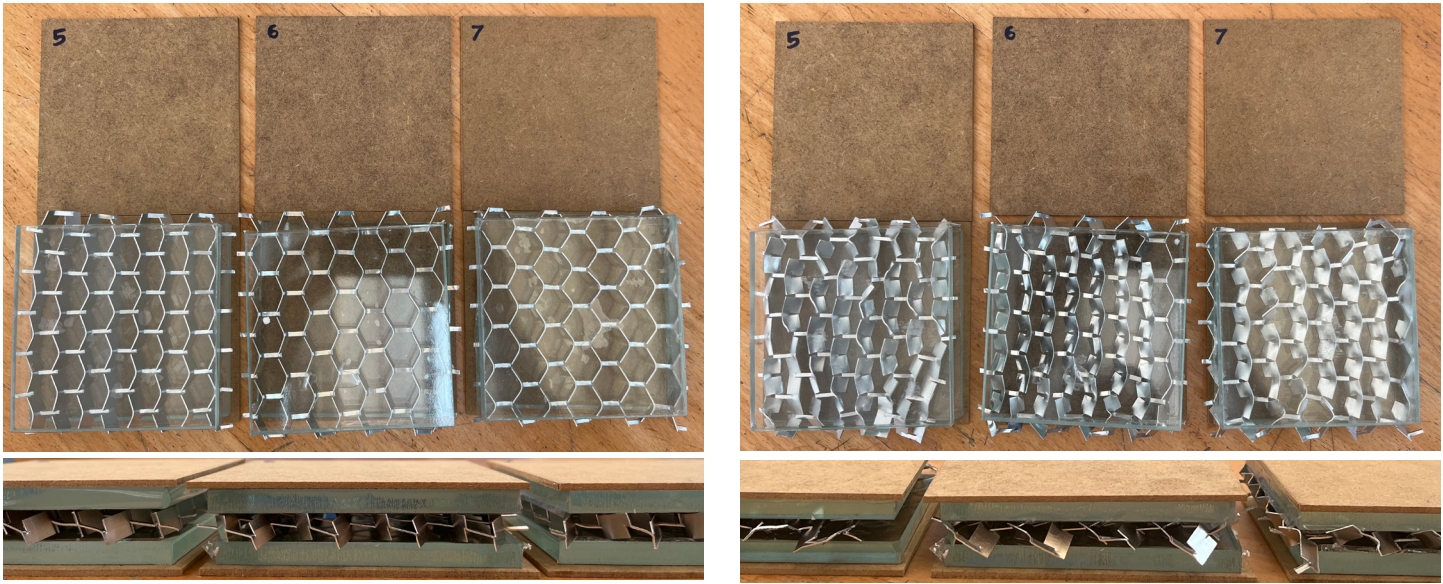


Figure 32: Specimens before testing.

Figure 33: Specimens after testing showing buckled kirigami

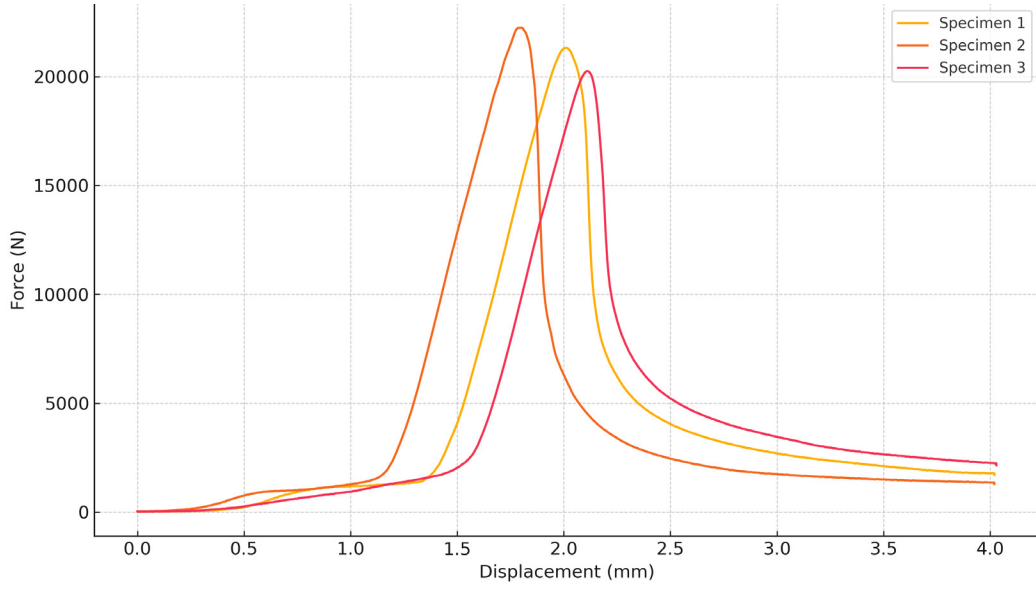


Figure 34: Force-displacement plot for the three specimen



*"This is not the final form, but the first layer- printed,
placed, and ready to support what comes next."*

